INFORMATION TO USERS

This dissertation was produced from a microfilm copy of the original document. While the most advanced technological means to photograph and reproduce this document have been used, the quality is heavily dependent upon the quality of the original submitted.

The following explanation of techniques is provided to help you understand markings or patterns which may appear on this reproduction.

1. The sign or "target" for pages apparently lacking from the document photographed is "Missing Page(s)". If it was possible to obtain the missing page(s) or section, they are spliced into the film along with adjacent pages. This may have necessitated cutting thru an image and duplicating adjacent pages to insure you complete continuity.

2. When an image on the film is obliterated with a large round black mark, it is an indication that the photographer suspected that the copy may have moved during exposure and thus cause a blurred image. You will find a good image of the page in the adjacent frame.

3. When a map, drawing or chart, etc., was part of the material being photographed the photographer followed a definite method in "sectioning" the material. It is customary to begin photoing at the upper left hand corner of a large sheet and to continue photoing from left to right in equal sections with a small overlap. If necessary, sectioning is continued again – beginning below the first row and continuing on until complete.

4. The majority of users indicate that the textual content is of greatest value, however, a somewhat higher quality reproduction could be made from "photographs" if essential to the understanding of the dissertation. Silver prints of "photographs" may be ordered at additional charge by writing the Order Department, giving the catalog number, title, author and specific pages you wish reproduced.

University Microfilms

300 North Zeeb Road
Ann Arbor, Michigan 48106

A Xerox Education Company

Downloaded from SHAREOK. Persistent Handle URL: https://hdl.handle.net/11244/3250

72-19,747

BROWN, Lester Edward, 1942-
AN EXPERIMENTAL AND ANALYTIC STUDY OF WOOD PYROLYSIS.

The University of Oklahoma, Ph.D., 1972
Engineering, chemical

University Microfilms, A XEROX Company, Ann Arbor, Michigan

THIS DISSERTATION HAS BEEN MICROFILMED EXACTLY AS RECEIVED

THE UNIVERSITY OF OKLAHOMA

GRADUATE COLLEGE

AN EXPERIMENTAL AND ANALYTIC STUDY OF WOOD PYROLYSIS

A DISSERTATION

SUBMITTED TO THE GRADUATE FACULTY

in partial fulfillment of the requirements for the

degree of

DOCTOR OF PHILOSOPHY

BY

LESTER EDWARD BROWN

Norman, Oklahoma

1972

AN EXPERIMENTAL AND ANALYTIC STUDY OF WOOD PYROLYSIS

APPROVED BY

C. M. Sliepcevich

Arthur Bernhart

J. Reed Welker

William E. Martinkus

Arthur Wm Wiley Jr

Hadi T. Hashemi

DISSERTATION COMMITTEE

PLEASE NOTE:

Some pages may have

indistinct print.

Filmed as received.

University Microfilms, A Xerox Education Company

ACKNOWLEDGMENTS

I would like to express my sincere gratitude to a number of persons who have contributed to this research effort.

Dr. C. M. Sliepcevich, George Lynn Cross Research Professor of Engineering, for his direction and support.

Dr. J. R. Welker, Associate Director of the Flame Dynamics Laboratory, for his helpful advice and assistance throughout the program.

Dr. H. T. Hashemi, for his suggestions in developing the thermal conductivity experiment.

Dr. A. F. Bernhart, Professor of Mathematics, Dr. A. W. Aldag, Assistant Professor of Chemical Engineering, and Dr. W. E. Martinsen, Assistant Professor of Material Science for their contributions as members of my graduate committee.

Dr. J. A. Havens, presently at the University of Arkansas, whose untiring efforts as a graduate student led to the development of unique experimental equipment.

My fellow graduate students Mr. C. A. Blomquist, and Mr. W. M. Woodard, for their helpful suggestions and discussions.

Mrs. Joyce Gerald and Mrs. Barbara Everidge for their assistance in the preparation of the manuscript.

I am especially grateful to the University of Oklahoma Research Institute, the National Science Foundation, and University Engineers, Inc., for providing financial support.

Finally I wish to acknowledge my wife and daughter; their encouragement and personal sacrifice have not waived.

Lester Edward Brown

ABSTRACT

Thermal, physical, and chemical changes that occur when white pine and oak woods pyrolyze have been studied. Quantitative data have been obtained describing the energy of pyrolysis, the overall chemical kinetics of pyrolysis, and the thermal conductivity of the residual char.

The heat of pyrolysis was measured using the technique of differential scanning calorimetery. The data obtained by this method combine sensible and pyrolysis heat effects. It is shown that the magnitude of the decomposition heat effect is dependent on wood composition.

The overall chemical kinetics for wood pyrolysis have been studied at temperature heating rates of 10, 20, 40, 80, and 160°C/min. Arrhenius parameters have been obtained from these data, and it has been demonstrated that these parameters are independent of heating rate.

An experimental procedure has been developed which consists of pyrolyzing wood cylinders to varying degrees and then measuring the thermal conductivity of the char phase. The thermal conductivity of white pine char has been measured at temperatures ranging from 345°C to 650°C using this method.

These data have been used in a mathematical model based on the law of heat conduction to predict temperatures and weight loss for pyrolyzing wood cylinders. The predicted results have been compared to experimental data for pyrolyzing white pine cylinders.

TABLE OF CONTENTS

		Page
LIST OF TABLES		ix
LIST OF ILLUSTRATIONS		xi
Chapter		
I.	INTRODUCTION	1
II.	REVIEW OF PREVIOUS WORK	3
	The Heat of Reaction for Wood Pyrolysis	7
	Transient Heat Balance Methods	8
	Summary of Transient Heat Balance Methods	13
	The Heat of Reaction via Thermal Analysis	15
	Experimental Thermal Analysis Studies of Wood	24
	Reaction Kinetics for Wood Pyrolysis	33
	Isothermal Kinetic Studies	33
	Dynamic Temperature Kinetic Studies	38
	Thermal and Physical Properties of Wood	56
	Specific Heat	58
	Density	61
	Thermal Conductivity	63
	Effect of Moisture Content	73
	Effect of Bulk Flow and Secondary Pyrolysis	74
	Mathematical Models	78
	Bamford, Crank, and Malan	78
	Weatherford and Sheppard	81
	Panton and Rittman	81
	Kung--Kanury	83
	Havens	84
III.	EXPERIMENTAL PROCEDURES AND RESULTS	10
	Kinetics of Wood Pyrolysis at High Heating Rates	10

Chapter Page

Equipment 104
Experimental Procedure and Data 112
Analysis of Data 125

Heat of Pyrolysis 134

Measurement of Wood Char Thermal Conductivity 147

Preparation of the Samples 150
Thermal Conductivity Test Run 155
Treatment of Data 157

Transient Temperature Profiles 161

IV. MATHEMATICAL MODEL 165

Effect of Heating Rate and Bulk Flow Neglected 168

Inclusion of the Effect of Heating Rate . . . 171

Effect of Bulk Flow 177

Mass Loss 177

V. DISCUSSION OF RESULTS 182

VI. SUMMARY OF WORK AND SPECULATION ON FUTURE STUDIES 192

BIBLIOGRAPHY 194

LIST OF TABLES

Table		Page
II- 1.	Summary of Qualitative DTA Data for Wood . . .	29
II- 2.	Activation Energies for Weight Loss of Wood Samples by Thermal Degradation	36
II- 3.	Activation Energy for Decomposition of Wood and Its Major Components	39
II- 4.	Activation Energies for Untreated Ponderosa Pine Samples	40
II- 5.	Summary of Robert's and Clough's Data for Thermal Decomposition of Wood	41
II- 6.	Kinetic Parameters for Pyrolysis of Wood from Dynamic Thermogravimetry	49
II- 7.	Kinetic Parameters for Pyrolysis of α-Cellulose	57
II- 8.	Thermal Conductivity Values for Wood	66
II- 9.	The Temperature Dependence for the Thermal Conductivity of White Pine	72
II-10.	Estimate of the Magnitude of Bulk Flow Heat Effects on Decomposing Cellulosic Materials	77
II-11.	Summary of Mathematical Analogs	102
III- 1.	Magnetic Standards for TGS-1b Furnace Calibration	112
III- 2.	Kinetic Parameters for the Pyrolysis of White Pine and Oak	134
III- 3.	Experimental Values for Thermal Conductivity of Char	161

Table		Page
IV- 1.	Temperature Correction Factors	172
V- 1.	Furnace Calibration Using Aluminum Oxide and Oak Beds	188

LIST OF ILLUSTRATIONS

Figure		Page
II- 1.	A Schematic Representation of Wood Pyrolysis .	4
II- 2.	Measured Central Temperature-Time Profile for Wood Slabs	9
II- 3.	Heat Generation Rate and Time as Dependent on Temperature in Pine Cylinders	14
II- 4.	Heat Generation Rate and Time as Dependent on Temperature in Pine Cylinders	14
II- 5.	Schematic Diagrams of DTA and DSC Test Cells .	17
II- 6.	Comparison of Sample Temperature, Reference Temperature, and Differential Temperature Curves in Differential Thermal Analysis . .	18
II- 7.	Hypothetical DSC Thermogram	23
II- 8.	Differential Thermal Analysis of α-Cellulose .	26
II- 9.	DTA Results for Cellulose in Nitrogen and Air	27
II-10.	DTA Results for α-Cellulose in Nitrogen and Air, Akita and Kase	30
II-11.	Energy Capacity of Pine Wood as a Function of Temperature in Nitrogen Atmosphere . . .	31
II-12.	Energy Capacity of Oak Wood as a Function of Temperature in Nitrogen Atmosphere . . .	32
II-13.	Experimental Pyrolysis Apparatus Used by Blackshear and Kanury	43
II-14.	Density and Its Dependence on Temperature for Decomposing α-Cellulose Cylinders with Radial Position as Parameters	44

Figure		Page
II-15.	Kinetics of Weight Loss Plot for Wood, α-Cellulose and Lignin	48
II-16.	Weight Loss and Its Dependence on Temperature for Beech Sawdust in Vacuum at Different Heating Rates	50
II-17.	Effect of Rate of Heating on Kinetics of Weight Loss of Dry Pine Wood in Nitrogen . .	53
II-18.	Effect of Rate of Heating on Kinetics of Weight Loss of Dry Oak Wood in Nitrogen Atmosphere	53
II-19.	Specific Heat, C, and Mean Specific Heat, C_m, for Charcoal as a Function of Temperature .	60
II-20.	Comparison of Density Data of Blackshear and Kanury (5) and TG Data of Havens (16) . . .	62
II-21.	Schematic of End Grain Pattern of Ash Board Showing Location of Test Specimens	64
II-22.	Computed and Measured Central Temperature Time Curves from Bamford, Crank, and Malan	80
II-23.	Predicted Temperature and Density Profiles in Pyrolyzing Wood	85
II-24.	Effect of Char Thermal Conductivity on Rate of Weight Loss	86
II-25.	A Mesh Region (i,j) and Its Adjacent Mesh Points	88
II-26.	Schematic of Resistance Wire Heater and Wood Cylinder	98
II-27.	Comparison of Measured and Predicted Temperature Profiles for White Pine at Two Radial Positions for Four Minute Runs	99
II-28.	Measured and Predicted Weight Loss for Pine Test Section	100
II-29.	Adjusted Thermal Conductivity Profile	101

Figure		Page
III- 1.	Perkin-Elmer TGS-1 Thermobalance and UU-1 Temperature Controller	105
III- 2.	Schematic of Perkin-Elmer TGS-1 Furnace and Weight Assemble	106
III- 3.	Modified Thermobalance Furnace	109
III- 4.	Schematic of TGS-1 Temperature Calibration System	111
III- 5.	Temperature Calibration Curves for TGS-1b Furnace	113
III- 6.	TG and DTG Curves for White Pine at a Nominal Heating Rate of 10°C/min	115
III- 7.	TG and DTG Curves for White Pine at a Nominal Heating Rate of 20°C/min	116
III- 8.	TG and DTG Curves for White Pine at a Nominal Heating Rate of 40°C/min	117
III- 9.	TG and DTG Curves for White Pine at a Nominal Heating Rate of 80°C/min	118
III-10.	TG and DTG Curves for White Pine at a Nominal Heating Rate of 160°C/min	119
III-11.	TG and DTG Curves for Oak at a Nominal Heating Rate of 10°C/min	120
III-12.	TG and DTG Curves for Oak at a Nominal Heating Rate of 20°C/min	121
III-13.	TG and DTG Curves for Oak at a Nominal Heating Rate of 40°C/min	122
III-14.	TG and DTG Curves for Oak at a Nominal Heating Rate of 80°C/min	123
III-15.	TG and DTG Curves for Oak at a Nominal Heating Rate of 160°C/min	124
III-16.	TG Curve for White Pine in an Air Atmosphere at a Nominal Heating Rate of 20°C/min . . .	126

Figure		Page
III-17.	Summary of TG Curves for White Pine in an Nitrogen Atmosphere	127
III-18.	Summary of TG Curves for Oak in an Nitrogen Atmosphere	128
III-19.	Log Rate as Dependent on Reciprocal Temperature for White Pine	130
III-20.	Log Rate as Dependent on Reciprocal Temperature for Oak	131
III-21.	Determination of the Order of Reaction and Frequency Factors for White Pine and Oak . .	133
III-22.	The Perkin-Elmer DSC-1b	136
III-23.	Purge Gas Flow Pattern in Differential Scanning Calorimeter Sample Head	139
III-24.	Relation Between Programmed and Actual Temperatures in Perkin-Elmer DSC-1b Instrument	142
III-25.	Power Calibration for the Differential Scanning Calorimeter	144
III-26.	Energy Capacity of White Pine as a Function of Temperature in a Nitrogen Atmosphere . .	146
III-27.	Energy Capacity of Oak as a Function of Temperature in a Nitrogen Atmosphere	148
III-28.	Radial X-Ray of White Pine Cylinder Showing Thermocouple Bead Location	152
III-29.	Photograph of Instrumented Wood Cylinder in Test Cell	153
III-30.	Schematic Diagram of Instrumented Wood Cylinder	154
III-31.	Temperature Dependence of Electrical Resistance of Trophet A 80-20 Nickel-Chromium Wire	156
III-32.	X-Ray Photographs of Pyrolyzing Wood	158

Figure		Page
III-33.	Char Temperature as a Function of Thermocouple Position	160
III-34.	Schematic of Section of Cylindrical Test Section Showing Boundary Condition	162
IV- 1.	Thermal Conductivity of White Pine as a Function of Temperature	169
IV- 2.	Comparison of Computed and Experimental Temperature Profiles for White Pine (Model of Havens)	170
IV- 3.	Estimate of Effect of Heating Rate on Heat of Pyrolysis	174
IV- 4.	Energy Capacity as a Function of Heating Rate for White Pine	176
IV- 5.	Computed and Experimental Temperature Profiles for White Pine. Computed Results Include Effect of Heating Rate	178
IV- 6.	Experimental and Computed Temperature Profile for White Pine. Model Includes Effect of Heating Rate	179
IV- 7.	Experimental and Computed Temperature Profile for White Pine. Model Includes Heating Rate and Bulk Flow Effects	180
IV- 8.	Computed and Experimental Weight Loss Profile for White Pine	181
V- 1.	Estimate of Heat of Pyrolysis for White Pine from DSC Data	184
V- 2.	Estimate of Heat of Pyrolysis for Oak from DSC Data	185
V- 3.	DTG Curves for White Pine and Oak at a Heating Rate of 20°C/min	186
V- 4.	Effect of Model Modifications on Computed Temperature Profiles	191

CHAPTER I

INTRODUCTION

Wood, fabrics, plastics, and other organic solids are used in applications where their thermal degradation or combustion is a safety hazard. A fundamental mathematical model describing the transient transport and chemical processes that precede ignition and combustion would be of value in evaluating fire retardants, fire hazards, and fire prevention systems. Although several such models have been proposed for wood, their usefulness has been limited since data describing the changes in wood composition and properties as wood pyrolyzes have not been available.

The Flame Dynamics Laboratory at the University of Oklahoma Research Institute initiated in 1966 a fundamental study of the thermal, physical, and chemical properties of pyrolyzing wood in an effort to develop a mathematical model which could be used to describe the transient temperature and density profiles of pyrolyzing wood. A thermal analysis system was purchased by the laboratory for use in determining wood properties during pyrolysis. The data obtained were incorporated into a numerical heat conduction model previously

developed at the University of Oklahoma (15). Unfortunately major assumptions regarding the chemical kinetics and thermal conductivity of pyrolyzing wood were required to obtain agreement between experimental and computed results.

The objectives of this study are: (1) experimentally measure the thermal conductivity of wood char, (2) determine the dependence of pyrolysis reaction kinetics on heat history, and (3) incorporate these findings into a mathematical model to describe the temperature profile and mass loss characteristics of pyrolyzing wood. Ideally, solution of the model should require only the physical and thermal properties of wood and the initial and boundary conditions for wood undergoing pyrolysis. A further objective is to test the reliability of the mathematical model by comparing computed and experimental temperature and weight loss profiles for large pyrolyzing wood samples.

CHAPTER II

REVIEW OF PREVIOUS WORK

Wood is a heterogenous, non-isotropic material consisting primarily of the natural polymers, cellulose, lignin, and hemicellulose. The individual polymer molecules combine to form fibers; these fibers preferentially order to form the well known solid called wood. The terms ignition and combustion of wood are somewhat misleading in that the solid does not ignite or burn; rather volatile gases formed by pyrolysis of the polymer components in wood ignite and burn at the surface of the wood. The development of an ignition criterion based on the rate of wood pyrolysis and the temperature profile in pyrolyzing wood required that a series of complicated transport and chemical processes be defined. An overall perspective of the pyrolysis process and the requirements for a predictive model can be obtained by qualitative consideration of the sequence of events that occur in pyrolyzing wood.

Figure II-1a represents the heating of a wood slab initially at temperature T_o by an external energy source of flux Q. During the initial heating period the slab temperature

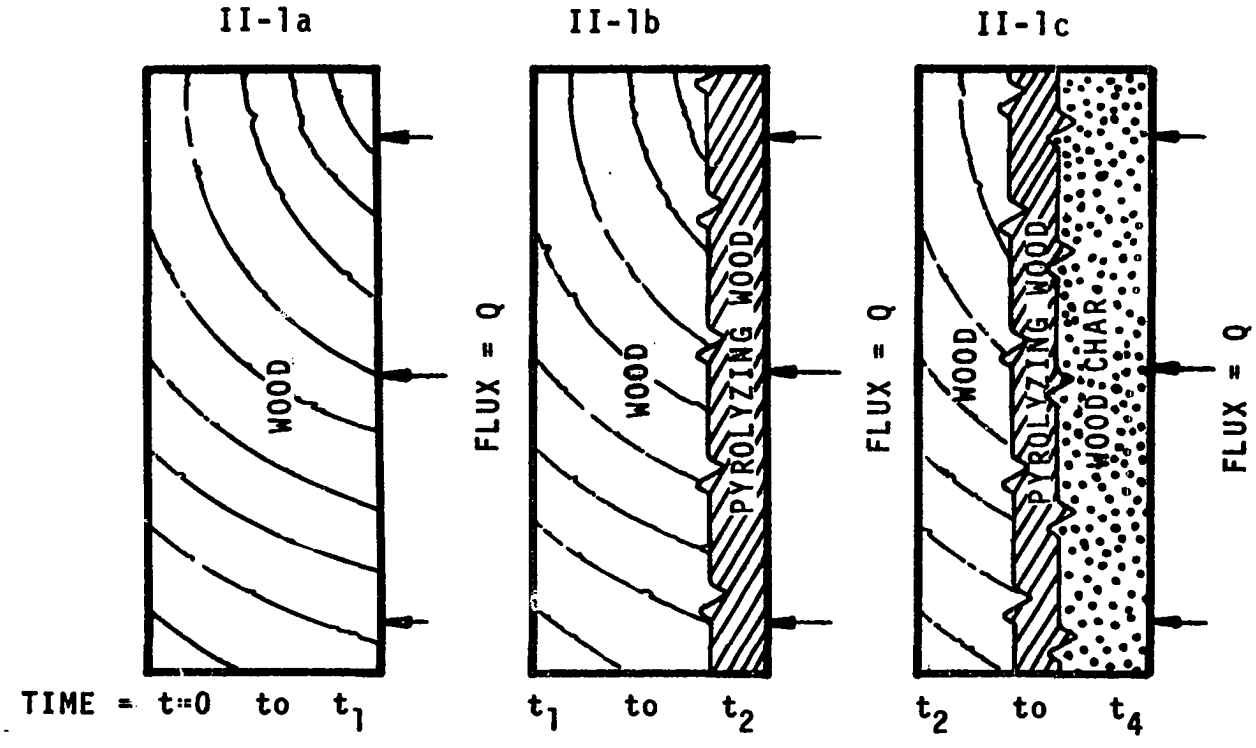

Figure II-1. A Schematic Representation of Wood Pyrolysis.

rises, its composition is unchanged, and its thermal and physical properties remain nearly constant. Assuming that no edge effects occur the transient temperature response of the wood slab can be computed by solving the heat conduction equation given below

$$K \frac{\partial^2 T}{\partial x^2} = C_p \rho \frac{\partial T}{\partial t} \qquad \text{II-1}$$

The boundary conditions for Equation II-1 are:

$$\text{at } t = 0, \quad T = T_o, \text{ for } 0 < x < L$$

$$t > 0, \; - K \frac{\partial T}{\partial x} = f(Q) \text{ at } x = L$$

$$t > 0, \; - K \frac{\partial T}{\partial x} = H(T) \text{ at } x = 0$$

where T = temperature (°C)

t = time (sec)

K = thermal conductivity of wood (cal/cm^2-sec-°C/cm)

C_p = heat capacity of wood (cal/gm-°C)

ρ = density of wood (gm/cm^3)

x = position along sample width (cm) (cm)

L = sample width (cm)

$f(Q)$, $H(T)$ = heat transfer rates at front and back surfaces of sample (cal/cm^2-sec)

Eventually the material nearest the heat source will accumulate sufficient energy so that pyrolysis begins as shown in Figure II-1b. The polymeric components fragment during pyrolysis forming volatile products which provide the fuel for

ignition and combustion. A number of modifications must be made in the heat conduction equation to define fully the heat and mass loss effects during pyrolysis. Among these changes are:

1. A term must be added for the heat of reaction associated with wood pyrolysis. Usually this term takes the form $q(\partial W/\partial t)$ where q is the heat of pyrolysis and $\partial W/\partial t$ the change in sample weight with respect to time. As shall be shown later in a dynamic heating process, the pyrolysis of wood occurs over a broad temperature range; therefore, q must be defined as a function of temperature and composition.
2. The kinetic term $\partial W/\partial t$ must be determined and its dependence on heating history must be considered.
3. Since the physical and thermal properties of wood are strongly dependent on the extent of pyrolysis, these variations in properties must be included in the model. As an example, in a fully developed pyrolysis zone, the density decreases by 80 percent across the pyrolysis zone.

As more energy is supplied to the wood, the pyrolysis zone as shown in Figure II-1c, moves through the wood sample leaving behind a char matrix. Since the physical and thermal properties of char are considerably different from those of either the original wood or the pyrolyzing wood, these differences must be taken into account. Additionally, the volatiles

formed in the pyrolysis zone flow through the char matrix and exit at the heated surface. The char is warmer than the volatiles; therefore, in a model the transfer of heat to the volatiles flowing through the char must be considered. Several investigators have also theorized that the volatiles are thermally cracked as they pass through the char.

A detailed mathematical description of pyrolyzing wood obviously requires that density, thermal conductivity, and heat capacity be specified for all three phases shown in Figure II-1c. Additionally, the kinetics of pyrolysis, the heat effects associated with pyrolysis chemistry, and the flow of volatiles must be known. In the remainder of this chapter, previous studies of these physical, thermal, and chemical properties will be considered, and the various pyrolysis models reported in the literature will be discussed.

The Heat of Reaction for Wood Pyrolysis

The heat of reaction for wood pyrolysis has been reported in the literature as exothermic, endothermic, and a combination of the two. Some investigators have assumed pyrolysis occurs over a narrow temperature range; others, over a wide temperature range. This confusion can be attributed to the two types of experiments that have been used to measure the heat of pyrolysis: transient heat balance methods and thermal analysis methods.

Transient Heat Balance Methods

Bamford, Crank, and Malan (4) computed the heat of reaction for wood pyrolysis from transient temperature profiles obtained at the center of wood slabs heated on both faces by flames. A typical central temperature profile, as shown in Figure II-2, exhibits a sharp temperature rise near 600°K which Bamford et al. attributed to an exothermic pyrolysis reaction. The heat balance given in Equation II-2 was written per unit volume of wood and was solved for the heat of pyrolysis based on the following assumptions:

1. The sudden rise in central temperature was only due to the heat of pyrolysis.
2. No heat was conducted away from the pyrolysis zone.
3. The physical properties of the wood remained constant throughout the experiment.

$$C_p \rho \Delta T = q W_o \qquad \text{II-2}$$

C_p = heat capacity of the wood (cal/gm°C)

ρ = density of wood (gm/cm^3)

ΔT = the magnitude of the sudden temperature rise (°C)

W_o = weight of wood decomposed (gm/cm^3)

q = heat of pyrolysis (cal/gm)

The value of W_o was experimentally determined, and the values for heat capacity and density were obtained from the literature. The computed value for heat of pyrolysis was reported

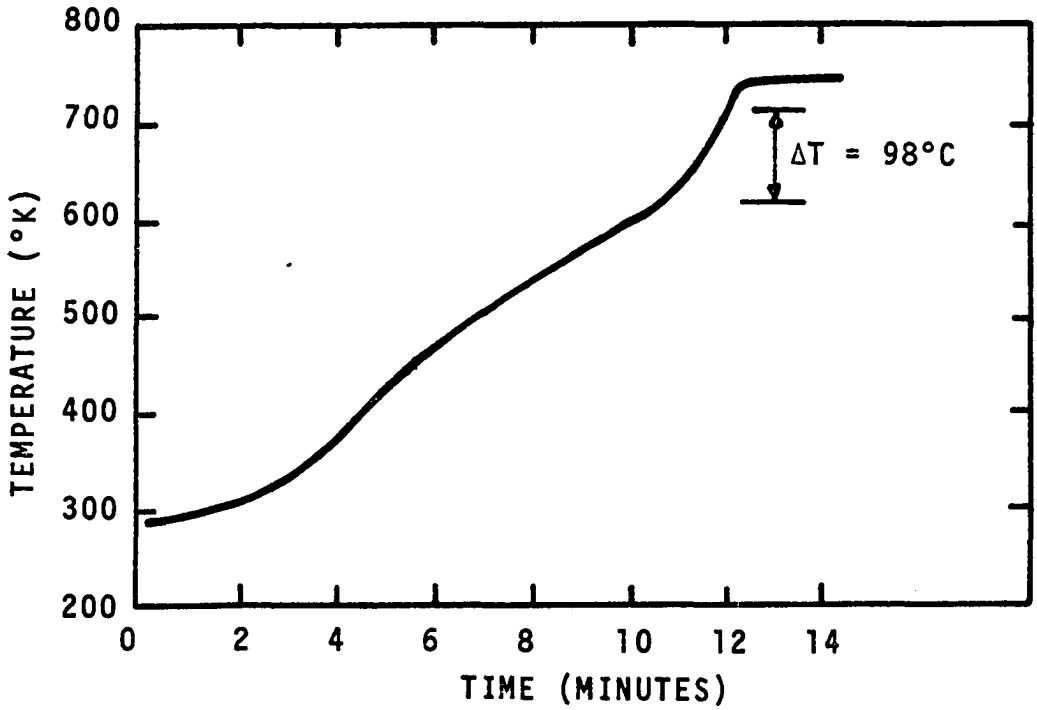

Figure II-2. Measured Central Temperature-Time Profile for Wood Slabs as Reported by Bamford, Crank and Malan (4).

to be 86 cal/gm, exothermic, which Bamford et al. claimed was in agreement with a value computed by taking the difference between the heat of combustion for wood and its decomposition products.

This value for the heat of pyrolysis was the first to be published and has been widely accepted. It may be questioned for the following reasons:

1. Temperature gradients in the samples are neglected; hence, no conduction effects were considered in determining the magnitude of the temperature effect due to pyrolysis.
2. The measured value of q assumes the decomposition and resulting heat effects occur over a narrow temperature range near 430°C, and that no appreciable heat effects are present at other temperatures.
3. Since the work of Bamford, Crank, and Malan, the properties of wood have been shown to change dramatically during pyrolysis. The sharp rise in temperature near 600°K may be attributable to the change in thermal and physical properties.

Akita (1) estimated the heat of pyrolysis for sawdust and Japanese cypress using a transient temperature profile obtained at the center of externally heated wood spheres. It was assumed that during pyrolysis heat was homogenously released as described in Equation II-3. The equation for heat conduction was solved using values for the reaction rate constant experimentally determined by Akita.

$$q \frac{dW}{dt} = qk(W - W_\infty) \qquad \text{II-3}$$

W = weight of reactant at time t (gm/cm^3)

k = rate constant (sec^{-1})

W_∞ = residue weight of reactants (gm/cm^3)

An approximate solution to the heat conduction equation yields

$$T_o = T_a + \frac{2qW_\infty}{C_p\rho} \sum_{n=1}^{\infty} (-1)^n \frac{a^2k}{\alpha\pi^2n^2 - a^2k} \left[\exp \frac{\alpha\pi^2n^2t}{a^2} - \exp(-\alpha t)\right] \qquad \text{II-4}$$

where T_a = surface temperature (or temperature of heating medium) (°C)

T_o = temperature at the center of the sphere of radius r (°C)

q = heat of pyrolysis (cal/gm decomposed)

C_p = specific heat (cal/gm°C)

ρ = density (gm/cm^3)

k = rate constant (sec^{-1})

α = thermal diffusivity (cm^2/sec)

Akita's experiments were run in an inert atmosphere, and Equation II-4 was fitted to the experimental data by adjusting q, the only unknown. The best fit for sawdust was a value of 30 cal/gm and for Japanese cypress, 32 cal/gm, both exothermic. Akita assumed that thermal diffusivity remained constant throughout pyrolysis.

Roberts and Clough (34) computed the heat of pyrolysis from transient temperature profiles obtained at several radial positions in cylindrical samples heated in a muffle furnace. They wrote a heat balance on a cylindrical element within the specimen as net heat transferred across the surface + heat generated within the element = accumulation of heat within the element. The first and third terms were computed from the measured temperature profiles. The heat of pyrolysis was determined by fitting a value of q to the experimental data. The value for heat of pyrolysis, when the sample temperatures exceeded 300°C, was 55-75 cal/gm, exothermic. At temperatures below 300°C a value of 280 cal/gm, exothermic, was obtained. Again it was assumed that all thermal and physical properties were constant throughout pyrolysis.

Widell (46) computed the heat of pyrolysis for pine, spruce, and birch from transient temperature profiles obtained at several radial positions in externally heated cylindrical samples. Widell solved the heat conduction equation (Equation II-5) for the heat of pyrolysis as a function of sample temperature by computing the first and second order variations in temperature with respect to radial position, and the derivative of temperature with respect to time, directly from the experimental data.

$$\frac{\partial T}{\partial t} = \alpha \left(\frac{\partial^2 T}{\partial r^2} + \frac{1}{r} \frac{\partial T}{\partial r} \right) + \frac{1}{C_p \rho} q \qquad \text{II-5}$$

Widell also assumed that the physical and thermal properties of wood were invariant throughout pyrolysis.

Data were obtained by Widell at isothermal furnace temperatures of 80°C and 300°C. The heat of pyrolysis was computed from the data as a function of temperature using Equation II-5. Figures II-3 and II-4 show the results of these computations for pine test rods of radii 11.2 mm and 45 mm. The entire heat of pyrolysis curve is endothermic for an 80°C surrounding temperature. For the case of 300°C surrounding temperatures the endothermic effect is deepest at a temperature of 125°C. It then decreases until the net effect appears to become exothermic at a temperature of approximately 250°C and higher.

Recently, Kanury (19) proposed that the heat of decomposition be computed using a model that accounts for the variation of physical and thermal properties with temperature and chemical composition. A computer program was written by Kung (24) for numerical solution of this model (which will be discussed later) but because of the lack of property data, the computations were not performed.

Summary of Transient Heat Balance Methods

Each of the transient heat balance methods discussed in this section required that a pyrolysis model be assumed. By adjusting the heat of pyrolysis to force experiment data to fit a model any differences between the true pyrolysis

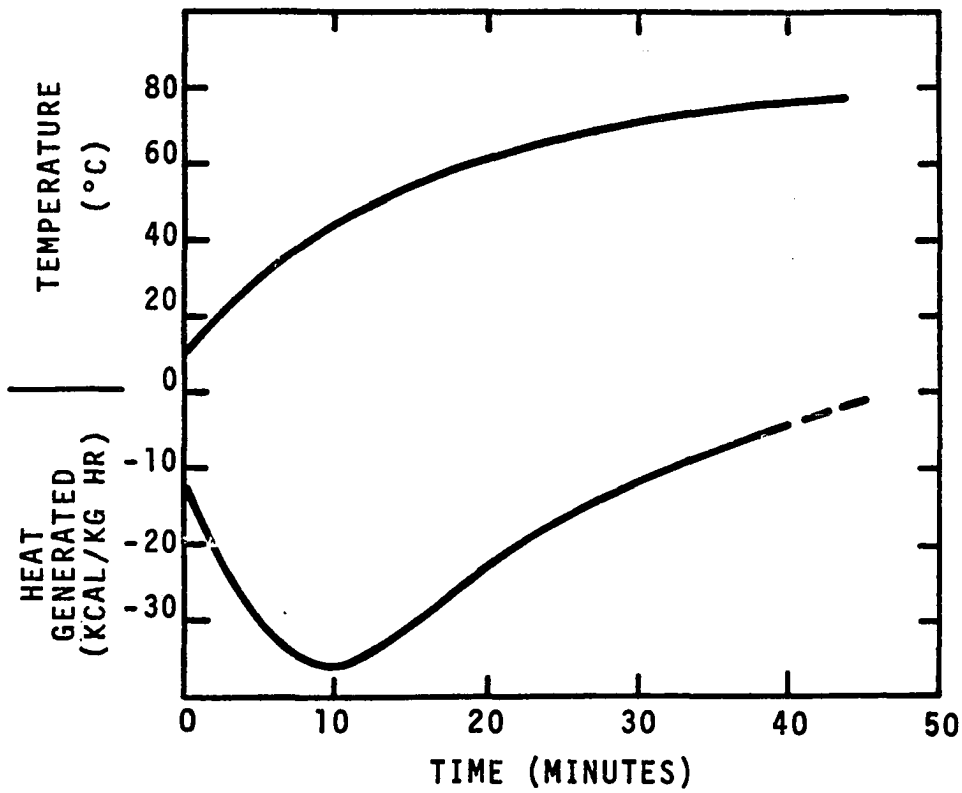

Figure II-3. Heat Generation Rate and Temperature as Dependent on Time in Pine Cylinder (r = 11.2 mm) with Surrounding Temperature = 80°C (46).

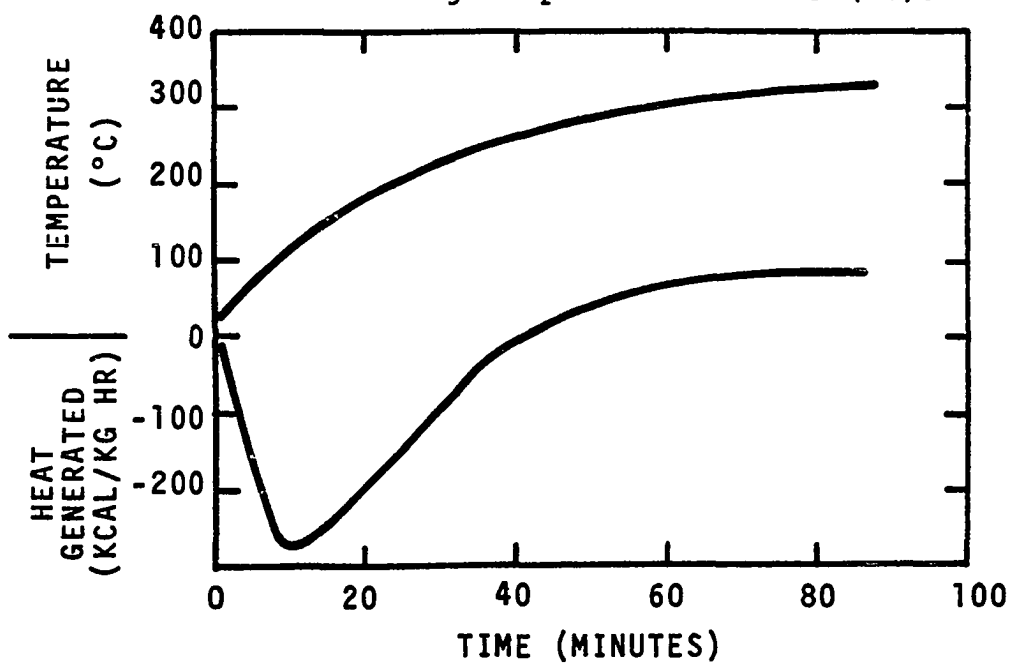

Figure II-4. Heat Generation Rate and Temperature as Dependent on Time in Pine Cylinder (r = 11.2 mm) with Surrounding Temperature = 300°C (46).

process and the model are incorporated into the heat of pyrolysis. The result is, at best, a semi-empirical quantity which only has meaning with respect to the experimental data from which it was derived if the model and real process are different. The values for heat of pyrolysis reviewed in this section were obtained using this procedure.

The Heat of Reaction via Thermal Analysis

Differential thermal analysis (DTA) and differential scanning calorimetry (DSC) may in theory both be used to measure the heat of pyrolysis for wood as a function of temperature. However, the practical performance of these two techniques differ somewhat in providing useful data. The assets and liabilities of both of these thermal analysis techniques will first be discussed, and then the experimental work reported in the literature for thermal analysis of wood will be reviewed.

Recent advances in DTA and DSC equipment, and the nomenclature each vendor has associated with his particular thermal analysis system, have resulted in considerable confusion as to the difference between DTA and DSC. This unfortunate situation has been encouraged by the many similarities between the two techniques, several of which are listed below.

1. Both systems are designed to identify and measure heat effects associated with chemical reactions and phase transitions.

2. The DTA and DSC test cells, shown in Figure II-5a and 5b, are strikingly similar. Such features as sample pan, reference pan and purge gas are common to both systems.
3. The fundamental experimental concept in both systems is that heat effects can be measured by comparing the temperatures of a linearly heated sample and a reference pan.

In this study any thermal analytical system in which the sample pan and reference pan are heated by a common source will be called a DTA system. A DSC test cell will be defined as a thermal analysis system in which the sample pan and reference pan will be maintained at the same temperature by use of a feedback control circuit.

The determination of heat effects using DTA techniques can be illustrated by considering a hypothetical pair of materials which are identical in all respects except that at temperature T_1, the material, which shall de denoted as the sample, undergoes an endothermic transition. The second inert material will be referred to as the reference. If one assumes that the heat input rate to the heating block is constant and the thermal properties of the reference material are invariant with temperature, then the time-temperature profile for the reference material would appear as a straight line similar to that shown in Figure II-6. If the sample is exposed to the same thermal environment as the reference, the temperature of the sample will rise identically with that of the reference

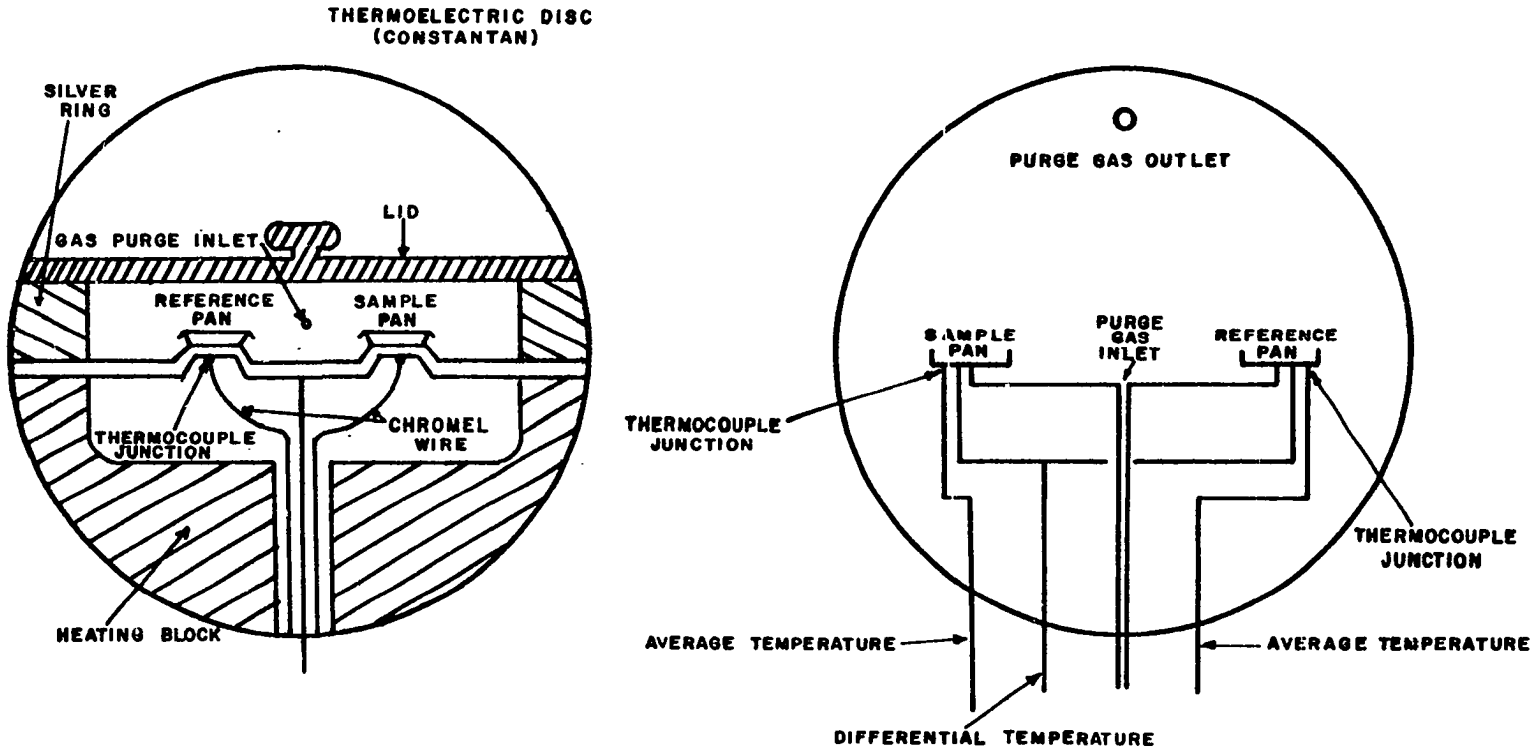

DTA CELL CROSS SECTION

DSC CELL CROSS SECTION

Figure II-5. Schematic Diagrams of DTA and DSC Cells.

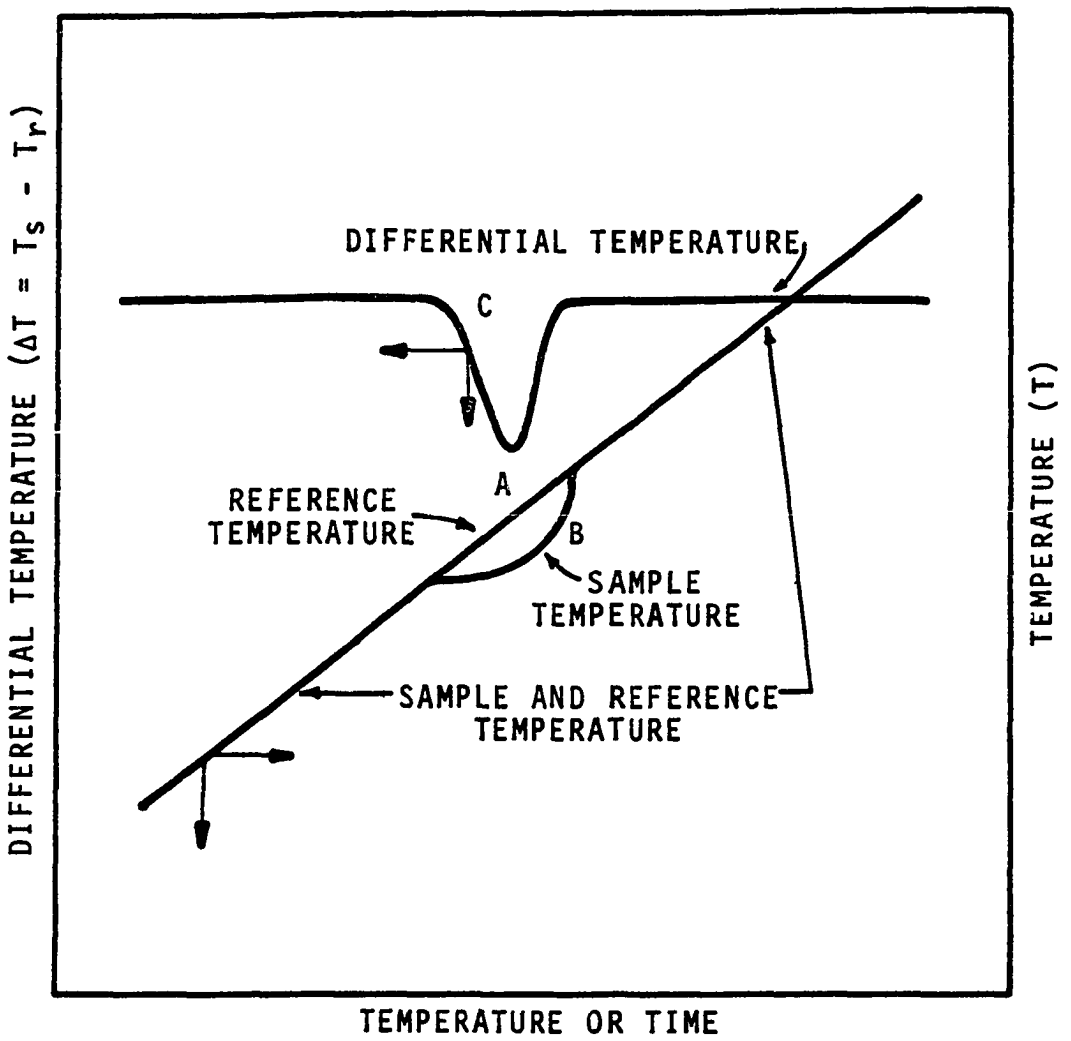

Figure II-6. Comparison of Sample Temperature, Reference Temperature, and Differential Temperature Curves in Differential Thermal Analysis.

until the temperature, T_1, is reached, at which time the absorption of heat due to the endothermic phase transition will cause the sample temperature to be lower than the reference. Upon completion of the phase transition the sample temperature will return again to that of the reference material as shown by Curve B of Figure II-6. Usually the difference in temperature ($\Delta T = T_S - T_R$) between the sample and reference materials is plotted versus time or reference temperature which gives a curve similar to C in Figure II-6.

DTA data must be converted to energy units to be useful. This conversion can be accomplished by comparing the sample DTA thermogram to that for a calibration material which undergoes a well defined heat effect. The thermal properties of real materials usually vary with temperature. Thus, the ideal straight line in Figure II-6 will not only be a curve, but will also vary from material to material even when a common reference is used. To minimize this non-ideal behavior on quantitative computations, the calibration heat effect should occur near the temperature at which the sample heat effect occurs. A series of calibration samples must be used for samples which decompose over a wide temperature range.

Reproduction of DTA thermograms is very difficult and frequently impossible. This problem has been attributed to a number of factors. The dominate factor appears to be changes in the radiative and conductive heat transfer properties of

the test cell from run to run. These changes cannot be easily identified in DTA experiments.

The Perkin-Elmer Corporation has developed a DSC which maintains both the sample and reference pans shown in Figure II-5b at very nearly the same temperature regardless of the heat effects taking place. This characteristic is accomplished by use of a feedback control circuit which supplies power to both pans in proportion to the temperature difference between the two pans. The significance of this feature can be demonstrated by considering a hypothetical DSC scan of a material having a heat effect of magnitude q_s.

The temperature difference between the sample and reference pans without feedback control is dependent on the magnitude and duration of the heat effect, q_s, and the thermal resistance between the sample holder and the surroundings as expressed in Equation II-6.

$$\Delta T = q_s R \qquad \text{II-6}$$

ΔT = temperature difference between sample and reference pans (without feedback control)

q_s = heat effect

R = resistance to heat flow from the sample and sample holder to the surroundings.

A DSC feedback circuit supplies instantaneous heat flow to the sample holder based on the actual temperature

difference, $\Delta T'$, between the sample and reference pans. The feedback energy supplied can be expressed as:

$$q = - K \Delta T' \qquad \text{II-7}$$

K = amplifier gain

$\Delta T'$ = temperature difference between sample and reference pans (with feedback control-closed loop system)

q = energy supplied by feedback control loop due to $\Delta T'$.

Since the magnitude of $\Delta T'$ is dependent upon the net heat flow seen by the temperature sensors, then from Equation II-6

$$\Delta T' = (q_s + q) R \qquad \text{II-8}$$

substituting from Equation II-7 for $\Delta T'$

$$- q/K = (q_s + q) R \qquad \text{II-9}$$

solving for q the energy supplied by the feedback controller Equation II-10 is obtained.

$$q = -q_s \left(\frac{1}{1 + \frac{1}{KR}}\right) \qquad \text{II-10}$$

The resistance to heat flow in Equation II-10 is fairly large, and if the amplifer gain approaches infinity

then the electrical energy supplied by the feedback control circuit just balances the unknown heat effect q_s. Thus in theory the heat effect q_s can be quantitatively determined by measuring the electrical energy supplied by the feedback control circuit.

The same hypothetical endothermic process used above for DTA can be analyzed for DSC to demonstrate the practical aspects of thermal analysis using a DSC. The DSC feedback control circuit cannot distinguish between inherent sample and reference pan heating difference and those caused by heat effect in the test specimen. Consequently in a DSC scan all of these heat effects are combined and thus in actual DSC studies the first task is to determine the difference in heat capacity and heat transfer characteristics of the sample and reference pans over the temperature range of interest. These data are referred to as the baseline, which is Curve A in Figure II-7. The sample thermogram is then obtained as shown in Curve B. The output data using the Perkin-Elmer DSC is the derivative of energy with respect to time and, hence, the total energy required to raise the specimen from its initial temperature, through an endothermic transition and to its final temperature is given by the area enclosed by Curves A and B. The peak in Curve B represents the endothermic heat effect. Note that the DSC method does not require a reference sample, only a reference pan, and that calibration is needed

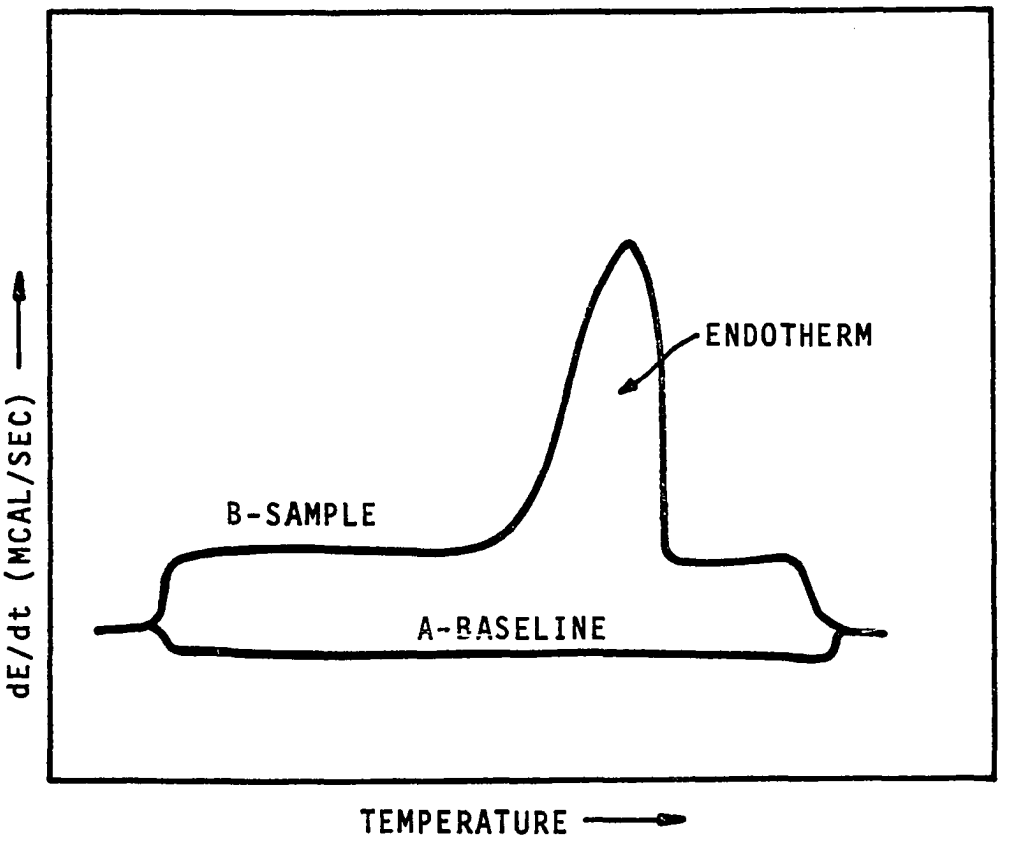

Figure II-7. Hypothetical DSC Thermogram.

only at one temperature. Also the effect of radiative and conductive heat transfer can be identified and minimized by requiring that the isothermal heat losses at the low and high temperature limits of the experiment be identical for both the base line and sample runs.

Experimental Thermal Analysis Studies of Wood

Widell (46) designed a thermal analysis experiment in an effort to determine the energy associated with the pyrolysis of wood. Wood test cylinders 150 mm in length and 45 mm in outside diameter, having a 20 mm diameter center hole along the longitudinal axis, were used. Each test specimen was heated using an electrical resistance heater inserted in the center hole and extending past both ends of the specimen. Three thermocouples were located along various radii inside each specimen. The instrumented specimen was placed in a brass cylinder provided with stainless steel end covers. The brass cylinder and test specimen were then placed in a second cylindrical container 300 mm in diameter, and the second container was filled with silica gel. The problem of determining the heat loss characteristics of the test unit was resolved by comparing the surface temperature of the brass cylinder to that of an identically constructed system excluding the test specimen. During a test a constant power level to the pyrolysis cylinder was maintained, while the power to the compensation cylinder was regulated in such a way that the

surface temperature of the two cylinders was equal throughout the experiment. Widell calculated heats of pyrolysis of 200 cal/gm (exothermic) and 0 cal/gm for 45 mm and 20 mm diameter rods respectively, by assuming that the difference in power input to the cylinders was due to the heat of pyrolysis. Widell partially reconciled these differences by noting that the amount of energy liberated during pyrolysis was obtained from the difference between numbers that are almost equal in magnitude.

Tang and Neill (39) estimated the heat of pyrolysis and combustion for α-cellulose using a commercial differential thermal analysis unit. Experimental data were obtained at a heating rate of 12°C/minute in both flowing helium and oxygen atmospheres. Typical DTA thermograms from this study are shown in Figure II-8. As can be seen, the pyrolysis reaction in an inert atmosphere is endothermic over the full temperature range, whereas the oxidation reaction is exothermic. The heat of pyrolysis was found to be 88 $\pm$ 3.6 cal/gm, endothermic, while the oxidation reaction liberated 3550 cal/gm.

Broido (6) studied the thermal decomposition of α-cellulose and ash free cellulose using the same DTA equipment as Tang and Neill. Thermograms were obtained in flowing nitrogen and air atmospheres. Broido's thermograms, as shown in Figure II-9, indicated that in both atmospheres pyrolysis was endothermic up to approximately 325°C and exothermic from

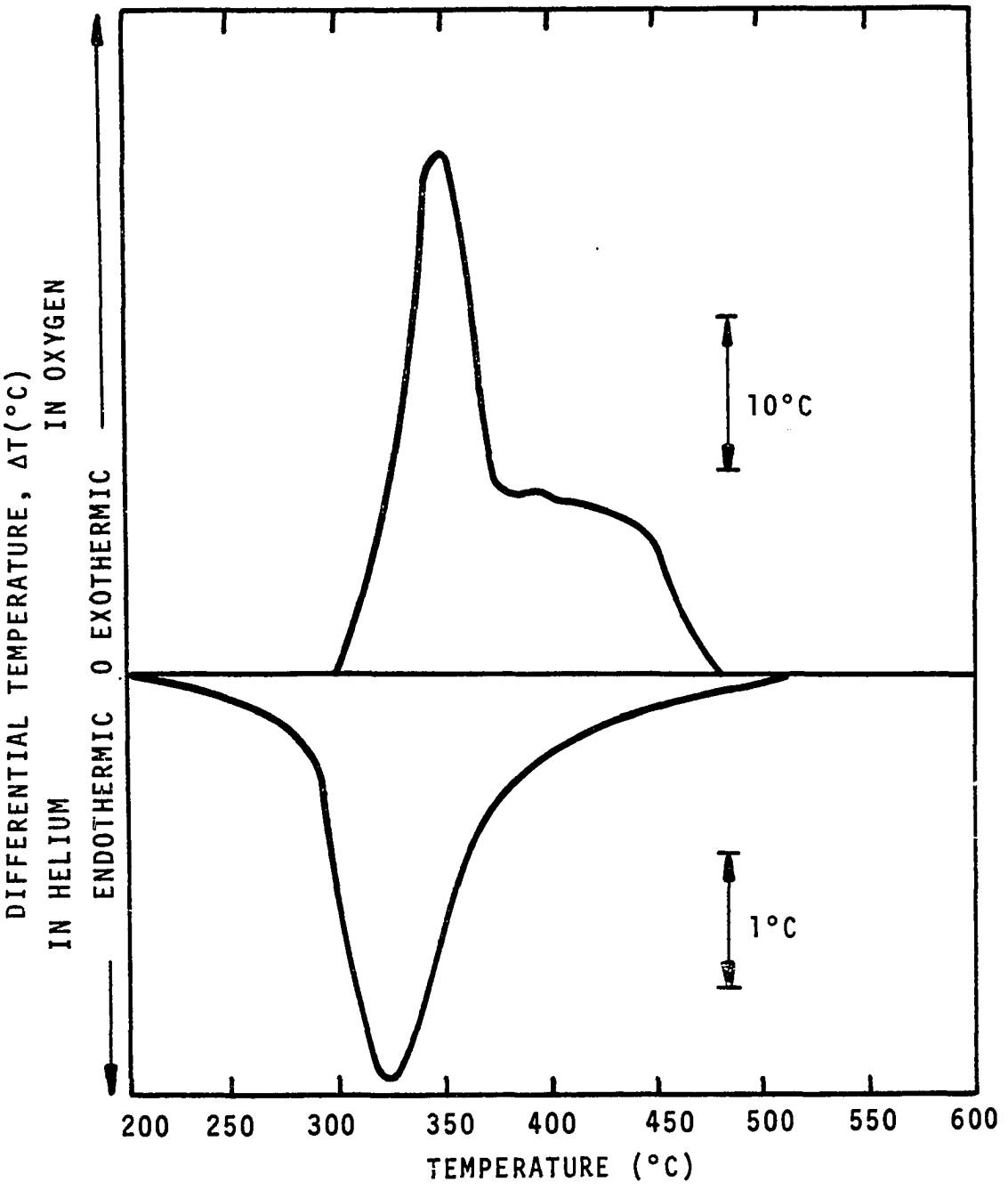

Figure II-8. Differential Thermal Analysis of α-Cellulose by Tang and Neill (39).

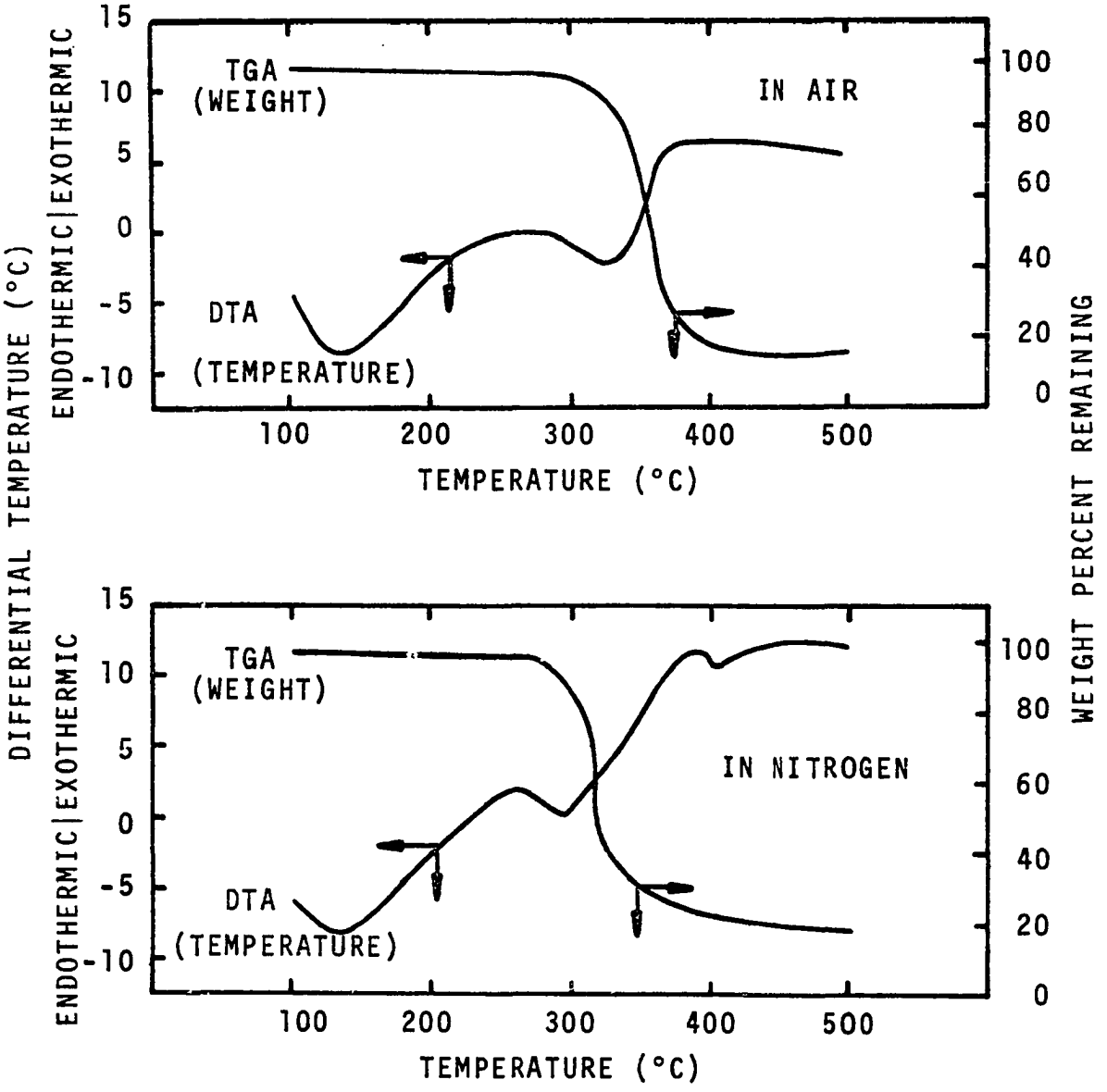

Figure II-9. DTA Results of Broida (6) for Cellulose in Nitrogen and Air.

325°C on up to 500°C. This result is obviously in conflict with the results obtained by Tang and Neill.

Akita and Kase (2) have also studied the pyrolysis of α-cellulose in flowing nitrogen and air atmospheres. Thermograms were obtained at a heating rate of 5°C/min. As shown in Figure II-10, the thermogram obtained in an inert atmosphere is endothermic over the entire temperature range, whereas that obtained in air is endothermic to about 325°C and exothermic over the remainder of the temperature range. The agreement between these results and those of Tang and Neill for inert atmospheres is surprisingly good in view of the difficulty normally encountered in reproducing DTA data between different laboratories.

A number of other investigators have obtained DTA thermograms for woods of various types and shapes. These data are qualitative and are summarized in Table II-1.

Havens (16) developed an experimental DSC procedure to measure the heat of pyrolysis for white pine and oak sawdust in a flowing nitrogen atmosphere. The experimental procedure, which is also used in this study, will be discussed in detail in a later chapter. Thermograms were obtained at a heating rate of 20°C/min and as shown in Figures II-11 and II-12 the pyrolysis was endothermic over the full temperature range studied. Assuming that the shaded area in Figure II-11 and II-12 represents the heat of pyrolysis, Havens obtained values of 47.5 and 26.2 cal/gm, endothermic, for white pine and oak

TABLE II-1

SUMMARY OF QUALITATIVE DTA DATA FOR WOOD

Investigator	Wood Types Studied	Temperature Range	Surrounding Atmosphere	Results
Arseneau (3)	Balsam filing and balsam components	50-420°C heated at 5.8°C/min	Air	Decomposition was endothermic to 270°C and exothermic above 270°C. Found balsam thermogram could be produced by superposition of component thermograms.
Domansky and Rendos (10)	Pine, beech, alder, poplar, oak; sample geometry not described.	50-420°C heated at 10°C/min	Air	Between 100°C and 170°C the decomposition exhibited a deep endotherm. Decomposition was exothermic from 215-350°C and above 350°C no heat effect was observed.
Heinrich and Kaesche-Krischer (17)	Beech, pine, and spruce cylinders 37 mm long, 25 mm diameter	100°C-420°C heated at 1°C/min	Nitrogen	Decomposition was endothermic up to 250°C. At both 270°C and 330°C the DTA curve exhibited a maximum ΔT
Sanderman and Augustin (36)	Wood as sawdust cellulose, lignin, hemicellulose	Temperature range not available	Nitrogen	Decomposition was endothermic up to 250°C. Two exothermic maxima were indicated, one at approximately 350°C, the other at 410°C.
			Air	Similar to that in nitrogen except for small exothermic peaks at 240° and 300°C.
Keyworth and Christoph (20)	Wood with and without fire retardants	Approximately 50-450°C	Air	Obtained a heat of combustion of 4500 cal/gm for untreated beech; from bomb calorimetry a value of 4000 cal/gm was obtained.
Tyulpanov (40)	Ground birchwood	Information not available	Nitrogen	The amount of individual decomposition products was independent of heating rate.

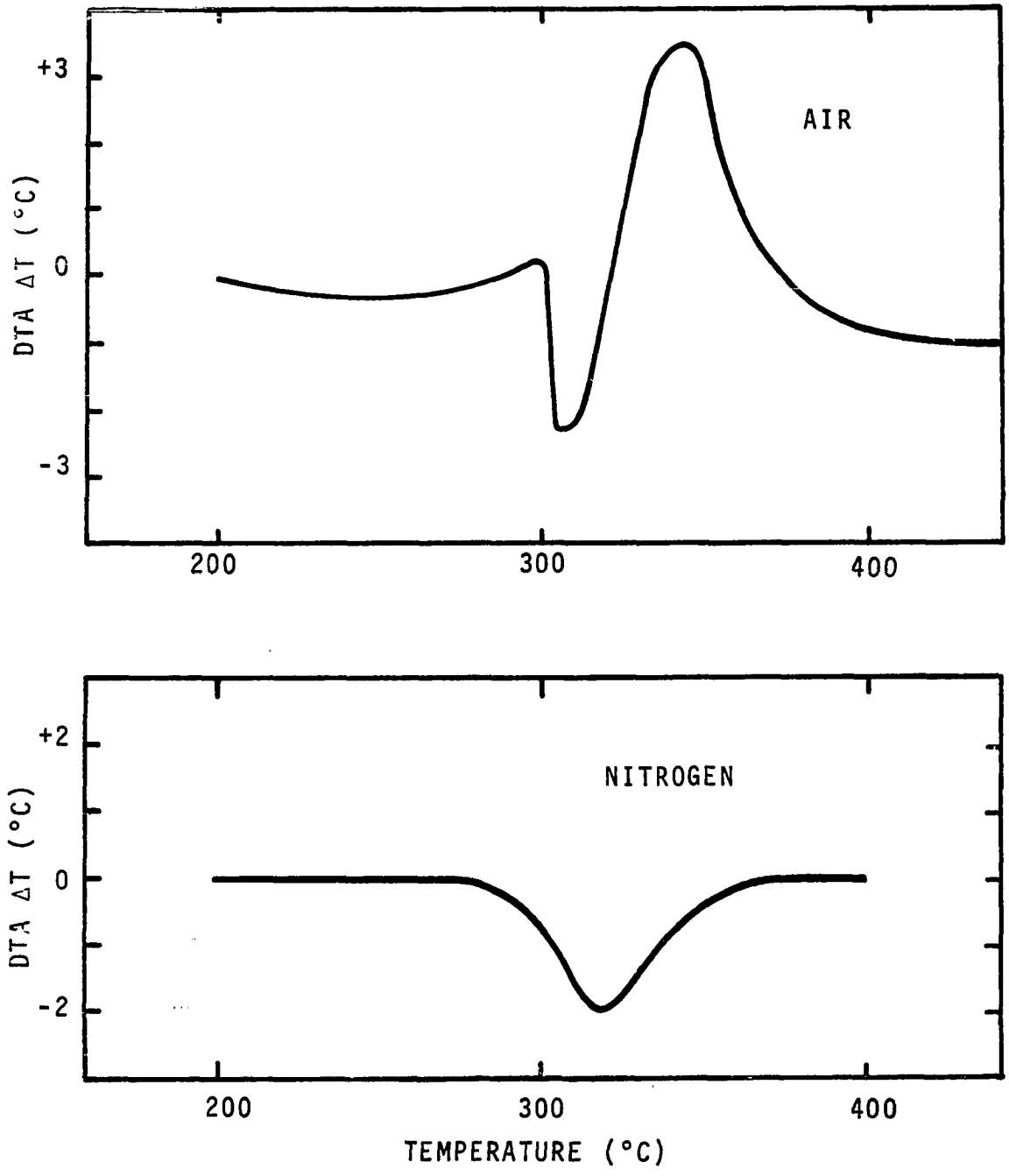

Figure II-10. DTA Results for α-Cellulose in Nitrogen and Air, Akita and Kase (2).

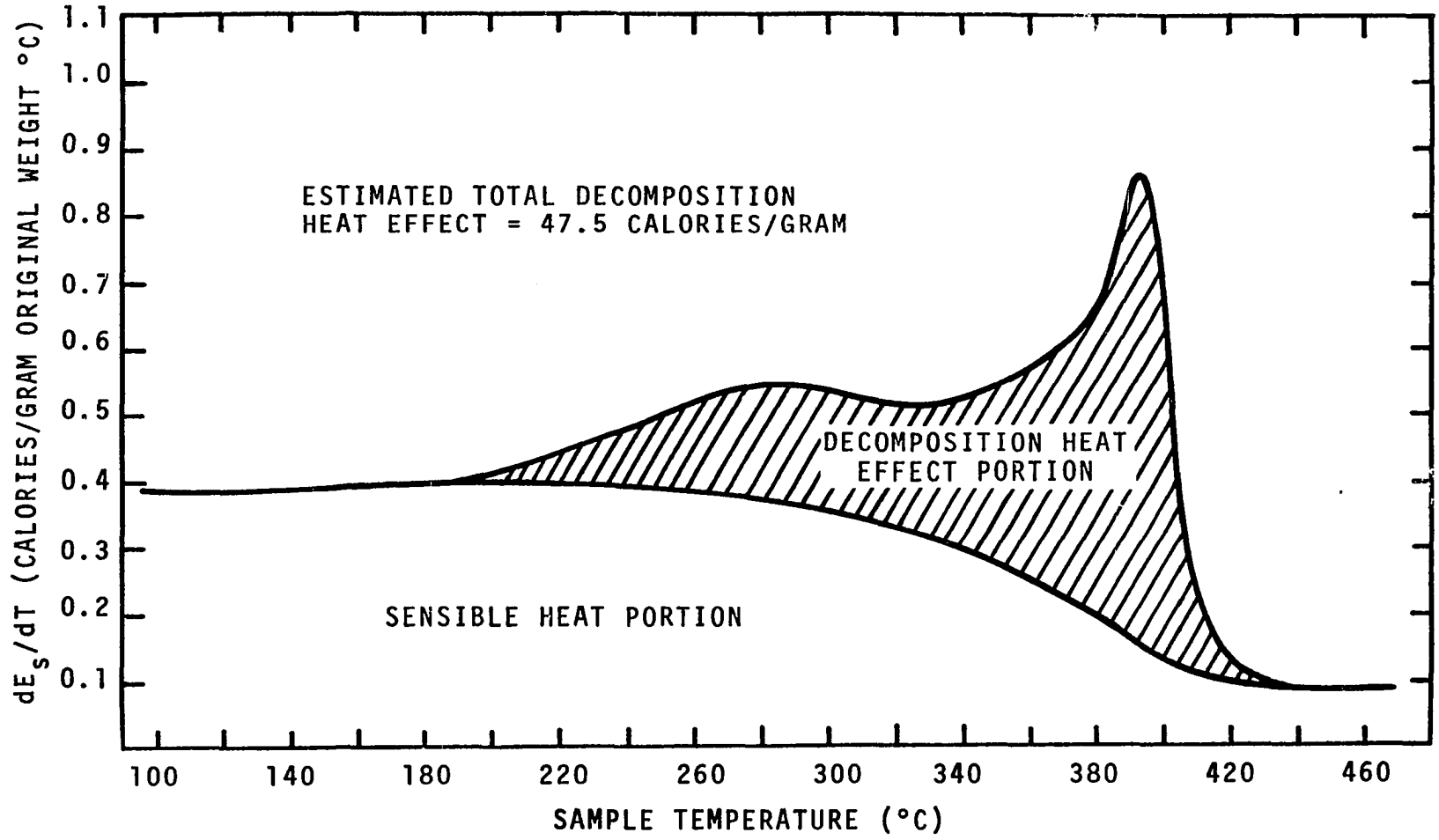

Figure II-11. Energy Capacity of Pine Wood as a Function of Temperature in Nitrogen Atmosphere from Reference (16).

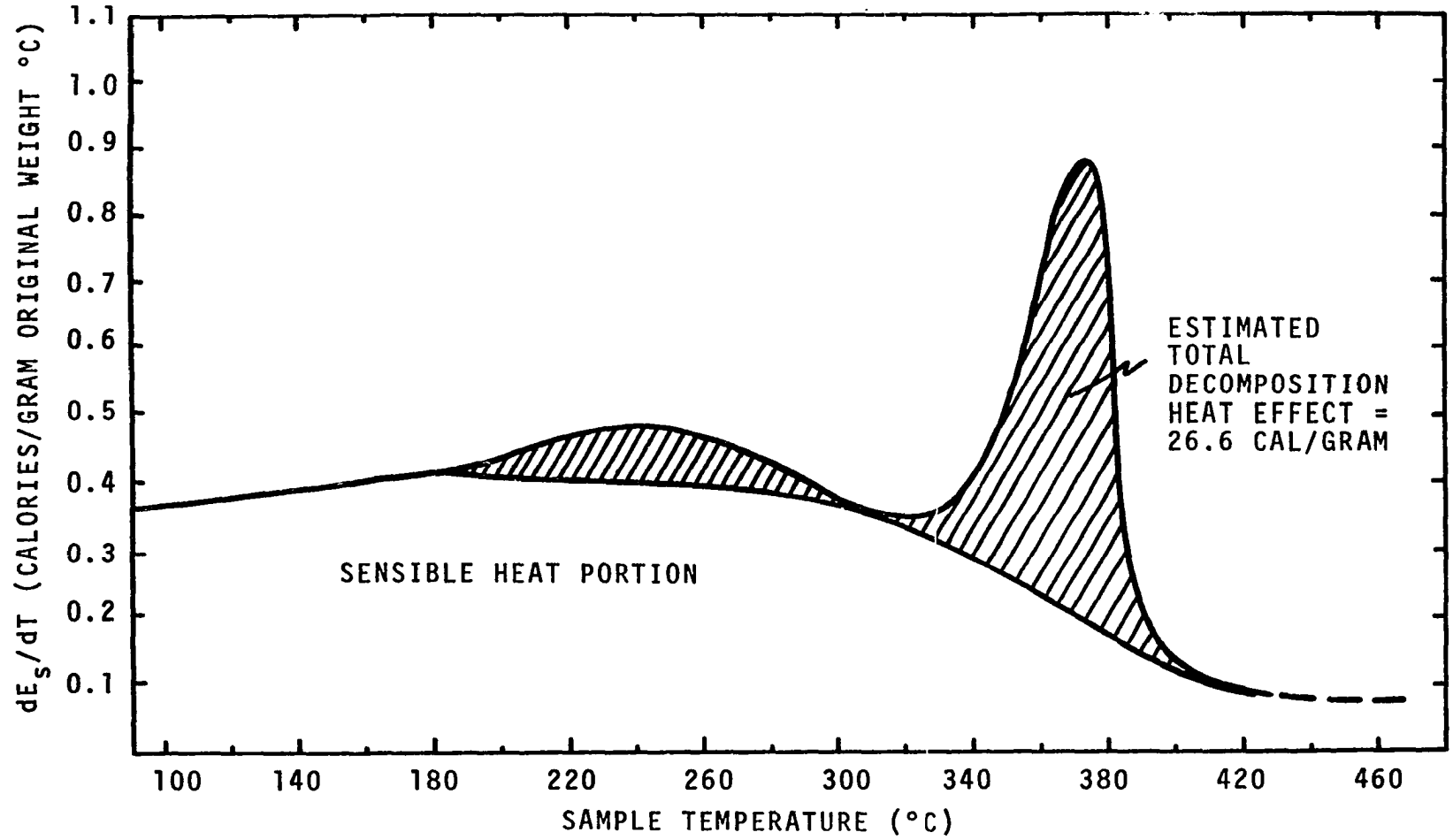

Figure II-12. Energy Capacity of Oak Wood as a Function of Temperature in Nitrogen Atmosphere (from Reference [16]).

respectively. Havens suggests the unshaded area represents sensible heat effects.

Reaction Kinetics for Wood Pyrolysis

Identification of the elementary chemical reactions which occur when wood thermally decomposes is virtually impossible due to the heterogenous composition of wood and the complex decomposition scheme which the components in wood follow. It has been suggested by Roberts (33) that the problem is further complicated by a fundamental change in the pyrolysis process as the rate of heating is increased. Fortunately, the pyrolysis model does not require a fundamental kinetic expression. It requires only an expression which accurately describes the rate of mass loss and its dependence on temperature, composition, and heating history. Two types of experiments have been used in determining the kinetic parameters of wood pyrolysis, isothermal and temperature-programmed.

Isothermal Kinetic Studies

A number of investigators have studied the kinetics of wood pyrolysis using pseudo-isothermal techniques. In this method a sample at ambient conditions is suddenly placed in a constant temperature oven and its weight measured at different time intervals. It is assumed that no significant decomposition occurs between the time the sample is placed in the furnace and the time it reaches thermal equilibrium with the

furnace. Generally, the data have been correlated using the law of mass action with an Arrhenius (temperature dependent) rate constant as given below.

$$\frac{dW}{dt} = kW^n = k_o e^{-E/RT} W^n \qquad \text{II-11}$$

where k = rate constant (sec^{-1})

W = weight of the sample

n = reaction order

k_o = frequency factor (sec^{-1})

E = activation energy cal/gm mole

R = gas constant 1.986 cal/gm mole-°K

T = temperature °K

Most investigators have assumed that the pyrolysis reactions obey first order kinetics, in which case Equation II-11 may be integrated to yield Equation II-12

$$\ln W = kt + \ln W_o \qquad \text{II-12}$$

where W_o = initial weight of specimen.

If the reaction is first order, a plot of ln W against time at each furnace temperature will yield a straight line of slope k. The Arrhenius temperature dependence may then be verified by plotting ln (k) at each furnace temperature against reciprocal temperature. The resulting straight line has a slope of -E/R and an intercept of k_o.

Stamm (37) used this method to correlate wood pyrolysis data obtained by himself and others (26, 30). Kinetic parameters for pine, fir, and spruce samples ranging in size from 1/16 x 1 x 5-7/8 inches to 1 x 1 x 6 inches were computed, as were those for Douglas Fir sawdust and its components. The samples were pyrolyzed in an oven or a molten metal bath at temperatures ranging from 93.5°C to 300°C and for times from 1 minute to 2.4 years. Sample weights were followed by removing each sample from the oven intermittantly and weighing it. A summary of Stamm's results are shown in Table II-2.

Based upon the assumption of first order kinetics Stamm obtained activation energies ranging in value from 23.0 Kcal/gm mole to 29.5 Kcal/gm mole. However, these values of activation energy include effects other than chemical kinetics. These include:

1. At higher furnace temperatures significant decomposition occurred before thermal equilibrium between the furnace and sample was obtained.
2. The pyrolysis occurred in an air atmosphere, thus the kinetic parameters for pyrolysis include the effect of exothermic oxidation at the surface of the sample.
3. Each time the sample was removed from the furnace for weighing, pyrolysis continued at transient temperature conditions until the sample cooled to some minimum temperature.

TABLE II-2

ACTIVATION ENERGIES FOR WEIGHT LOSS OF WOOD SAMPLES
BY THERMAL DEGRADATION [Stamm (37)]

Material	Heating Condition	Time Range	Temperature Range (°C)	Frequency Factor (sec^{-1})	Activation Energy (kcal/gm mole)
Southern and white pine, Sitka spruce, Douglas fir sticks, and Sitka spruce veneer*	Oven	1 hr-2.4 yr	94-250	5.1×10^{11}	29.5
	Under molten metal	1 min-6 days	167-300	2.3×10^{11}	29.8
Douglas fir sawdust	Oven	16 hr-64 days	110-220	1.9×10^{9}	25.0
α-cellulose from Douglas fir	Oven	16 hr-64 days	110-220	4.8×10^{9}	26.0
Hemicellulose from Douglas fir	Oven	2 hrs-64 days	110-220	3.6×10^{10}	26.7
Lignin from Douglas fir	Oven	16 hr-64 days	110-220	1.4×10^{10}	23.0

*The values for these different types of samples were said to be approximately the same; the value reported is an average.

Akita (1) studied the isothermal pyrolysis of wood at temperatures ranging from 150°C to 400°C in the presence of air at pressures from 2 mm Hg to 1 atm. Samples were pyrolyzed in a molten metal bath. The weight of the sample while in the bath was monitored using a spring balance technqiue. Akita proposed that the law of mass action, Equation II-11, would better represent the true pyrolysis phenomena if the right hand side was changed to a summation over the components in wood as shown in Equation II-13.

$$\frac{dN}{dt} = \sum_i k_i \, (N_{\infty i} - N_i) \qquad \text{II-13}$$

where N = total number of moles of gas evolved at time t

N_i = number of moles of gas evolved at time t by i th constituent

$N_{\infty i}$ = total number of moles of gas evolved by i th constituent

k_i = rate constant for i th constituent (sec^{-1})

Since wood consists essentially of three components, Akita wrote Equation II-13 as a summation of three terms, one each for cellulose, lignin, and hemicellulose.

The experimental data for cellulose, hemicellulose, and lignin were said to fit first order kinetic models with the rates computed on the bases of decomposible material. Akita found that an apparent change of mechanism for cellulose pyrolysis occurred at a temperature of approximately 340°C,

resulting in two distinct activation energies for cellulose (one above and one below 340°C). His experimentally determined kinetic parameters are summarized in Table II-3.

Tang (38) studied the pyrolysis kinetics of pine using a constant temperature thermogravimetric technique. Pyrolysis was studied over a temperature range from 300°C to 385°C. As shown in Table II-4, the computed kinetic parameters are dependent on sample weight and size. Tang in a later paper (39) stated that these results were strongly influenced by weight loss of up to 35 percent during the preheating period.

Dynamic Temperature Kinetic Studies

The study of wood pyrolysis kinetics using a dynamic temperature technique has several advantages over the isothermal method.

1. Kinetic data (weight versus time) over a broad temperature range can be obtained in only a few minutes.
2. The problem of decomposition before reaching the desired test temperature is not encountered in the dynamic method since the test may be initiated well below the incipient decomposition temperature.
3. Different heating rates may be studied.

Along with these advantages there are two problem areas. First, depending on the sample size and thermal properties, conduction heat transfer effects may alter the rate of weight loss such that the weight loss reflects heat transfer effects rather

TABLE II-3

ACTIVATION ENERGY OF DECOMPOSITION OF WOOD AND ITS MAJOR COMPONENTS [Akita (1)]

Material	Temperature Range (°C)	Activation Energy (kcal/gm mole)
Lignin	270-400	26.0
Hemicellulose	270-400	17.0
Cellulose	270-340	36.0
Cellulose	340-370	24.0
Wood (Japanese Cypress)*	270-340	26.0 (average)
	340-370	23.0 (average)

*Wood specimens were 25 x 15 x 1.2 mm.

TABLE II-4

ACTIVATION ENERGIES FOR UNTREATED PONDEROSA PINE SAMPLES [Tang (38)]

Geometry of Specimen	Thickness of Specimen (cm)	Activation Energy (kcal/gm mole) Below 330°C	Above 330°C
Veneers	0.013	45.6	45.6
	0.028	44.9	44.9
	0.318	37.8	37.8
Dowels	0.635	44.1	44.1
	0.952	41.1	28.5
	1.270	40.7	28.7

than decomposition chemistry. Second, the techniques used to date for obtaining kinetic parameters from dynamic weight loss requires that one, and frequently two, of the Arrhenius parameters be assumed.

Two types of experiments have been used to determine the kinetics of wood pyrolysis in a dynamic temperature environment.

Roberts and Clough (34) studied the pyrolysis of 2 cm x 15 cm beech cylinders, heated at 10°C/min in a purged muffle furnace. The weight of each specimen was continuously measured and the temperature monitored by five thermocouples located at various radial positions parallel to the longitudinal axis. The experimental data from five runs are summarized in Table II-5.

TABLE II-5

SUMMARY OF ROBERT'S AND CLOUGH'S DATA FOR THERMAL DECOMPOSITION OF WOOD (34)

	Experiment Number				
	1	2	3	4	5
Maximum temperature achieved by specimen (°C)	445.0	353.0	505.0	394.0	282.0
$\frac{\text{Final Weight}}{\text{Initial Weight}} \times 100$ (%)	30.9	52.5	28.0	39.9	78.6
Maximum rate of weight loss (mg/sec)	92.0	26.0	193.0	40.0	8.0
Surface area of specimen (cm^2)	97.0	88.0	88.0	88.0	85.0

The data were fitted to the first order kinetic expression given below.

$$-\frac{dW}{dt} = (W - W') \exp(-E/RT) \qquad \text{II-14}$$

W = weight of specimen at time t (gm)

W' = final weight of specimen (gm)

The activation energy obtained for the first four runs was found to be 15 Kcal/gm mole with a frequency factor of 9.1×10^4 min^{-1}. The activation energy and frequency factor for Test #5 were 25 Kcal/gmole and 2.6×10^8 min^{-1} respectively. Roberts and Clough suggested that this difference was due to different decomposition mechanisms above and below 500°C.

Blackshear and Kanury (5) have studied the pyrolysis of cellulose cylinders in both nitrogen and air atmospheres. A schematic diagram of the experimental apparatus used by these investigators is shown in Figure II-13. The copper tube shown in Figure II-13 was rotated at a velocity such that Couette flow was maintained in the space between the tube and the cellulose specimen. Radial x-ray photographs were taken during decomposition, and the transient density profile at any radial position was computed from these photographs using a densiometer calibrated against the absorption of x-rays by a graphite wedge. Temperatures inside the specimen were measured using Chromel-Alumel thermocouples. Temperature-density profiles for various radial positions are shown in Figure II-14.

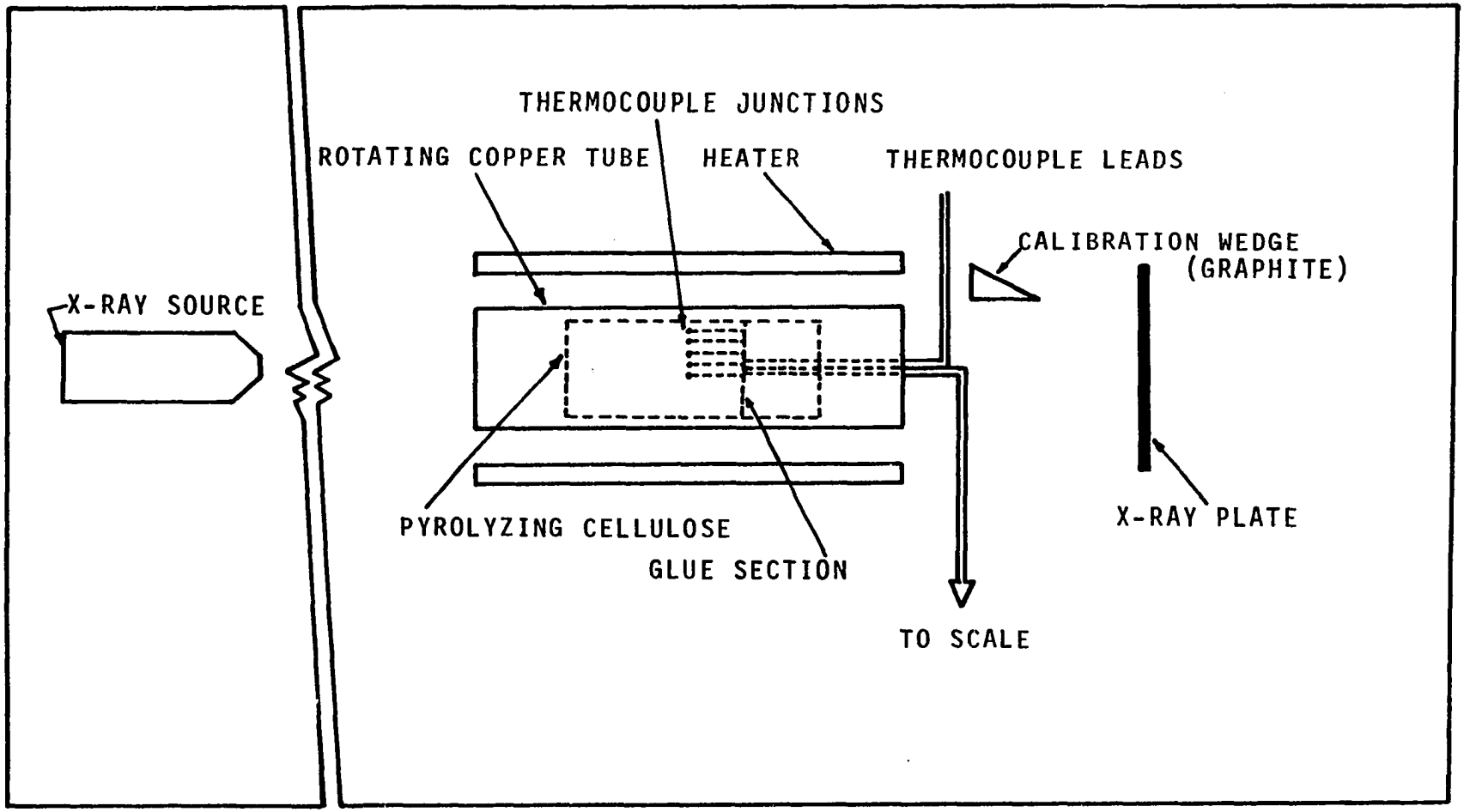

Figure II-13. Experimental Pyrolysis Apparatus Used by Blackshear and Kanury (5).

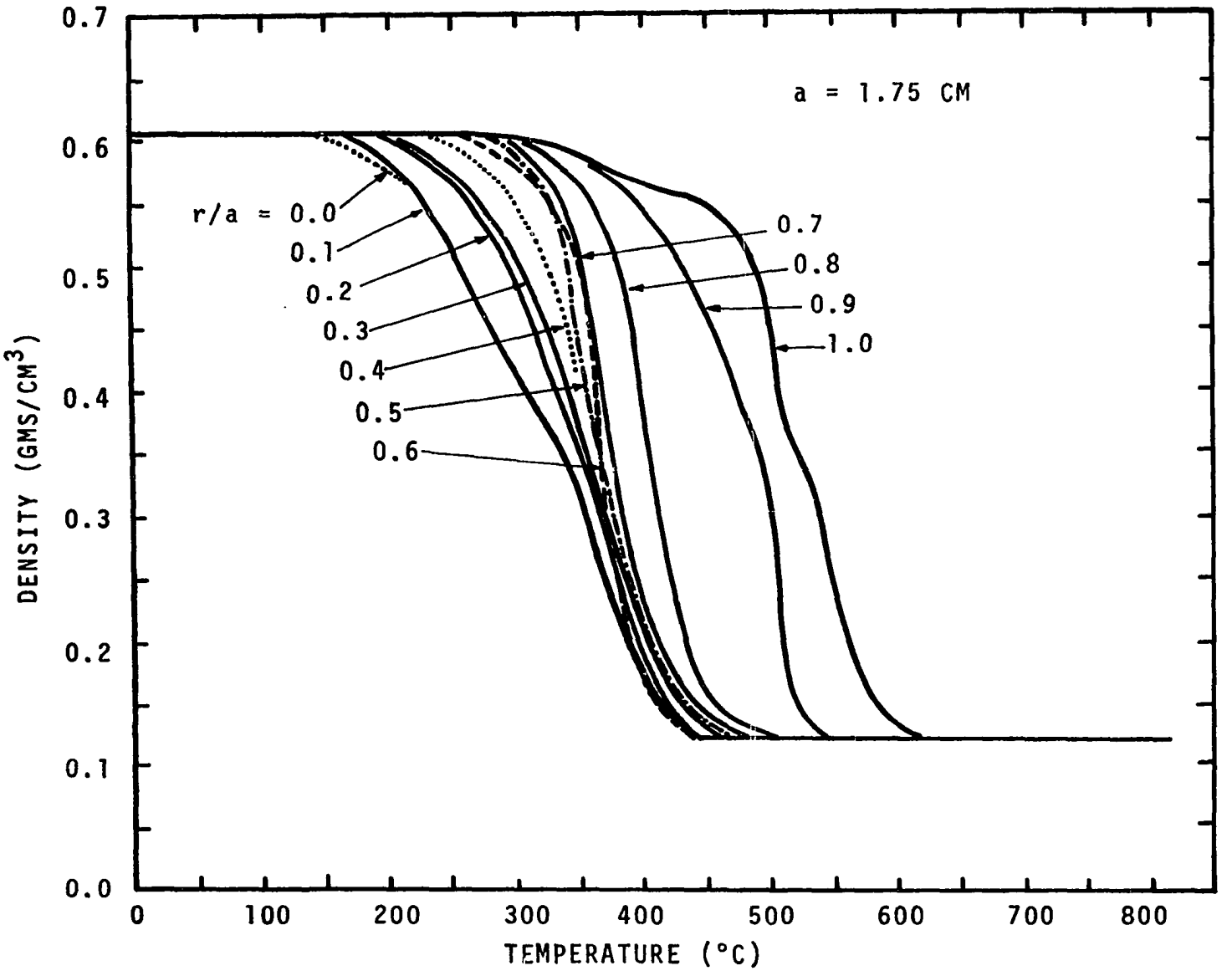

Figure II-14. Density and its Dependence on Temperature for Decomposing α-Cellulose Cylinder with Radial Position as Parameter (5).

These investigators correlated their data assuming first order kinetics and a frequency factor of 10^6/min. The resulting activation energy was found to be 19,000 cal/gmole. D. J. Brown (7) has recently shown that the wavelength range of the x-ray unit used by Blackshear and Murty Kanury was such that errors in weight loss measurement of up to 25 percent could occur.

The kinetic parameters obtained by Roberts and Clough and Blackshear and Kanury are strongly influenced by changes in wood properties with pyrolysis. Simply, the kinetic parameters include heat transfer effects and thus are dependent on test sample size and shape. Such kinetic parameters would be of little value in developing a mathematical analog generalized for wood geometry.

A number of companies manufacture thermogravimetric balances, TG, in which a small sample, 1-100 mg, can be heated at selected rates of temperature increase with continuous weight measurements. The sample size can be kept small enough in theory such that heat transfer effects may be neglected. Goldfarb et al. (13) have reviewed eleven different procedures for obtaining kinetic parameters from TG data. Additionally, Akita and Kase (2), Burningham and Seader (8), and Goldfarb, et al. (13), have recently proposed new methods.

Tang (39) has used the procedure of Freeman and Carrol (12) to extract kinetic parameters for wood pyrolysis from TG data. The technique is developed by first solving for the

rate constant in both equalities of Equation II-11 and setting the two expressions equal to one another as given in Equation II-15.

$$k_o\, e^{-E/RT} = -\frac{1}{W^n}\frac{dW}{dt} \qquad \text{II-15}$$

Taking the logarithms of both sides of Equation II-15 yields Equation II-16, which when differentiated with respect to temperature, results in Equation II-17.

$$\ln k_o - E/RT = \ln\,(-dW/dt) - n \ln W \qquad \text{II-16}$$

$$\frac{Edt}{RT^2} = \frac{d \ln\,(-dW/dt)}{dT} - n\,\frac{d \ln W}{dT} \qquad \text{II-17}$$

Integrating Equation II-17 over a finite temperature range ΔT and dividing through by $\Delta(\ln W)$ yields Equation II-18.

$$\frac{-E/R\ \Delta(T^{-1})}{\Delta\ (\ln W)} = \frac{\Delta \ln\,(-dW/dt)}{\Delta\ (\ln W)} - n \qquad \text{II-18}$$

A plot of $[\Delta\ (T^{-1})]/[\Delta \log W]$ versus $\Delta[\log\,(-dW/dt)]/\Delta[\log W]$ should yield a straight line of slope E/2.303R and intercept n.

Tang obtained TG data for Ponderosa Pine samples 0.14 mm thick and 100 mg initial weight. Samples were heated at 10°C/min in vacuum. Tang's data substantiated the assumption of first order kinetics; however, the above mentioned difference plot reflected a large scatter of data during the initial stages of pyrolysis. Also, the best fit line through these

data for initial pyrolysis did not have the same slope as that at higher conversions. Tang attributed this scatter to two factors: (1) The initial pyrolysis, that at low temperatures, proceeds via a different mechanism than that at higher temperatures. (2) Experimental errors in weight loss data occurred during the low temperature stage due to the very small weight loss.

Tang noted that the low temperature data would fit a pseudo zero order kinetic expression. He alleviated much of the inherent error associated with difference techniques by making pseudo-first order plots directly from the experimental values of rate dW/dt, and Equation II-19.

$$\frac{dW}{dt} = k_o \exp\ (-E/RT)\ W \qquad \text{II-19}$$

One such plot is shown in Figure II-15. The activation energies and frequency factors for the woods studied are shown in Table II-6. It is interesting to note that the activation energies for cellulose and wood are lower in the low temperature range than in the high ranges, which are in direct contrast to the static results of Tang (38) and Akita (1).

Heinrich and Kaesche-Krisher (17) used dynamic thermogravimetry to study the weight loss kinetics of beech sawdust subjected to linearly increasing heating rates of 1, 2, 3, 4, and 12°C per minute in vacuum. As shown in Figure II-16, essentially no weight loss occurred up to 200°C, but weight loss

TABLE II-6

KINETIC PARAMETERS OF PYROLYSIS FROM DYNAMIC THERMOGRAVIMETRY [Tang (38)]

Material	First Stage			Second Stage		
	T(°C)	k_{01} (min^{-1})	E_2 (Kcal/gm mole)	T(°C)	k_{02} (min^{-1})	E_2 (Kcal/gm mole)
Pine wood	280-325	1.98×10^{7}	23	325-350	3.92×10^{18}	54
α-cellulose	240-308	3.85×10^{11}	35	308-360	2.37×10^{19}	54
Lignin	280-344	9.86×10^{5}	21	344-435	5.6×10^{10}	9

*For 100 mg samples in vacuum (0.3 mm Hg absolute).

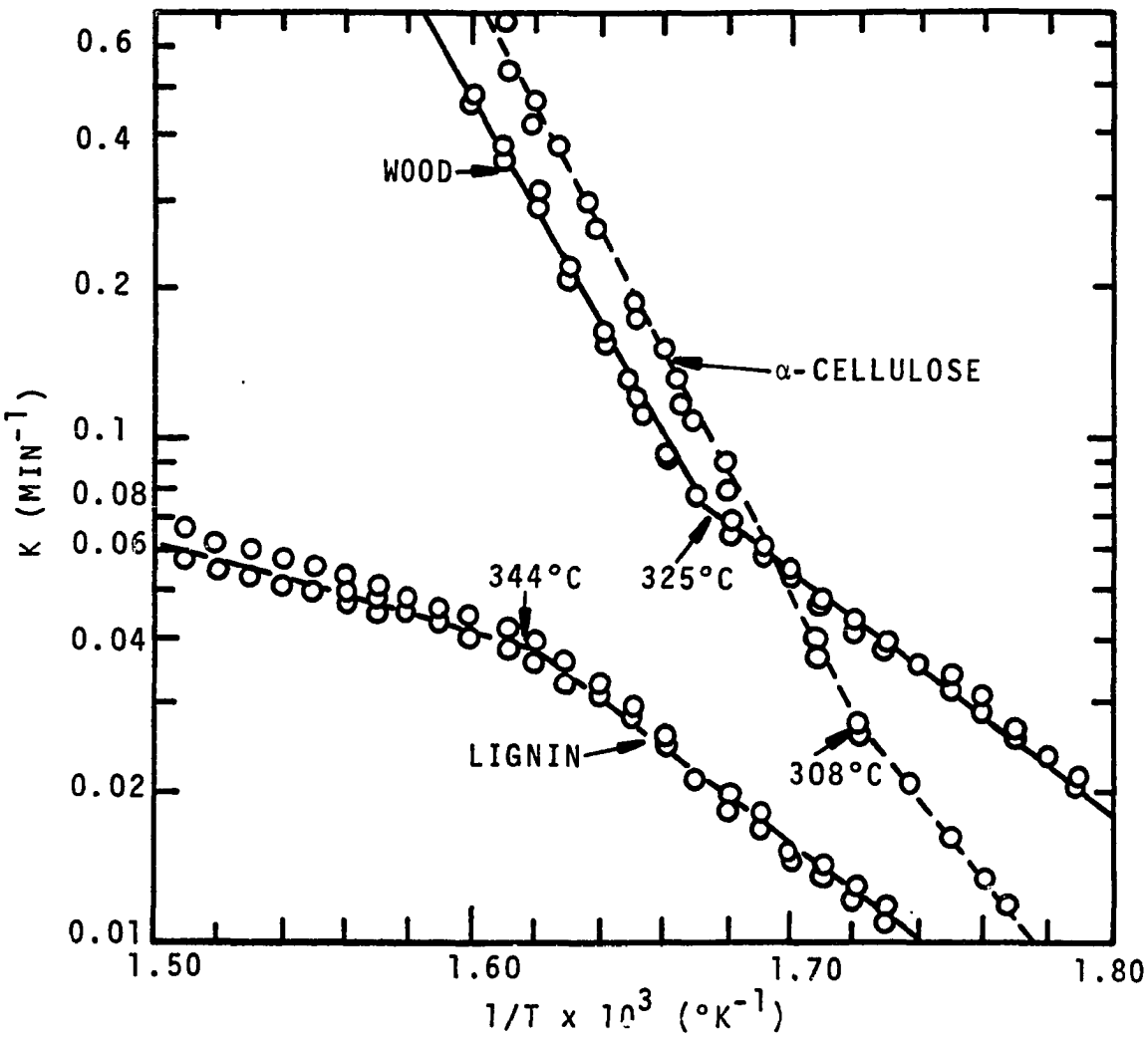

Figure II-15. Kinetics of Weight Loss Plots for Wood, α-Cellulose, and Lignin (38).

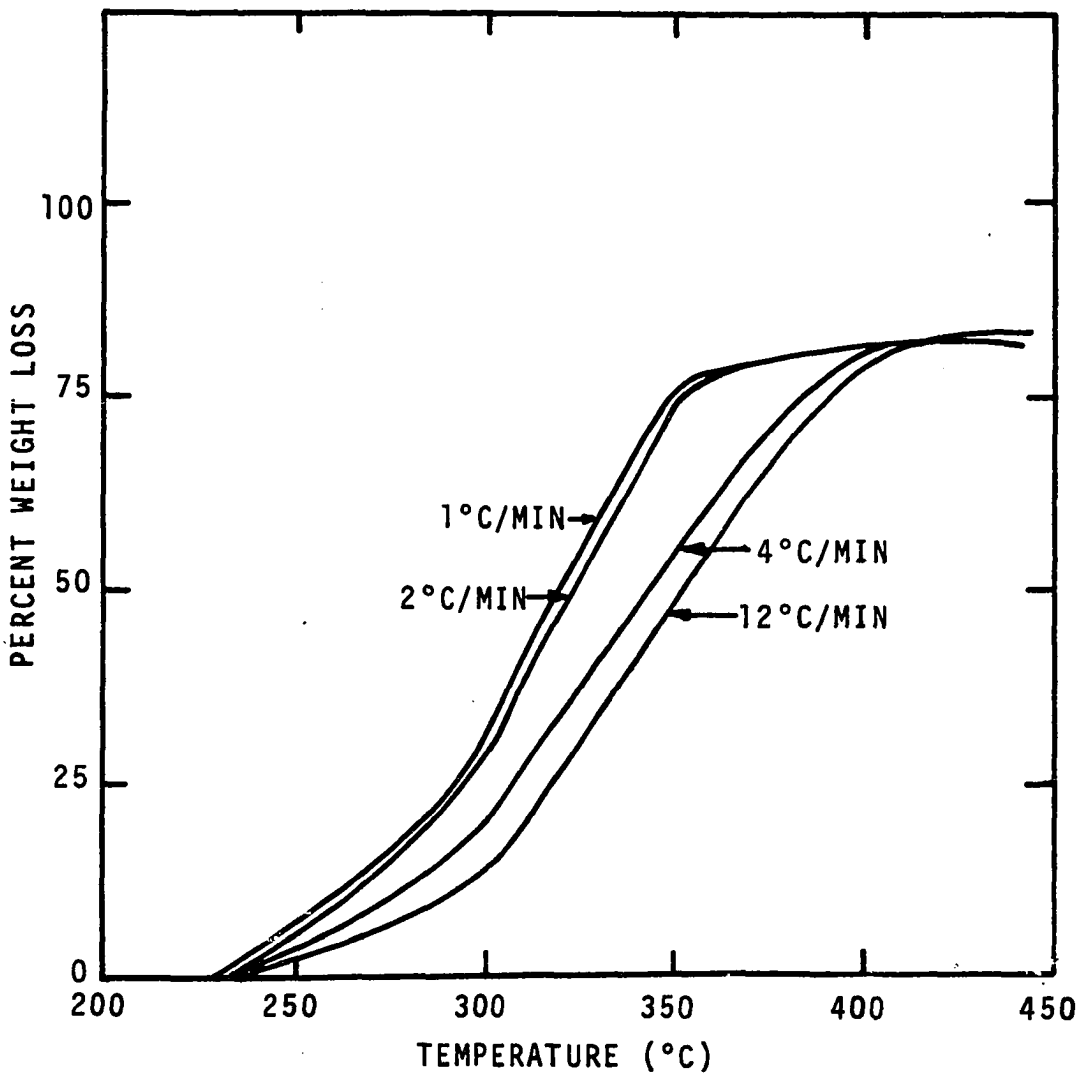

Figure II-16. Weight Loss and its Dependence on Temperature for Beech Sawdust in Vacuum at Different Heating Rates from the Studies of Heinrich and Kaesche-Krisher (7).

became rapid above about 250°C and continued to 400°C with a final weight loss at all heating rates of 83 percent of the initial material. At higher heating rates the weight loss curve shifted to higher temperatures. This shift can be explained by a number of factors:

1. As shown by Kanury (19), the Arrhenius type temperature dependent rate constant must be modified as shown in Equation II-20.

$$k = k_o \exp(-E/R\phi t) \qquad \text{II-20}$$

where ϕ = heating rate (°C/min)

t = time (min)

(Other terms as previously defined)

As ϕ is increased the weight curve will shift to the right.

2. Depending on the size of the sample, the furnace type, the heating rate, and the furnace calibration technique, the true sample temperatures may lag far behind the recorded temperature. This lag is predominant at high heating rates as discussed by Goldfarb, et al. (13).
3. The chemistry of pyrolysis may change as the sample is heated at a higher rate, resulting in a shift of the weight loss curve.

Heinrich and Kaesche-Krisher felt that their data indicated a change in the chemistry of decomposition as heating rate was increased; they, therefore, concluded that the

rate of weight loss could not be treated as a pseudo-first order process.

Havens (16) studied the pyrolysis of white pine and oak sawdust at TG heating rates of 20, 40, 80 and 160°C per minute in an inert atmosphere. Because the furnace used had a very small inertial heat effect and combined with the small sample size (less than 5 mg of sawdust) Havens concluded that the lag between the true sample temperature and recorded temperature was minimal. Havens' data, as shown in Figures II-17 and II-18, are typical for multiple heating rates. Havens did not extract kinetic parameters from his data, but he did note that the slight shift in weight loss to higher temperatures with increased heating rate would not greatly affect the model that he proposed. (It should be noted that the heating rates used by Havens are sufficient to cause wood to ignite in an air atmosphere.)

Akita and Kase (2) studied the pyrolysis of α-cellulose at TG heating rates ranging from 0.23°C/min to 2.4°C/min. Tests were run in air, nitrogen, and under vacuum. These investigators assumed that the sample temperature increased with the linear relationship

$$T = T_o + \phi t$$

where T = temperature (°K)

T_o = initial temperature (°K)

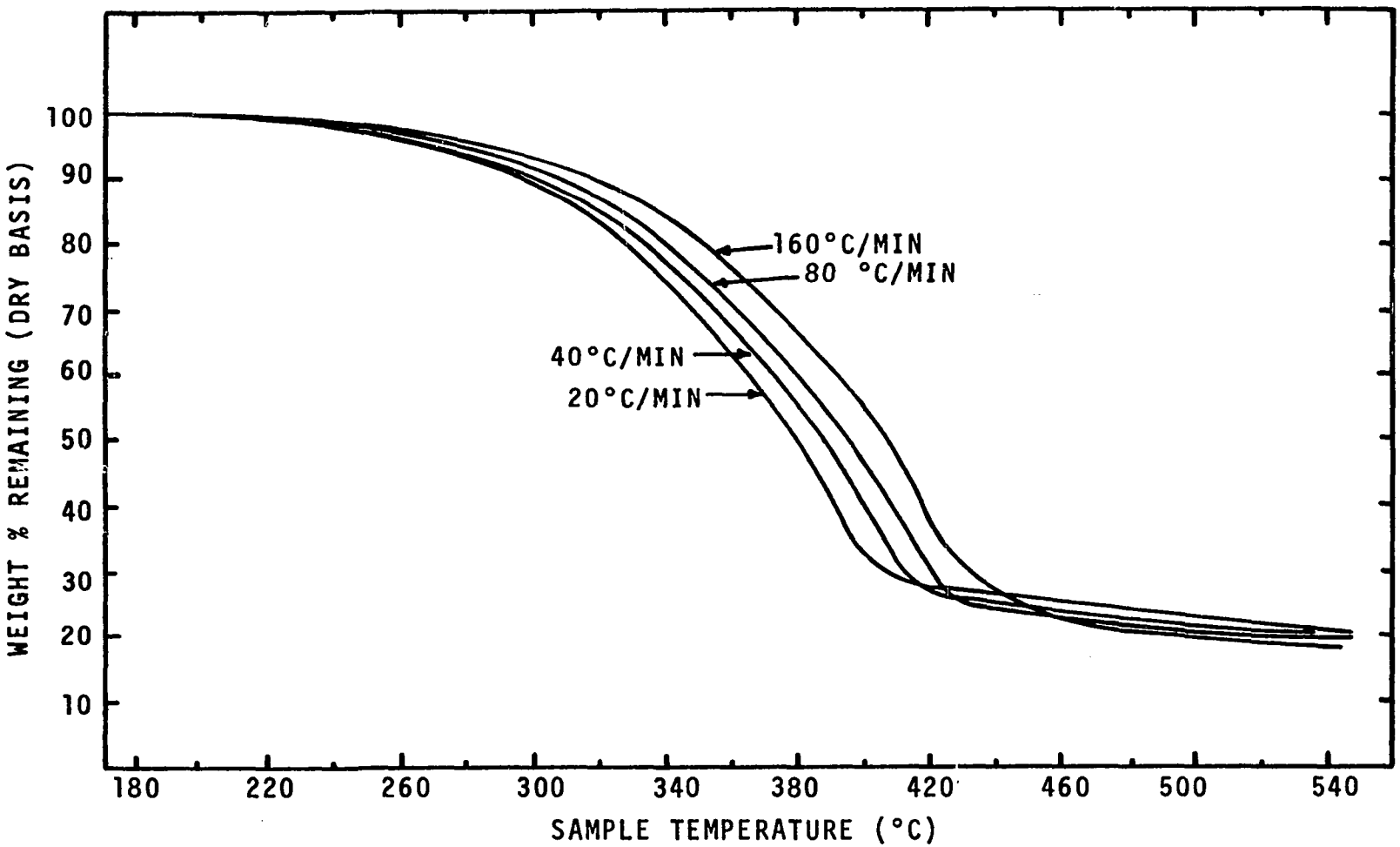

Figure II-17. Effect of Rate of Heating on Kinetics of Weight Loss of Dry Pine Wood in Nitrogen Atmosphere, Havens (16).

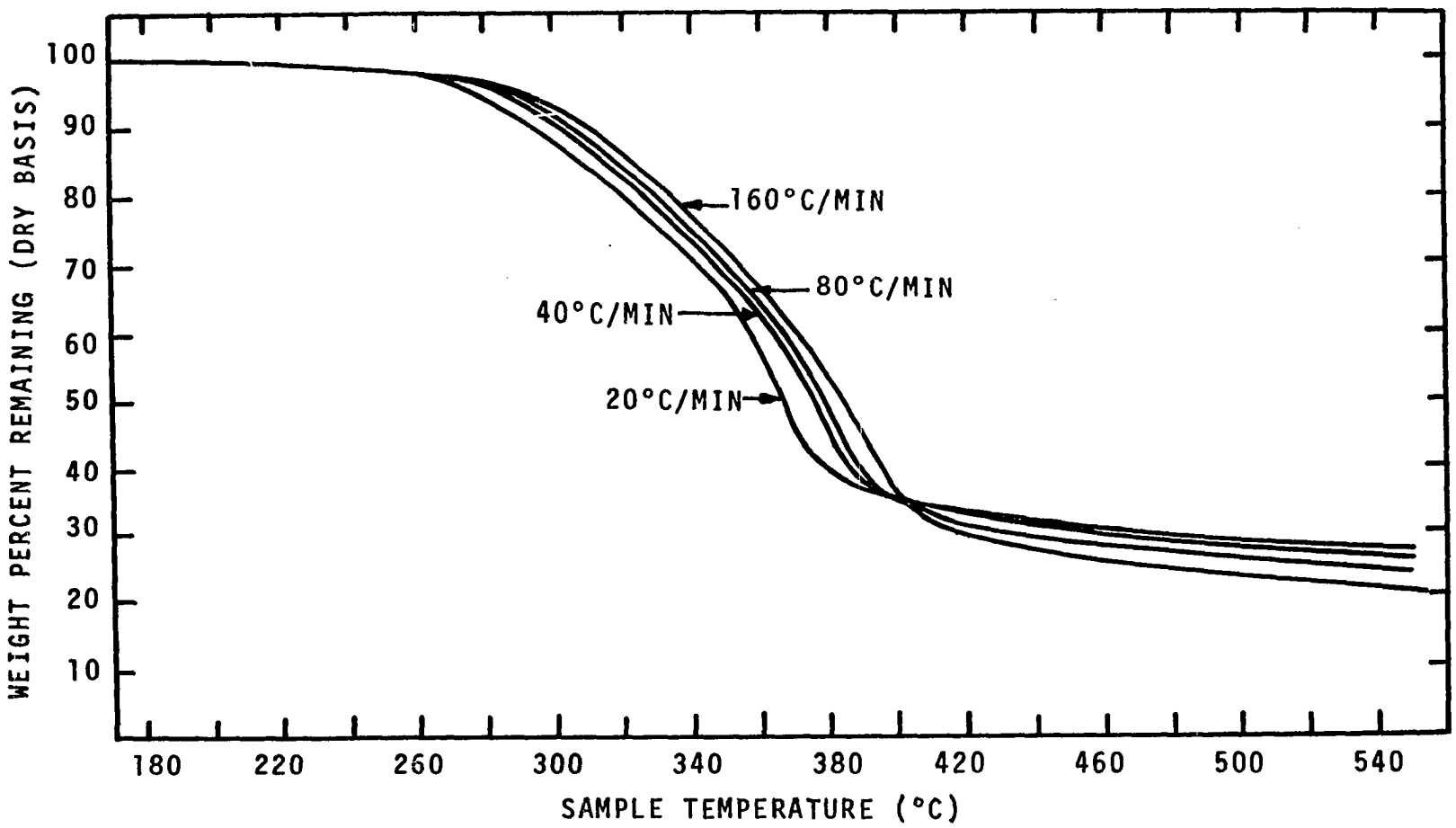

Figure II-18. Effect of Rate of Heating on Kinetics of Weight Loss of Dry Oak Wood in Nitrogen Atmosphere, from the Study of Havens (16).

ϕ = rate of heating (°C/min)

t = time (min)

This temperature relationship was substituted into Equation II-11, which yielded

$$\frac{dW}{dt} = k_o \exp \{\frac{-E}{R(T_o+\phi t)}\}(W_o - W)^n \qquad \text{II-21}$$

The maximum rate of weight loss was obtained from Equation II-21 by setting $(d/dt)(dW/dt) = 0$ and was found to be

$$(\frac{dW}{dt})_m = (\frac{W_o-W_m}{n})(\frac{E\phi}{RT_m^2}) \qquad \text{II-22}$$

where m = maximum rate of weight loss

Equating II-22 and II-11 at the maximum rate of weight loss,

$$\ln (\frac{\phi}{T_m^2}) = \ln [\frac{nR}{Ek_o(W_o-W)^{n-1}}] - \frac{E}{RT_m} \qquad \text{II-23}$$

Akita and Kase then plotted $\ln (\phi/T_m^2)$ versus $1/T_m$ to obtain the activation energy at the maximum rate of weight loss. They also obtained the order of reaction and frequency factor by integration of Equation II-21,

$$\int_0^{W_m} \frac{dW}{(W_o-W)^n} = \frac{k_o}{\phi} \int_0^{T_m} \exp (\frac{-E}{RT}) \, dT \qquad \text{II-24}$$

Assuming that k_o and n did not change with weight loss the right hand side of II-24 was integrated by partials resulting in

$$\ln\left(1 - \frac{W_m}{W_o}\right) = \frac{1}{n-1} \ln\left\{1 - \frac{n-1}{n}\left[1-2\left(\frac{RT_m}{E}\right) + 6\left(\frac{RT_m}{E}\right)^2 - \ldots\right]\right\}, \quad n \neq 1 \qquad \text{II-25}$$

$$\ln\left(1 - \frac{W_m}{W_o}\right) = -\left[1-2\left(\frac{RT_m}{E}\right) + 6\left(\frac{RT_m}{E}\right)^2 - \ldots\right], \quad n=1 \qquad \text{II-26}$$

For the condition $RT_m/E << 1$, Equations II-25 and II-26 reduced to

$$\left[1 - \frac{W_m}{W_o}\right]^{1-n} \simeq n, \quad n \neq 1$$
$$\left[1 - \frac{W_m}{W_o}\right] \simeq e^{-1}, \quad n = 1 \qquad \text{II-27}$$

The frequency factor was computed directly from Equation II-11. At the maximum rate of heat loss an average activation energy of 53.51 Kcal/gmole, an order of 1.054 and a frequency factor of $10^{18.8}$ were computed. As is evident from Table II-7, the pyrolysis kinetics at the maximum rate of weight loss is independent of heating rate at temperature heating rate up to 2.4°C/min.

Thermal and Physical Properties of Wood

Prediction of the transient temperature distribution in a wood specimen requires knowledge of the density, heat capacity, and thermal conductivity of the wood as a function of temperature and decomposition history. The density variations in wood as a function of temperature can be deduced from the thermogravimetric and x-ray studies discussed

TABLE II-7

KINETIC PARAMETERS FOR PYROLYSIS OF α-CELLULOSE [Akita and Kase (2)]

No.	ϕ °C/min	W_m/W_o x 10^{-2}	T_m °K	t_m x 10^{-2} min	n	E Kcal/mole	log k_o min^{-1}
1	2.40	38.5	598	6.92	0.97	43.4	18.8
2	2.20	39.4	603	6.51	1.02	54.3	18.9
3	0.95	40.1	587	3.03	1.05	54.2	19.1
4	0.94	39.4	588	2.84	1.02	53.2	18.7
5	0.50	40.9	579	1.64	1.10	52.5	18.4
6	0.47	40.0	578	1.58	1.05	55.2	19.5
7	0.24	39.4	568	0.83	1.02	53.0	18.7
8	0.23	42.4	570	0.78	1.20	52.2	18.3
				Average	1.054	53.51	18.80
				Standard deviation	0.065	0.94	0.36

in the previous section. Very little information is available with regard to the specific heat of partially pyrolyzed wood or char except for that obtained using DSC techniques. Thermal conductivity data are even more limited than that of specific heat. Only two experimental measurements on wood above 100°C were found in the literature; no data on thermal conductivity for partially pyrolyzed wood or char were located.

The properties of wood not only vary due to pyrolysis, but as previously mentioned, wood is a non-homogenous, non-isotropic material. Common examples of the non-isotropic character of wood are grain pattern, growth rings, knots, checks, and compressions. Less well known non-uniformities are those attributable to heart wood, the relatively inactive center of the tree, and sapwood, the outer portion of the tree trunk which carries the sap from roots to leaves. Additional non-uniformities are due to wood rays which connect the various layers from the central core to the bark for storage and transfer of nutrients. This review will be limited to the variation in properties due to directional growth patterns, growth rings, wood rays and the distribution of sapwood and heart wood.

Specific Heat

The specific heat of wet and dry virgin woods has been measured by several investigators. Dunlap (11) measured the specific heat of small cylinders (about 6 grams) of oven-dry

wood in the temperature range 0°C to 106°C using a modified Bunsen's ice calorimeter. It was reported that the specific heat of 20 species ranging in density from 0.23 to 1.10 gm/cm^3 could be described by Equation II-28.

$$C = 0.266 + 0.00116\ T \qquad \text{II-28}$$

where C = specific heat (cal/gm°C)

T = temperature (°C)

Dunlap reported that there was no significant difference between the specific heat of heart wood and sapwood of the same species, that geographic origin did not appear to influence the specific heat, and that there appeared to be no significant difference among the different wood species studied.

Kollman (22) studied the effect of free moisture on the specific heat of wood. He proposed an expression for the specific heat of wet wood as given in Equation II-29.

$$C_x = (x)C_w + (1-x)C \qquad \text{II-29}$$

C_x = mean specific heat of moist wood (cal/gm°C)

x = moisture content as a fraction of net weight

C_w = specific heat of water (cal/gm°C)

C = specific heat of oven-dry wood (cal/gm°C)

The specific heat and mean specific heat for charcoal have been presented by Widell as shown in Figure II-19.

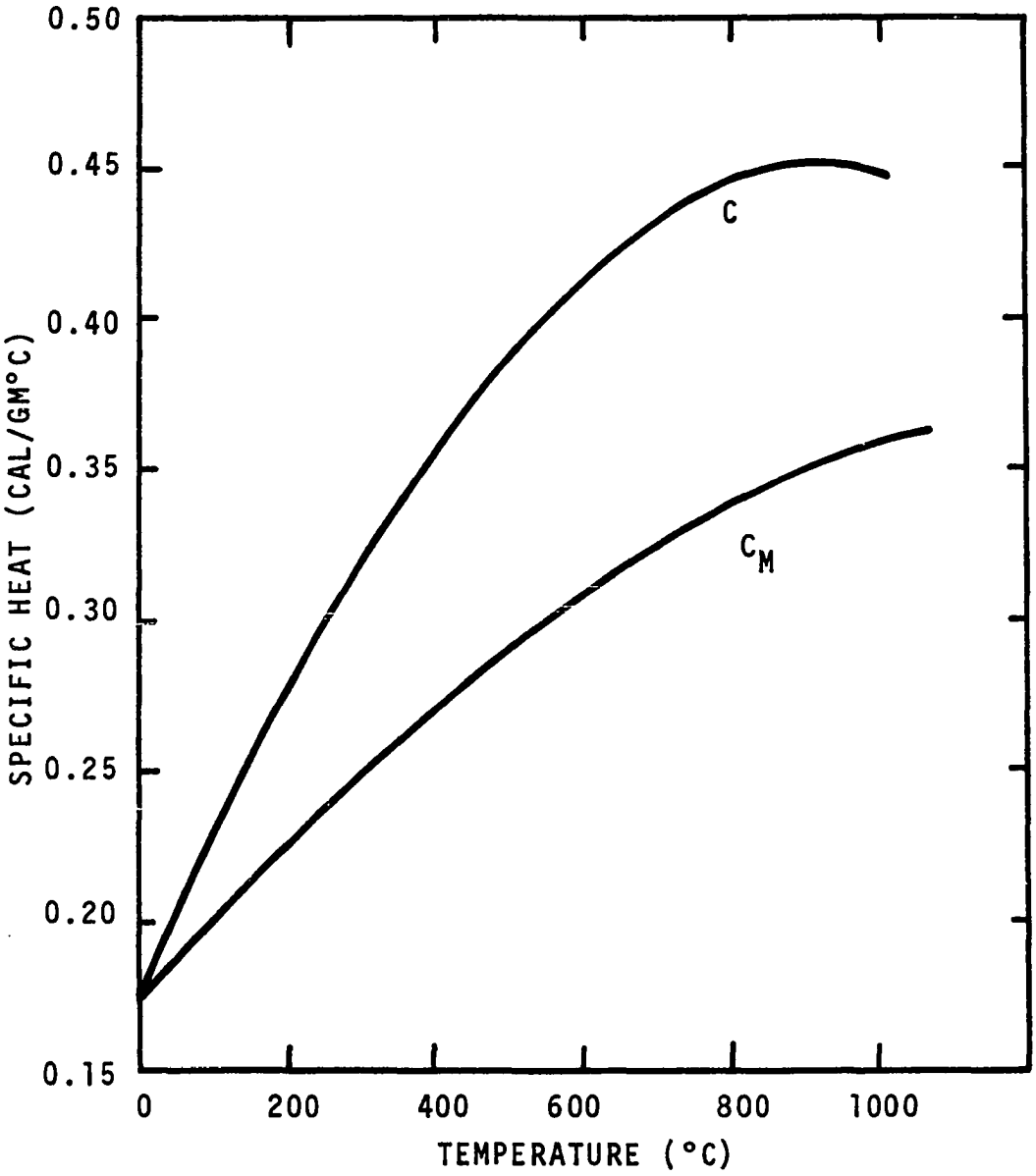

Figure II-19. Specific Heat C and Mean Specific Heat C_M for Charcoal as a Function of Temperature (46).

When discussing the applications of DSC to determining the heat of pyrolysis it was noted that the thermogram includes both the heat of pyrolysis and sensible heat effects. It is evident from the DSC thermogram in Figures II-11 and II-12 that above and below the temperature range in which decomposition occurs, the thermograms represent the specific heat of char and virgin wood respectively. In the decomposition range, Havens suggested that the sensible heat of partially pyrolyzed wood is included in the unshaded areas of Figures II-11 and II-12. The specific heat data of Havens' for partially pyrolyzed wood are the only such data available in the literature.

Density

The local density variation in a wood specimen during pyrolysis can be obtained from thermogravimetric data if the specimen is assumed to retain its original size and exterior boundaries. The x-ray work of Blackshear and Kanury (5) indicates this assumption is true so long as the wood maintains its mechanical strength.

The applicability of thermogravimetric data is also supported by the density-temperature profile obtained by Blackshear and Kanury. The similarity of the density temperature profiles for α- cellulose cylinders reported by them and the weight loss temperature profile obtained by Havens are shown in Figure II-20.

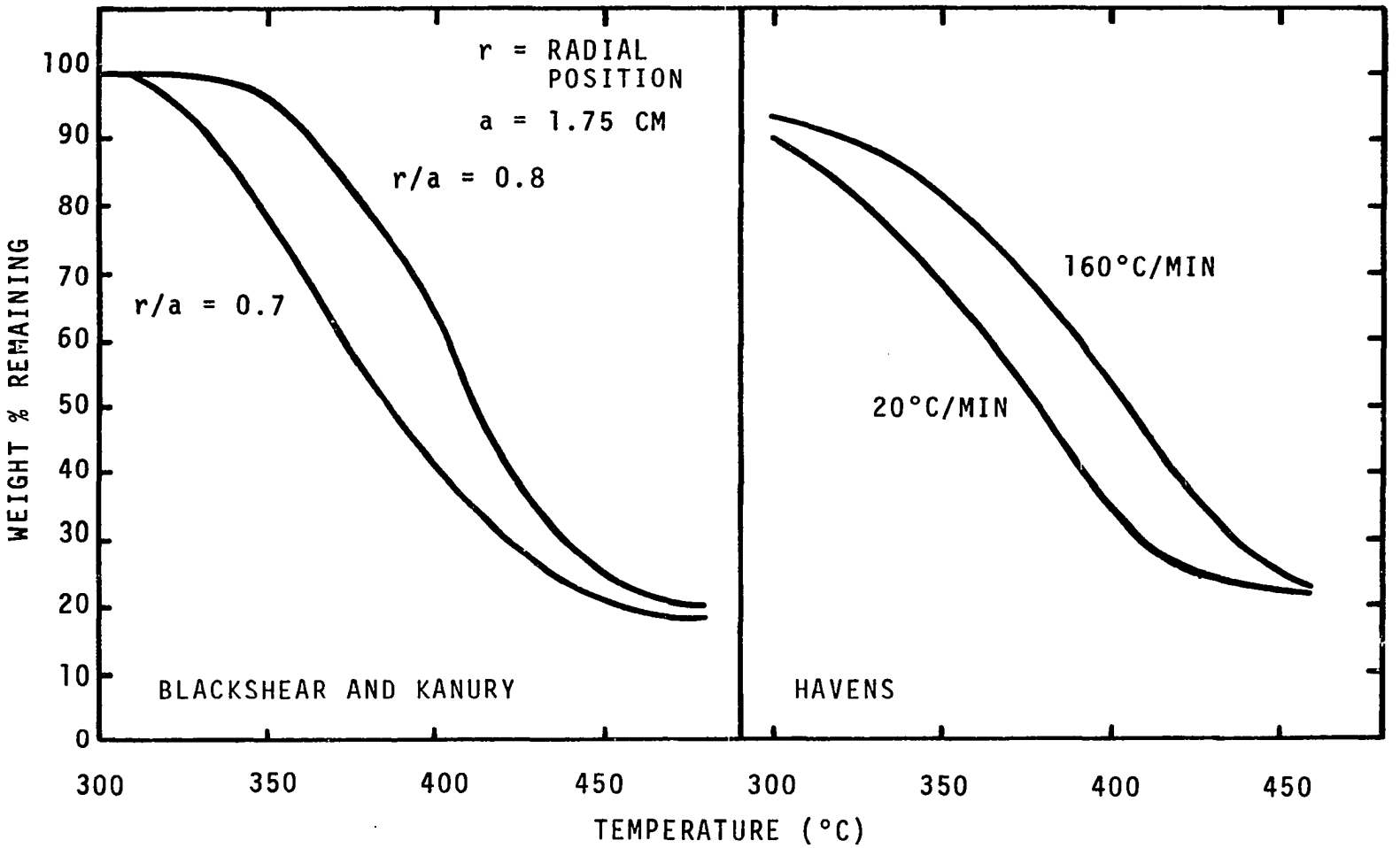

Figure II-20. Comparison of Density Data of Blackshear and Kanury (5) to TG Data of Havens (16).

Thermal Conductivity

The thermal conductivity of wood is known to be strongly dependent on wood grain direction, local non-homogenities, and density variations within the specimen. Several studies have been made which shed considerable light on the effect of these non-homogenities on the thermal conductivity of wood. The thermal conductivity of wood in the pyrolysis zone and char have been discussed by several workers but no experimental studies have been undertaken.

Griffith and Kaye (14) studied the effect of wood structure, direction of heat flow, and moisture content on the thermal conductivity of eight different woods. These investigators defined three nearly perpendicular axis of reference in the end grain pattern of each species as shown in Figure II-21. These axis are:

1. Parallel to the grain or wood fiber (Nos. 1 and 4 in Figure II-21).
2. Across the grain, perpendicular to fiber length, and radial to the annual growth rings (Nos. 5 and 3).
3. Across the grain, perpendicular to fiber length, and tangential to the annual growth rings (Nos. 6 and 2).

Test discs 3/4 inches in diameter were obtained at each of the numbered positions in Figure II-21. Test specimens were obtained at several locations along each axis to determine the effect of location on thermal conductivity.

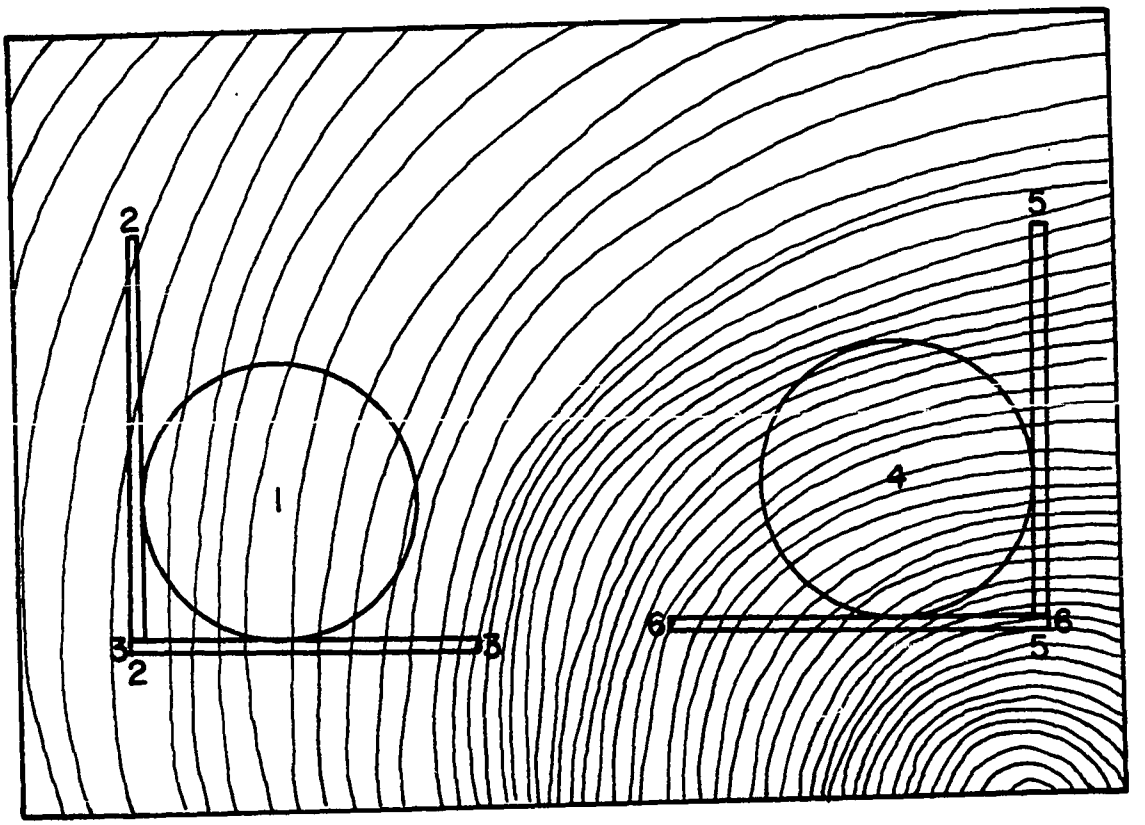

Figure II-21. Schematic of End Grain Pattern of Ash Board Showing Location of Test Specimens (14).

Griffith and Kaye measured the thermal conductivity of these wood specimens using the hot plate method. Data were obtained on a mean sample temperature of 30°C with a temperature drop across the samples of from 3°C to 20°C. A summary of the thermal conductivity values obtained is given in Table II-8. Although all the samples tested contained appreciable quantities of moisture, the data show the effect of direction of heat flow on the thermal conductivity. Griffith and Kaye concluded that longitudinal conductivity is approximately twice the conductivity in either transverse direction. The radial conductivity was found to be 5 to 10 percent higher than the tangential conductivity. They attributed the higher longitudinal conductivity to the relatively smooth heat flow path in that direction as contrasted to either transverse direction. Errors in these tests due to moisture content and inherent errors in the hot plate method would suggest that the differences in tangential and radial conductivities are not statistically significant.

Rowley (35) reported that the following conclusions were made based on over 100 tests for 14 different woods at the U.S. Forest Products Laboratory.

1. Thermal conductivity varies approximately as a linear function of density in any given wood.
2. In woods with well defined annual rings the conductivity in the tangential direction is greater than that in the radial direction.

TABLE II-8

THERMAL CONDUCTIVITY VALUES FOR WOOD
[Griffith and Kaye (14)]

Species	Density (gm/cm^3)	Position	Thermal Conductivity* (cal/cm^2-sec-°C/cm)
Ash	0.74	1	0.000365
	0.74	2	0.000369
	0.74	3	0.000714
	0.74	4	0.000464
	0.74	5	0.000416
	0.74	6	0.000754
Mahogany	0.70	1	0.000391
	0.70	2	0.000351
	0.70	3	0.000701
	0.70	4	0.000416
	0.70	5	0.000387
	0.70	6	0.000776
Spruce	0.41	1	0.000341
	0.41	2	0.000264
	0.41	3	0.000550
	0.41	4	0.000242
	0.41	5	0.000237
	0.41	6	0.000509
Walnut	0.65	1	0.000346
	0.65	2	0.000326
	0.65	3	0.000794
Teak	0.72	2	0.000314
	0.72	5	0.000341

*Mean sample temperature = 20°C.

3. In woods of uniform grain the position of annual rings can be neglected.
4. Thermal conductivity varies as a linear function of moisture content expressed as weight per unit volume of wood.

Rowley's conclusion that wood conductivity in the tangential direction is higher than in the radial direction is the reverse of Griffith and Kaye's conclusion.

Wangaard (41, 42) studied the effects of density, moisture content, direction of heat flow, and composition on the thermal conductivity of 40 types of wood. Measurements were made using the hot plate method at a mean sample temperature of approximately 28°C. Wangaard compared his data to that of Rowley and found an average difference of only 0.86 percent which was shown to be statistically insignificant. It was also concluded by Wangaard that:

1. The thermal conductivity of wood is strongly dependent on density and moisture content below the fiber saturation point.
2. Radial conductivity exceeds tangential conductivity in hardwoods by a small but statistically significant amount, attributable to radially oriented wood rays. For the softwoods the difference in conductivity in the radial and transverse direction is insignificant.
3. Variations in longitudinal cellular structure have little influence on the transverse conduction of heat.

4. Peculiarities in gross structure or chemical composition within individual wood types have little or no influence upon thermal conductivity other than that resulting from variations in density.

MacLean (25) studied the effect of density, moisture content, compression, and direction of heat flow on the thermal conductivity of 32 woods both of the hardwood and softwood varieties. Tests were made using the hot plate method with mean sample temperatures of 30°C and temperature drops from 22 to 28°C across the specimen. MacLean demonstrated that the variation in thermal conductivity due to density in moisture-free wood could be expressed by the linear relationship

$$K = 0.00478\rho + 0.000568 \qquad \text{II-29}$$

where K = thermal conductivity (cal/cm^2 sec-°C/cm)

ρ = density of wood (gm/cm^3)

The thermal conductivity at zero density approximates the conductivity of air at the average temperature of the specimen. MacLean compared experimental values of conductivity obtained for 18 wood species in 84 tests to those predicted by Equation II-29 and found a maximum error of 8.4 percent with an average absolute deviation of only 2.9 percent.

MacLean also determined the thermal conductivity of Douglas Fir in the radial and tangential direction. He

observed that the tangential conductivity tended to be slightly higher than the radial, but the difference was so small that MacLean concluded it was insignificant. The longitudinal conductivities determined by MacLean were 2-1/4 to 2-3/4 times higher than those obtained in the transverse directions.

The thermal conductivity of wood at temperatures up to the threshold of pyrolysis has been measured by Kanury (18), Koohyar (23), and Havens (16). All three of these investigators used a transient technique proposed by Chung and Jackson (19) for determining the temperature dependence of conductivity for materials having low conductivity. The technique utilizes the physical anomalie that thermal diffusivity is nearly independent of temperature even though its components, density, conductivity, and specific heat, are strongly temperature dependent. Thus, if the temperature dependence of density and specific heat are known, the thermal conductivity may be computed from Equation II-30.

$$K = \alpha\rho c = \text{constant} \qquad \text{II-30}$$

where α = thermal diffusivity (cm^2/sec)

c = heat capacity (cal/gm-°C)

(All other terms are defined as before)

An experiment may be designed to measure thermal diffusivity based upon heat transfer in the radial direction of an infinitely long cylinder. Transient heat transfer along the radial direction is given by

$$\alpha \left(\frac{\partial^2 T}{\partial r^2} + \frac{1}{r}\frac{\partial T}{\partial r}\right) = \frac{\partial T}{\partial t} \qquad \text{II-31}$$

where T = temperature (a function of r and t) (°C)

r = radial position (cm)

t = time (sec)

If a long cylindrical rod of radius R, initially at a uniform temperature T_o, is suddenly immersed in a fluid having a constant temperature T_B, the transient temperature response in the rod can be obtained by solving Equation II-32 with the following boundary conditions.

$$\begin{aligned} &\text{At } t < 0,\ T = T_o,\ 0 \le r \le R \\ &\quad t > 0,\ \partial T/\partial r = h(T_B - T)/K,\ r = R \\ &\quad t \ge 0,\ \partial T/\partial r = 0,\ r = 0 \end{aligned} \qquad \text{II-32}$$

The solution of Equation II-32 with these boundary conditions is given by Equation II-33.

$$\frac{T_B - T}{T_B - T_o} = \sum_{v=1} \frac{2J_1(X_v)}{X_v[J_o^2(X_v) + J_1^2(X_v)]} e^{-(X_v^2 \frac{\alpha t}{r^2})} [J_o(X_v \frac{1}{R})] \qquad \text{II-33}$$

Chung and Jackson have shown that the series given by Equation II-33 converges rapidly; after a short time all terms except the first are negligible. Equation II-33 then reduced to

$$Y = Ae^{-bt} \qquad \text{II-34}$$

where $$Y = \frac{T_B - T}{T_B - T_o} \qquad \text{II-35}$$

$$A = \frac{2J_1(X_1)}{X_1[J_o^2(X_1) + J_1^2(X_1)]} J_o(X_1 \frac{r}{R}) \qquad \text{II-36}$$

$$b = \frac{X_1^2 \alpha}{R^2} \qquad \text{II-37}$$

A plot of ln Y versus t should yield a straight line of slope -b from which one can calculate α using Equation II-37. The term X_1 is the smallest root of the transcendental equation given by:

$$\frac{X}{hR/K} = \frac{J_o(X)}{J_1(X)} \qquad \text{II-38}$$

The limiting value of X_1 as $hR/K \to \infty$ is 2.405 (8). For practical applications $hR/K > 100$; thus, no significant error will result from assuming $X_1 = 2.405$.

Koohyar and Havens both immersed cylindrical pine samples in hot liquid baths and followed the response of the specimen at several internal radial positions. The bath temperature, T_B, used by Koohyar was 70°C and those used by Havens were 197°C and 97°C. The temperature dependence of white pine thermal conductivity from the work of Havens is given in Table II-9.

Kanury obtained the thermal conductivity of α-cellulose from the temperature rise of cylinders which were suddenly inserted into the heated copper tube shown in

TABLE II-9

TEMPERATURE DEPENDENCE FOR THE THERMAL CONDUCTIVITY OF WHITE PINE

Temperature °C	Thermal Conductivity cal/cm^2 sec-°C/cm
30	0.00023
40	0.000253
200	0.000273
240*	0.00032

*Data extrapolated to 240°C assuming thermal diffusivity to be independent of temperature.

Figure II-13. Cellulose cylinders were prepared by pressing wet α-cellulose into cylindrical molds and then drying. The thermal diffusivities obtained were three to four times larger than those expected. Roberts (33) recently noted that this error can probably be attributed to the forced alignment of the α-cellulose fiber in the pressing operation.

There have been no experimental data reported in the literature regarding the thermal conductivity of wood char or partially pyrolyzed wood. Panton and Rittman (32) have suggested that the thermal conductivity of pyrolyzing wood and char are linearly dependent on the conductivity of the virgin wood and the densities of the pyrolyzing wood and char. Similarly Havens (16) has proposed that the thermal conductivity of wood char and partially pyrolyzed wood can be

calculated using MacLean's correlation of wood thermal conductivity with density given by Equation II-29, modified to account for changes in density due to weight loss during pyrolysis. The correlation used by Havens is shown in Equation II-39 and implicitly states that the thermal conductivity of wood during pyrolysis is independent of the composition of the pyrolyzing material.

$$K = 0.00478\rho f + 0.000568 \qquad \text{II-39}$$

where f = fraction of wood pyrolyzed determined from TG data

Effect of Moisture Content

It is well known that wood absorbs moisture from the surrounding air. If the wood is heated that moisture will have an effect on the heat transfer characteristics and the wood pyrolysis products. Although moisture will act as a heat sink, its quantitative effects have not been studied.

Blackshear and Kanury (5) have suggested that when wood is heated moisture migrates away from the hot surface toward the interior where it "pre-heats" the virgin wood and alters its decomposition mechanism. This conclusion was based on the pyrolysis of α-cellulose cylinder, previously discussed on pages 45 and 72, for which the apparent activation energy decreases with distance from the heated surface. It is reported by Roberts (33) that this effect can also be attributed to the forced alignment of cellulose fibers in the sample preparation process.

Effect of Bulk Flow and Secondary Pyrolysis

Bulk flow of the volatile pyrolysis products from the pyrolysis zone through the much warmer char matrix results in heat transfer from the char matrix to the volatiles. The effects of this heat sink on the temperature profile of pyrolyzing wood has been examined by Blackshear and Kanury (5).

Blackshear and Kanury have assumed that pyrolyzing wood consists of a solid matrix that remains inert while an entrained active material within the matrix is gasified. They also assume that the gasified material and the inert matrix are in thermal equilibrium. Blackshear and Kanury developed the following mathematical model for a one-dimensional system in which the pyrolysis process is described by a first-order kinetic equation.

$$\frac{\partial}{\partial T}(\rho h) = \frac{\partial}{\partial x} K \frac{\partial T}{\partial x} + C_g W_g \frac{\partial T}{\partial x} + \rho_g^{\circ} (C_g T + H_r) \qquad \text{II-40}$$

$$\rho_g^{\circ} = \frac{\partial W_g}{\partial x}$$

$$\rho^{\circ} = \rho_g^{\circ} = -(\rho - \rho_m) k_o e^{-E/RT}$$

where ρ = total density (gm/cm^2)

k_o = frequency factor (sec^{-1})

K = effective thermal conductivity (cal/cm^2-sec-°C/cm)

C_g = specific heat of the gaseous materials (cal/gm-°C)

h = enthalpy of local gaseous and solid components (cal/gm)

T = temperature (°K)

H = heat of pyrolysis (cal/gm)

W_g = mass flux of gasified material across surface (gm/sec-cm^2)

This model includes terms for energy transport by conduction, bulk flow and primary decomposition effects. It neglects any cracking of pyrolysis products in the char layer.

Blackshear and Kanury suggested that the effect of bulk flow on the temperature profile can be visualized using a characteristic length ℓ and the ratio of the bulk flow term ($C_g W_g \, \partial T/\partial x$) to the conduction term ($\partial/\partial x \; K \; \partial T/\partial x$) as given by

$$\frac{\text{Energy flow by bulk flow}}{\text{Energy flow by conduction}} = C_g W_g / K \qquad \text{II-41}$$

This ratio has the form of a modified Peclet number. If $C_g W_g / K << 1$, Blackshear and Kanury suggested that bulk flow effects could be neglected. Blackshear and Kanury assumed that the characteristic length ℓ of a specimen should be its thickness L after a time, t, defined as

$$t = \frac{\rho C L^2}{K} \qquad \text{II-42}$$

where ρ = density of wood (gm/cm^3)

C = heat capacity of wood (cal/gm°C)

K = thermal conductivity of the wood (cal/cm^2 sec-°C/cm)

L = thickness of specimen (cm)

They then suggested that a criterion for the neglect of the convection term in Equation II-40 for $t \geq \rho CL^2/K$ would be a lower limit on the value of $W_g C_g L/K < 0.1$. They tested the data of Bamford, Crank and Malan (4), and Roberts and Clough (34), for the effect of bulk flow. The results are presented in Table II-10. Note that W_g at the surface of the material is denoted by M". It can be seen from Table II-10 that in no case is $W_g C_g \ell/K$ less than 0.1; therefore, Blackshear and Kanury concluded that bulk flow must be included in a mathematical model.

Welker (44) has pointed out that the amount of heat transferred to the volatiles is dependent on the temperature drop across the char zone and, hence, its thermal conductivity and thickness. Thus the ratio given in Equation II-41 appears at best to indicate the conditions required for bulk flow to effect the temperature profile in the uncharred portion of the wood and implies nothing about the effect of bulk flow on the temperature profile in the char zone. Since the temperature profile across the char zone is of interest in this study the analysis of Blackshear and Kanury provides information of only limited interest.

TABLE II-10

ESTIMATES OF MAGNITUDE OF INTERNAL CONVECTION HEAT EFFECT IN DECOMPOSING MATERIAL
[Blackshear and Murty (5)]

Source	Remarks	L (cm)	K (cal/cm-sec°C)	C_g (cal/gm-°C)	$\dot{m}''$ (gm/cm^2-sec)	$\frac{\dot{m}''C_gL}{K}$
Blackshear and Murty (5)	$\dot{m}''$ = maximum value measured after $t = \rho C_g L^2/k$ L = radius of cylinder K obtained from measured values of thermal diffusivity and density, and an assumed specific heat for the solid C = 0.55; C_g, estimated.	0.667	16×10^{-4}	0.27	11.8×10^{-4}	0.133
		0.687			11.69	0.135
		0.696			9.26	0.109
		0.762			10.30	0.133
		0.909			8.14	0.125
		1.016			8.56	0.146
		1.028			8.91	0.155
		1.048			8.80	0.156
		1.175			9.16	0.181
		1.206			8.28	0.169
		1.276			6.70	0.144
		1.479			8.05	0.200
		1.606			7.86	0.214
		1.619			8.34	0.229
		1.835			6.28	0.194
		3.225			5.84	0.320
Bamford, Crank, Malan (4)	$\dot{m}''$: taken from Table 1 reference 4 $\dot{m}'' = L/t \times 0.375$ L = 1/2 thickness of specimen t = total heating and burning time K taken from reference 4 C_g estimated.	0.555	2.7×10^{-4}	0.27	6.96×10^{-4}	0.380
		1.035			5.08	0.521
		1.270			7.92	1.001
		1.035			5.88	0.602
		1.585			4.50	0.715
		1.900			4.16	0.792
		2.070			3.37	0.700
Reference 4, Table 3	Data for 5 cm thick specimen of Columbian pine heated radiantly on one side $\dot{m}''$ = (final depth of char/total time) 0.375.	0.435	2.7×10^{-4}	0.27	13.5×10^{-4}	0.635
		0.50			11.6	0.370
		0.83			10.35	0.860
		0.75			9.90	0.745
		5.0			5.47	2.74
Roberts and Clough (34)	Data from Table 1 of reference 34 $\dot{m}''$ measured directly L = radius K and C_g estimated.	0.5	2.7×10^{-4}	0.27	81.0×10^{-4}	8.1
		0.5			25.0	2.5
		0.5			170.0	11.0
		0.5			30.0	3.0
		0.5			7.6	0.76

Mathematical Models

The first mathematical model used to describe the pyrolysis of wood was that of Bamford, Crank and Malan (4). This model was solved based on the information available to these investigators regarding the pyrolysis phenomena. This original model was improved by other investigators as new insight was gained into the pyrolysis phenomena. Also, as new mathematical techniques were developed, the procedure for solving the mathematical model was improved. It is unfortunate that most of the early investigators made fundamental statements about ignition and combustion criterion for wood based on solutions of these highly simplified mathematical models. In the following discussion of mathematical models, only the model, the assumptions made, and the solution technique will be discussed.

Bamford, Crank, and Malan (4)

Bamford, Crank and Malan proposed that the transient temperature response and the rate of mass loss from a slab of wood undergoing thermal decomposition could be described by the heat conduction equation with a source term for the heat of decomposition given by

$$K \frac{\partial^2 T}{\partial x^2} - q \frac{\partial W}{\partial t} = C\rho \frac{\partial T}{\partial t} \qquad \text{II-43}$$

where q = heat of decomposition of material decomposed (cal/gm)

The weight loss term was determined by assuming a first order decomposition reaction,

$$-\frac{\partial W}{\partial t} = k_o W e^{-E/RT}$$

All other terms are defined as before (page 34). For a slab of wood of thickness 2ℓ heated on both faces by an open flame, the boundary conditions for Equation II-43 were written as:

$T = T_o$ at $t = 0$ and $0 < x < 2\ell$

W = constant at $t = 0$ and $0 < x < 2\ell$

$-K\ \partial T/\partial x = H(T_o)$ at $t > 0$ and $x = 0$, $x = 2\ell$

where T_o is the surface temperature of the wood for times greater than t_o. The rate of heat transfer to the surface, $H(T_o)$, was defined by Bamford, Crank, and Malan as

$$H(T_o) = \alpha(T_f - T_o) + \sigma(\varepsilon T_f^4 - T_o^4) \qquad \text{II-44}$$

where T_f = flame temperature (°K)

ε = emissivity of the flame (dimensionless)

σ = Stefan-Boltzmann constant (cal/cm^2-sec-°K)

α = overall convection plus conduction heat transfer coefficient (cal/cm^2-sec-°K)

Assuming constant values of specific heat, density, and thermal conductivity, a single first-order decomposition reaction and a heat of decomposition (as discussed previously) these investigators solved Equation II-43 using a finite difference method. A computed temperature response is shown in Figure II-22 and as can be seen central temperature data was predicted with good accuracy.

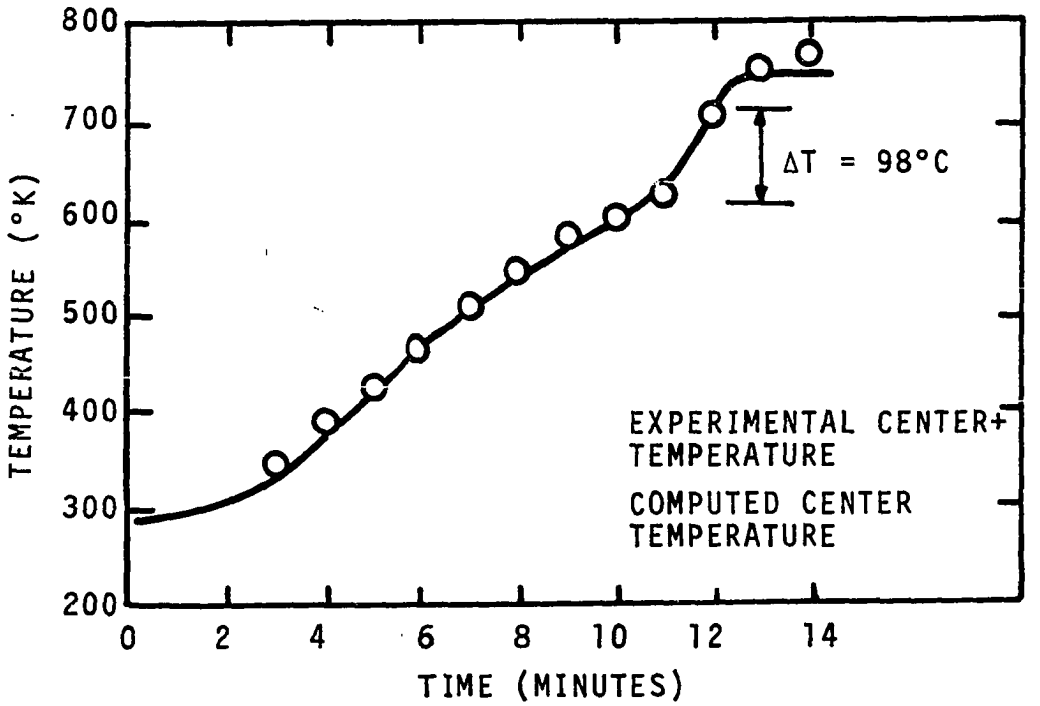

Figure II-22. Computed and Measured Central Temperature-Time Curves from Bamford, Crank and Malan (4).

Weatherford and Sheppard (43)

Weatherford and Sheppard solved Equation II-43 using a finite difference method and the same properties for wood as those proposed by Bamford, Crank, and Malan but with an internal heat balance given in Equation II-45.

$$\frac{\partial[K(\partial T/\partial x)]}{\partial x} = C\rho \left(\frac{\partial T}{\partial t}\right) + q \left(\frac{\partial W}{\partial t}\right) \qquad \text{II-45}$$

These investigators pointed out that the stability of the solution obtained was dependent on the incremental sample widths used. They found that the sample widths used by Bamford, Crank, and Malan led to a non-stable solution.

Weatherford and Sheppard compared the computed temperature profile for an inert model with that for the active model containing a heat source term. They found that for Biot number less than 10 the computed surface temperatures for the inert and active models were within 10 percent of one another.

Panton and Rittman (32)

Panton and Rittman were the first investigators to include the variation in physical and thermal properties and multiple decomposition reactions into the heat conduction problem. These investigators proposed that the thermal conductivity of pyrolyzing wood can be described as a function of density as given in Equation II-46.

$$K = K_o \, \rho/\rho_o \qquad \text{II-46}$$

where ρ_o = density of the virgin wood (gm/cm^3)

K_o = thermal conductivity of wood at density ρ_o (cal/cm^2-sec-°C/cm)

ρ = density of pyrolyzing wood (gm/cm^3)

K = thermal conductivity of pyrolyzing wood (cal/cm^2-sec-°C/cm)

Substitution of Equation II-46 into Equation II-43 yields Equation II-47

$$\frac{\partial T}{\partial t} = \frac{K_o}{\rho_o C} \frac{\partial^2 T}{\partial x^2} + \frac{K_o}{\rho_o C \rho} \frac{\partial \rho}{\partial x} \frac{\partial T}{\partial x} + \frac{\dot{Q}}{\rho C} \qquad \text{II-47}$$

where $\dot{Q}$ = the rate of heat of pyrolysis.

Panton and Rittman hypothesized a number of possible reaction mechanisms for wood pyrolysis including series, competing, and parallel reactions. Each of the proposed reactions was examined in the model. The effect of bulk flow through the char matrix and the change in specific heat due to pyrolysis were neglected. The heat of pyrolysis was assumed to be represented by a single value. Several values for each of the physical and thermal properties in Equation II-47 were chosen such that parametric computation could be made. Equation II-47 was solved using an integral technique which the authors said gave smoother results and better convergence than finite difference methods. This parametric study is of historical importance since it was the first to recognize variations in thermal and physical properties. The later studies of Kung (18) and Kanury (24) are more general.

Kung (18)--Kanury (24)

The mathematical model for wood pyrolysis proposed by Kanury and given in Equation II-48 includes the effects of variable thermal and physical properties, bulk flow, chemical kinetics, and the heat of pyrolysis.

$$\frac{\partial}{\partial t}(\rho_a h_a + \rho_c h_c) \equiv \frac{\partial}{\partial x}(K \frac{\partial T}{\partial x}) + \frac{\partial}{\partial x}(M_g h_g) - Q_p[- \frac{\partial \rho}{\partial t}] \quad \text{II-48}$$

where h = enthalpy (cal/gm)

M_g = mass flow rate of gas through the char matrix (gm/sec)

Q_p = heat of pyrolysis assumed to be a constant (cal/gm of decomposed material)

Subscripts

a = virgin wood

c = char

g = gas

(All other terms are as previously defined.)

Kanury proposed that the thermal conductivity of char be described as a linear function of density between the values for conductivity of wood and char.

Kung solved Equation II-48 numerically using the technique of Crank and Nicholsen which was said to be stable regardless of the size of the time step used in the iterative computations. A series of dimensionless values was assumed for each of the unknown quantities in Equation II-48, and the

equation was solved for time-temperature-density profiles. A typical result for a wood slab undergoing pyrolysis is shown in Figure II-23. The most striking computations are those which demonstrate the effects of char thermal conductivity on mass loss. The results of these computations are shown in Figure II-24. It is evident that the conductivity of char may play a significant role in the pyrolysis of wood. Kung concluded that before any significant comparison can be made between experimental and computed pyrolysis phenomena the thermal conductivity of char must be known.

Havens (16)

The mathematical model used by Havens is somewhat different from those previously discussed. The model is based on a method developed by Hashemi (15) for predicting transient temperature profiles in frozen soil. In this method, a region of interest is divided into a set of cells of finite dimensions, and a heat balance is written on each cell. The requirement of heat balance for each cell can be guaranteed using this procedure even though the rates of heat transfer at the boundaries are approximate. Using this technique the problem in obtaining a consistent set of difference equations is avoided. This technique will also be used in this study; therefore, it will be reviewed in detail.

To illustrate the procedure for setting up such a set of difference equations, consider a two-dimensional region in

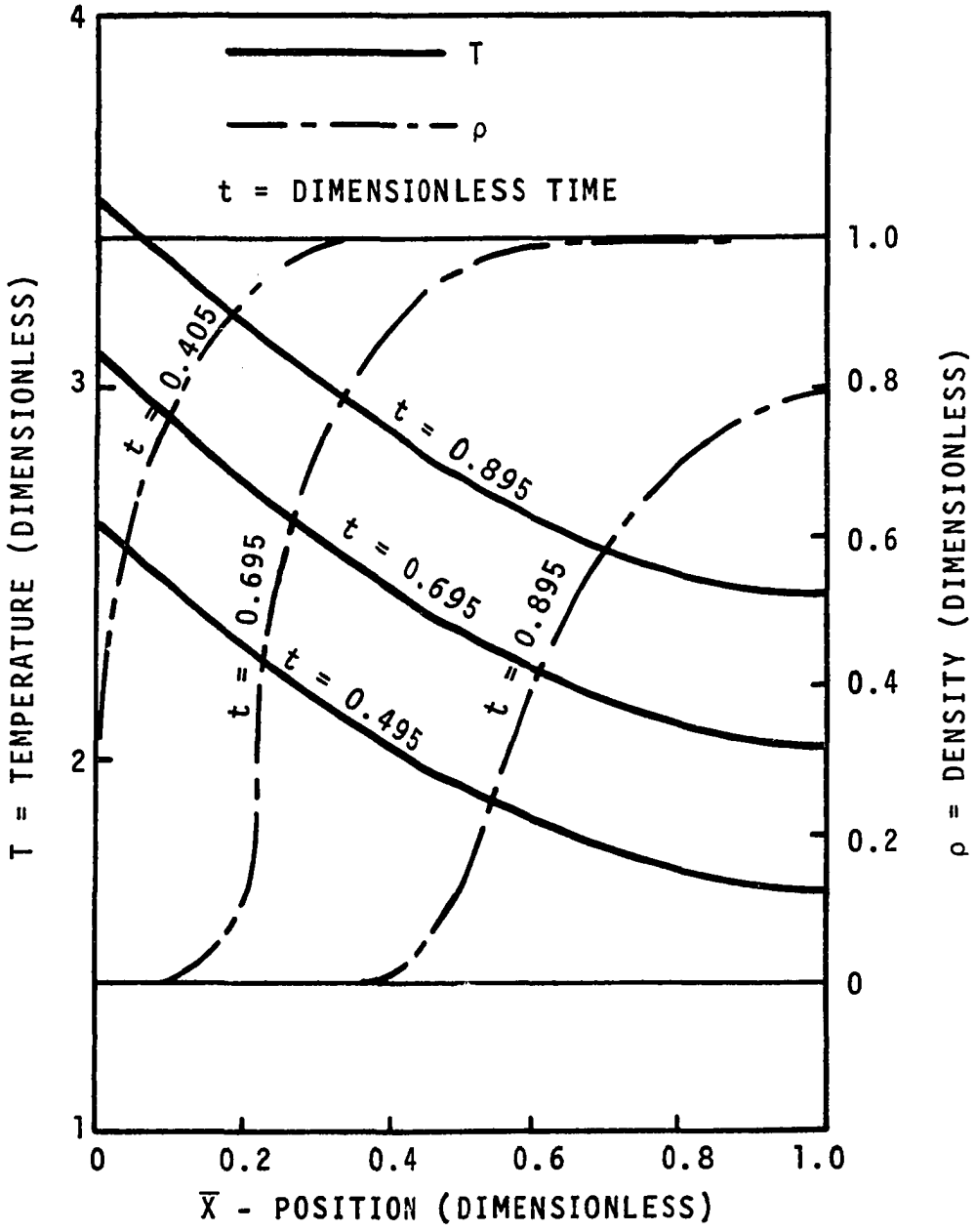

Figure II-23. Predicted Temperature and Density Profiles in Pyrolyzing Wood from Study of Kung (24).

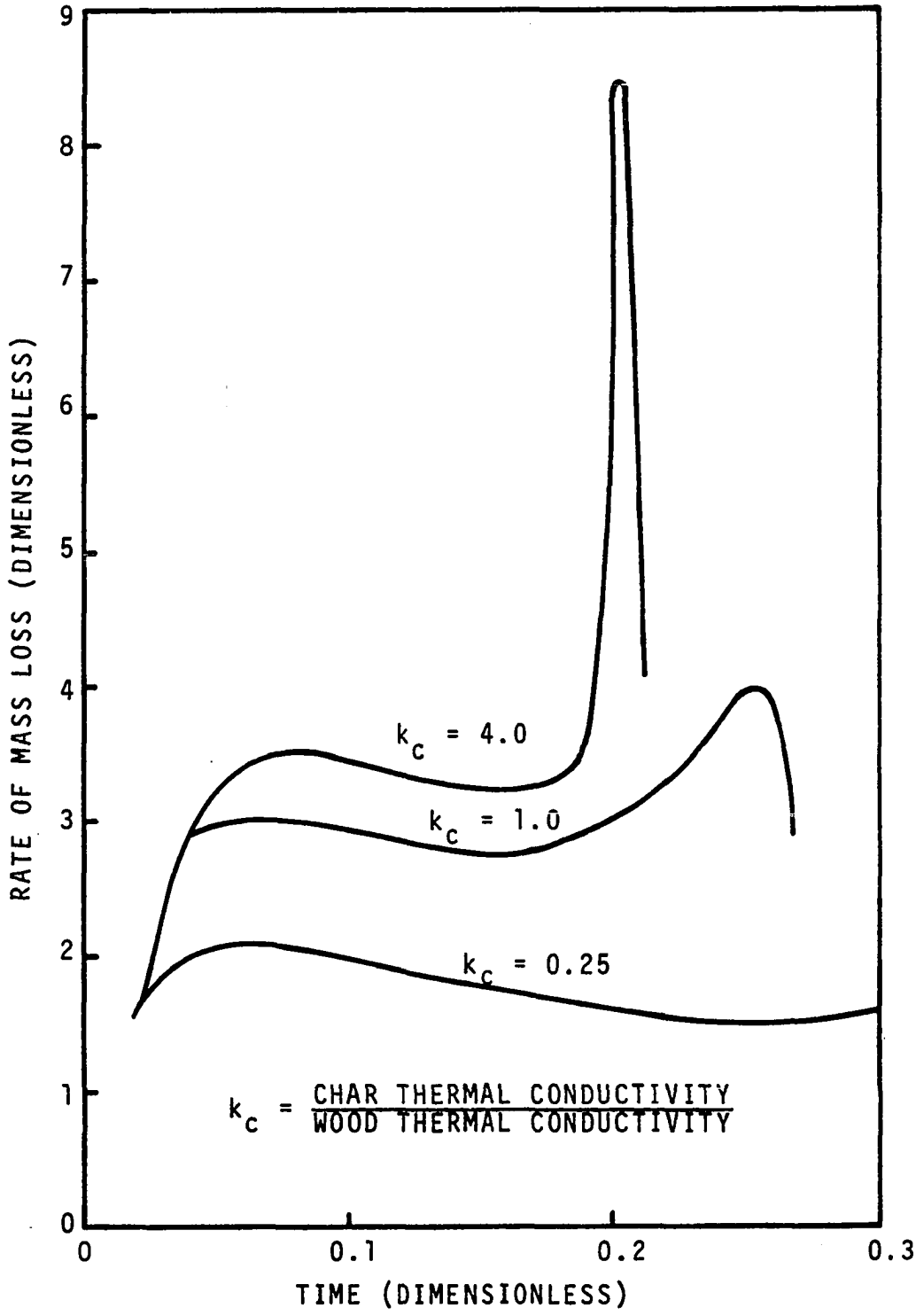

Figure II-24. Effect of Char Thermal Conductivity on Rate of Weight Loss--Reference (24).

which a network of mesh points has been developed by the intersection of N_x lines parallel to the x-axis and N_y lines parallel to the y-axis. Let the intersection of the ith line parallel to the x-axis and j^{th} line parallel to the y-axis (the point x_i, y_j) be a mesh point, denoted as (i,j). Let the distance between mesh points (i,j) and (i-1, j) be h_i, $1 \leq i \leq N_x$, and the distance between mesh points (i,j) and (i, j-1) be k_j, $1 \leq j \leq N_y$. Let the rectangle defined by lines $x_i - 1/2\ h_i$, $x_i + 1/2\ h_{i+1}$, $y_j - 1/2\ k_j$, and $y_j + 1/2\ k_{j+1}$ be the mesh region (i,j). Figure II-25 shows one such mesh region and its adjacent mesh points.

Assume that for a two-dimensional locally isotropic medium the heat fluxes in the x and y directions obey Fourier's Law and are given by Equation II-49

$$j_x = -K \frac{\partial T}{\partial x} \simeq - \frac{T(x+\Delta x,\ y) - T(x,y)}{R\Delta x}$$

and

$$j_y = -K \frac{\partial T}{\partial y} \simeq - \frac{T(x,\ y+\Delta y) - T(x,y)}{R\Delta y} \qquad \text{II-49}$$

where j_x, j_y = heat fluxes in x and y directions respectively (cal/cm^2-sec)

K = thermal conductivity (cal/cm^2-sec-°C/cm)

T = temperature (°C)

R = 1/K, the thermal resistivity (cm-sec-°C/cal)

Let the temperature T at a mesh point (i,j) by $T_{i,j}$ and the average value of the thermal resistivity, R, and the internal

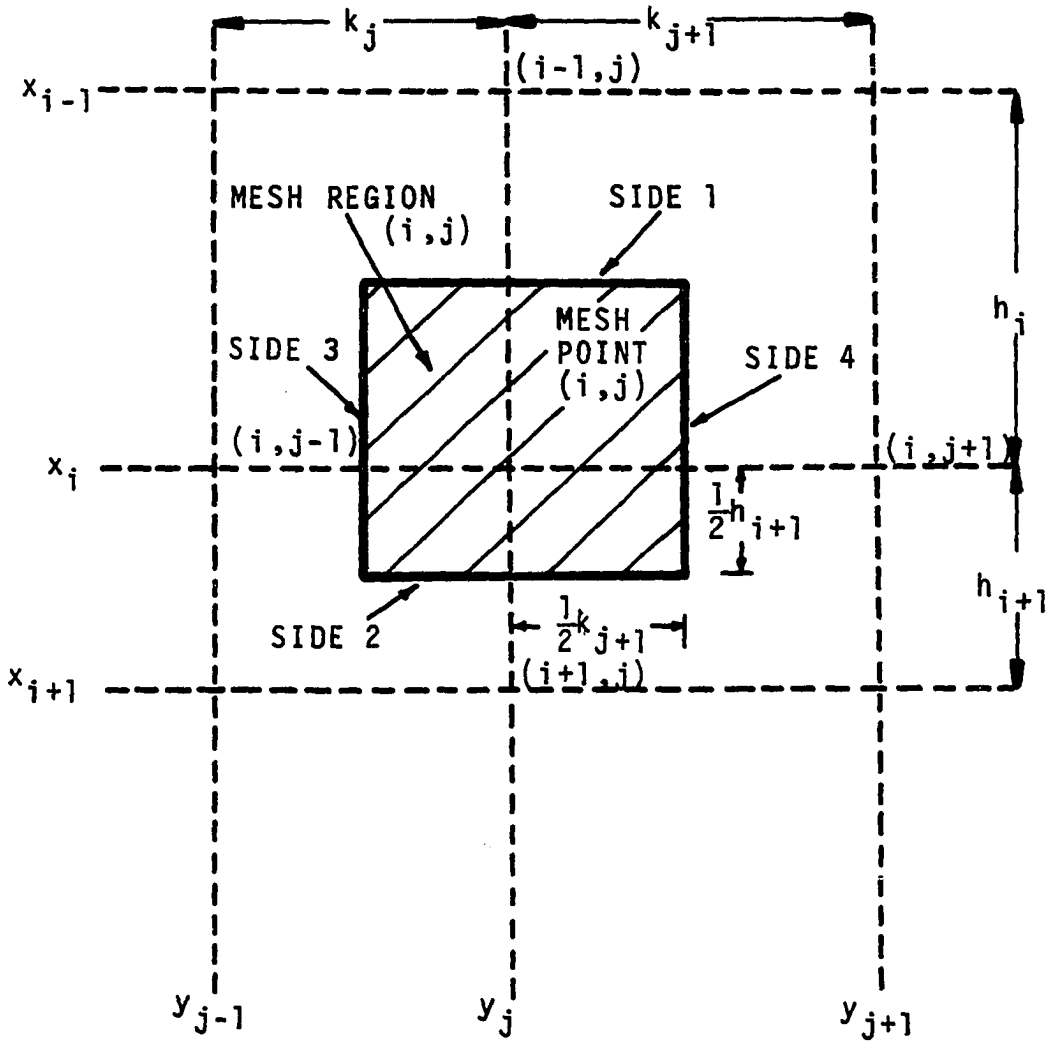

Figure II-25. A Mesh Region (i,j) and Its Adjacent Mesh Points.

energy, E, for a mesh region (i,j) by $R_{i,j}$ and $E_{i,j}$ respectively. Let the average values of $R_{i,j}$ and $E_{i,j}$ be those obtained at the temperature $T_{i,j}$ of the mesh point (i,j).

Let the rates at which heat is transferred by conduction into the mesh region (i,j) through sides 1, 2, 3 and 4 (see Figure II-25) be q_1, q_2, q_3 and q_4 respectively. Then the heat balance around a mesh region (i,j) is

$$(q_1 - q_2) + (q_3 - q_4) = \Delta V_{i,j} \frac{dE_{i,j}}{dt} \qquad \text{II-50}$$

where $\Delta V_{i,j}$ is the volume of the mesh region (i,j) and is given by

$$\Delta V_{i,j} = \Delta z \ (1/2\ h_i + 1/2\ h_{i+1})(1/2\ h_j + 1/2\ h_{j+1}) \qquad \text{II-51}$$

where Δz = the thickness of the region

q_1, q_2, q_3 and q_4 can be approximated with the aid of Equation II-49 to obtain

$$q_1 = -1/2\ \Delta z(k_j + k_{j+1})(T_{i,j} - T_{i-1,j})/[1/2\ h_i(R_{i,j} + R_{i-1,j})]$$

$$q_2 = -1/2\ \Delta z(k_j + k_{j+1})(T_{i+1,j} - T_{i,j})/[1/2\ h_{i+1}(R_{i,j}+R_{i+1,j})]$$

$$q_3 = -1/2\ \Delta z(h_i + h_{i+1})(T_{i,j} - T_{i,j-1})/[1/2\ k_j(R_{i,j} + R_{i,j-1})]$$

$$q_4 = -1/2\ \Delta z(h_i + h_{i+1})(T_{i,j+1} - T_{i,j})/[1/2\ k_{j+1}(R_{i,j}+R_{i,j+1})]$$

II-52

Equations II-52, when substituted in Equation II-50, result in the desired difference equations. However, it is helpful to write the resulting difference equation in terms of dimensionless variables. To this end let

$$u_{i,j} = (T_{i,j} - T_1)/(T_2 - T_1)$$
$$r_{i,j} = 1/2\ K_o R_{i,j}$$
$$e_{i,j} = E_{i,j}/[C_o(T_2 - T_1)]$$
$$\tau = K_o t/(C_o h^2)$$
$$C_i = 2h^2/h_i(h_i + h_{i+1})$$
$$C_j = 2h^2/k_j(k_j + k_{j+1})$$
$$b_i = 2h^2/h_{i+1}(h_i + h_{i+1})$$
$$b_j = 2h^2/k_{j+1}(k_j + k_{j+1})$$

Substituting Equations II-52 into Equation II-50, rearranging, and dividing by $K_o(T_2 - T_1)\Delta V_{i,j}/h^2$ gives

$$\frac{-C_i u_{i-1,j}}{r_{i,j} + r_{i-1,j}} + \left(\frac{C_i}{r_{i,j} + r_{i-1,j}} + \frac{b_i}{r_{i,j} + r_{i+1,j}}\right) u_{i,j}$$
$$- \frac{b_i u_{i+1,j}}{r_{i,j} + r_{i+1,j}} - \frac{C_j u_{i,j-1}}{r_{i,j} + r_{i,j-1}} + \left(\frac{C_j}{r_{i,j} + r_{i,j-1}}\right.$$
$$\left. + \frac{b_j}{r_{i,j} + r_{i,j+1}}\right) u_{i,j} - \frac{b_j u_{i,j+1}}{r_{i,j} + r_{i,j+1}} + \frac{de_{i,j}}{d\tau} = 0 \qquad \text{II-54}$$

where u = dimensionless temperature $T-T_2/T_2-T_1$

r = dimensionless thermal resistivity $(1/2\ K_o/K)$

K_o = reference state thermal conductivity (cal/cm^2-sec-°C/cm)

$E_{i,j}$ = internal energy (including sensible and decomposition heats) (cal/cm^3-°C)

$e_{i,j}$ = dimensionless internal energy

C_o = reference state specific heat (cal/cm^3-°C)

τ = dimensionless time

h = a geometrical scaling factor (cm)

c_i, c_j = dimensionless geometrical factors

b_i, b_j = dimensionless geometrical factors

For each mesh point at which the dimensionless temperature $u_{i,j}$ is unknown one obtains one equation such as Equation II-54. For N mesh points one then has a set of N simultaneous equations to be solved for N unknowns.

The nonlinearity of the problem of heat conduction accompanied by decomposition is due to the strongly non-linear relation between $e_{i,j}$ and $u_{i,j}$, particularly in the range of temperatures where thermal decomposition occurs. If the internal energy $e_{i,j}$, which includes decomposition and sensible heat effects, is assumed to be an explicit function of temperature only, and not a function of the rate of change of temperature (in other words, if it is assumed to be independent of the rate of heating), one can write

$$\frac{de_{i,j}}{d\tau} = \frac{de_{i,j}}{du_{i,j}} \frac{du_{i,j}}{d\tau} = \phi_{i,j} \frac{du_{i,j}}{d\tau} \qquad \text{II-55}$$

where $\phi_{i,j}$ can be thought of as an "energy capacity."

Utilizing the relation given by Equation II-55, the N simultaneous equations (Equation II-54) for the N unknown values of $u_{i,j}$ can be expressed in matrix notation as

$$\Phi \frac{dU(\tau)}{d\tau} + (H + V)\, U(\tau) = S(\tau) \qquad \text{II-56}$$

where Φ = an NxN diagonal matrix whose entries are the values of $\phi_{i,j}$

U = an N-dimensional vector whose entries are the unknown values of $u_{i,j}$

S = an N-dimensional source vector whose entries are zero when the mesh region (i,j) is not adjacent to the boundary, and contain information related to boundary conditions when the mesh region (i,j) is adjacent to the boundary

H and V are real NxN matrices with positive diagonal entries and non-positive off-diagonal entries, and both H and V have at most three non-zero entries per row. If one orders the mesh points by rows, i.e., from left to right, top to bottom, then H is the direct sum of tridiagonal matrices, i.e.,

$$H = \begin{bmatrix} H_1 & & & \\ & H_2 & & \\ & & \ddots & \\ & & & H_{Nx} \end{bmatrix}$$

where H_i, $1 \leq i \leq N_x$ are tridiagonal matrices whose diagonal entries are $[c_i/(r_{i,j} + r_{i-1,j}) + b_i/(r_{i,j} + r_{i+1,j})]$ and the off diagonal entries are $- c_i/(r_{i,j} + r_{i-1,j})$ and $- b_i/(r_{i,j} + r_{i+1,j})$. If instead, the mesh points are ordered by columns, i.e., from top to bottom, left to right, then V is the direct sum of tridiagonal matrices V_j, $1 \leq j \leq N_y$, i.e.,

$$V = \begin{bmatrix} V_1 & & & \\ & V_2 & & \\ & & \ddots & \\ & & & V_{Ny} \end{bmatrix}$$

where V_j, $1 \leq j \leq N_y$ are tridiagonal matrices whose diagonal entries are $[c_j/(r_{i,j} + r_{i,j-1}) + b_j/(r_{i,j} + r_{i,j+1})]$ and the off-diagonal entries are $- c_j/(r_{i,j} + r_{i,j-1})$ and $- b_j/(r_{i,j} + r_{i,j+1})$.

Equation II-55 is applicable to all mesh regions of interest, including the mesh regions adjacent to the boundary surface. For example, if side 1 of a mesh region (i,j) is insulated, then one sets $r_{i-1,j} = \infty$ (in practice a very large number, say 10^6, would be used). If, instead, the temperature on side 1 of mesh region (i,j) (i.e., $u_{i-1,j}$) is prescribed, then one sets $r_{i\pm1,j} = 0$ and moves the expression $c_i u_{i-1,j}/r_{i,j}$ to the right hand side of Equation II-54. Obviously one can use a similar method to specify a prescribed temperature on any other side or more than one side of any mesh region.

All natural boundary conditions fall into two categories; (a) the heat flux at the boundary is prescribed, or (b) the environment temperature is prescribed. When the heat flux is prescribed, the thermal resistivity of the external region is set equal to infinity and the prescribed value(s) of q_i, $1 \leq i \leq 4$, after being divided by $K_o(T_2-T_1)V_{i,j}/h^2$ is added to the right hand side of Equation II-54. When the temperature of the environment is prescribed, the value of thermal resistivity of the external mesh region is set equal to the heat transfer resistance at the boundary. When this resistance is zero, the boundary temperature is equal to the environment temperature.

Computer programs for solution of the temperature distribution in the region of interest (i.e., the solution of the system of first order, differential Equations II-54) have been developed by Hashemi (15). The numerical procedure is based on a variant of the Peaceman-Rachford alternating direction, implicit, iterative method.

Havens, in applying the numerical technique of Hashemi, stated that if the "energy capacity" (which includes energy effects due to pyrolysis as well as sensible heating) and the thermal conductivity K(u) can be specified, the transient temperature distribution satisfying Equation II-50 can be computed. Additionally, if the weight loss behavior of wood as a function of temperature can be specified, stepwise

integration of the weight versus temperature distribution can be made to predict the transient weight loss behavior of a large wood specimen.

The energy capacity data used by Havens were obtained from DSC measurements of white pine and oak at heating rate of 20°C/min. These data are shown in Figures II-11 and II-12. The rate of weight loss data used was obtained from TG measurements at 20°C/min as shown in Figures II-17 and II-18. Thermal conductivity was specified as a function of temperature using TG data obtained at a heating rate of 20°C/min to predict density and then using MacLean's thermal conductivity density correlation to compute conductivity.

Havens demonstrated the validity of the model, the energy capacity data, and the weight loss data by comparing computed temperature profiles and mass losses to experimental data.

Havens measured the temperature profiles in a cylindrical sample 15.3 cm in length and 4.45 cm outer diameter with an axial hole 0.635 cm in diameter. Heat was supplied to the inside surface of the wood cylinder from an 18 gage, 80-20 nickel-chromium resistance wire. The wood sample was cut into three cylindrical samples of equal length and the center section was instrumented with thermocouples. The three cylinders were taped together in their original order and with the wood grain lined-up. The resistance wire was positioned in the center hole using lava blocks as shown in

Figure II-26. Tests were run in a Plexiglas enclosure with a slow but continuous nitrogen purge.

A typical comparison of experimental temperatures and computed temperatures is shown in Figure II-27 and for mass loss in Figure II-28. To obtain these values of computed temperature, a major adjustment in the thermal conductivity-temperature profile was required. This adjustment, as shown in Figure II-29, required that the thermal conductivity of undecomposed wood be raised approximately 20 percent and that for char increased 75 percent. Also, the predicted temperature profiles were all in virgin material and were based on data obtained at heating rates of 20°C/min.

It will be shown in a later chapter that the large adjustment in thermal conductivity is a result of assuming that the thermal conductivity of pyrolyzing wood decreases in proportion to weight loss during pyrolysis and is independent of composition changes that occur during pyrolysis.

Each of the mathematical analogs reviewed and their development is summarized in Table II-11. As is evident from Table II-11, each group of investigators has developed more complex analogs in an effort to include every heat and mass transfer effect that occurs during pyrolysis. Unfortunately, the absence of data describing the reaction kinetics and thermal conductivity of pyrolyzing wood has precluded comparison of the results obtianed from the simpler models to the

results obtained from the more complex analogs. In fact, other than in the studies of Bamford, Crank and Malan and those of Havens, where values of thermal properties were assumed, no direct comparison has been made between experimental and computed time and temperature profiles. If the type models summarized in Table II-11 are to be used to establish ignition criterion, then the physical and thermal properties needed to solve these analogs must be obtained.

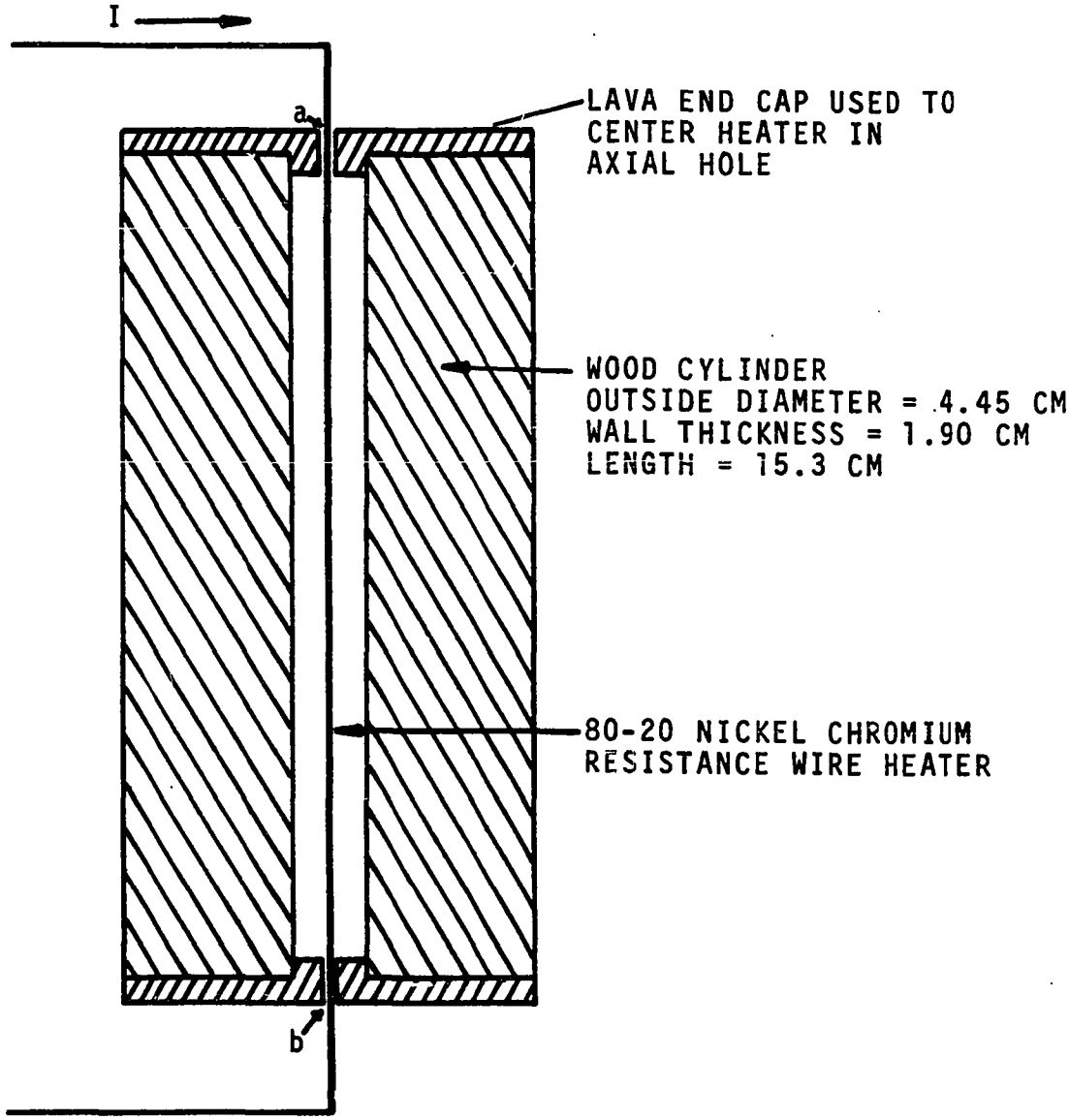

Figure II-26. Schematic of Resistance Wire Heater and Wood Cylinder from Work of Havens (16).

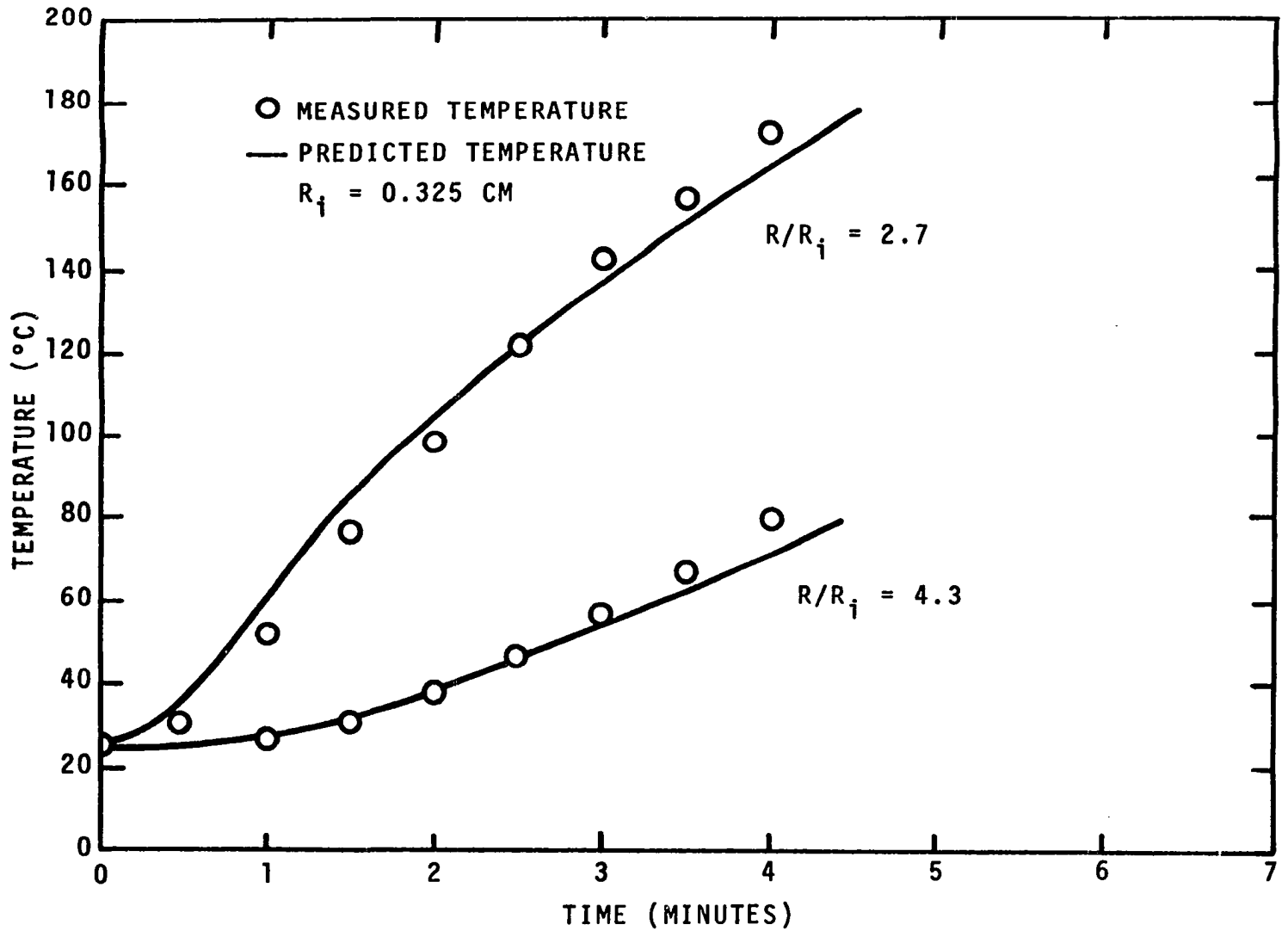

Figure II-27. Comparison of Measured and Predicted Temperature Profiles of White Pine at Two Radial Positions for Four Minute Run as Given by Havens (16).

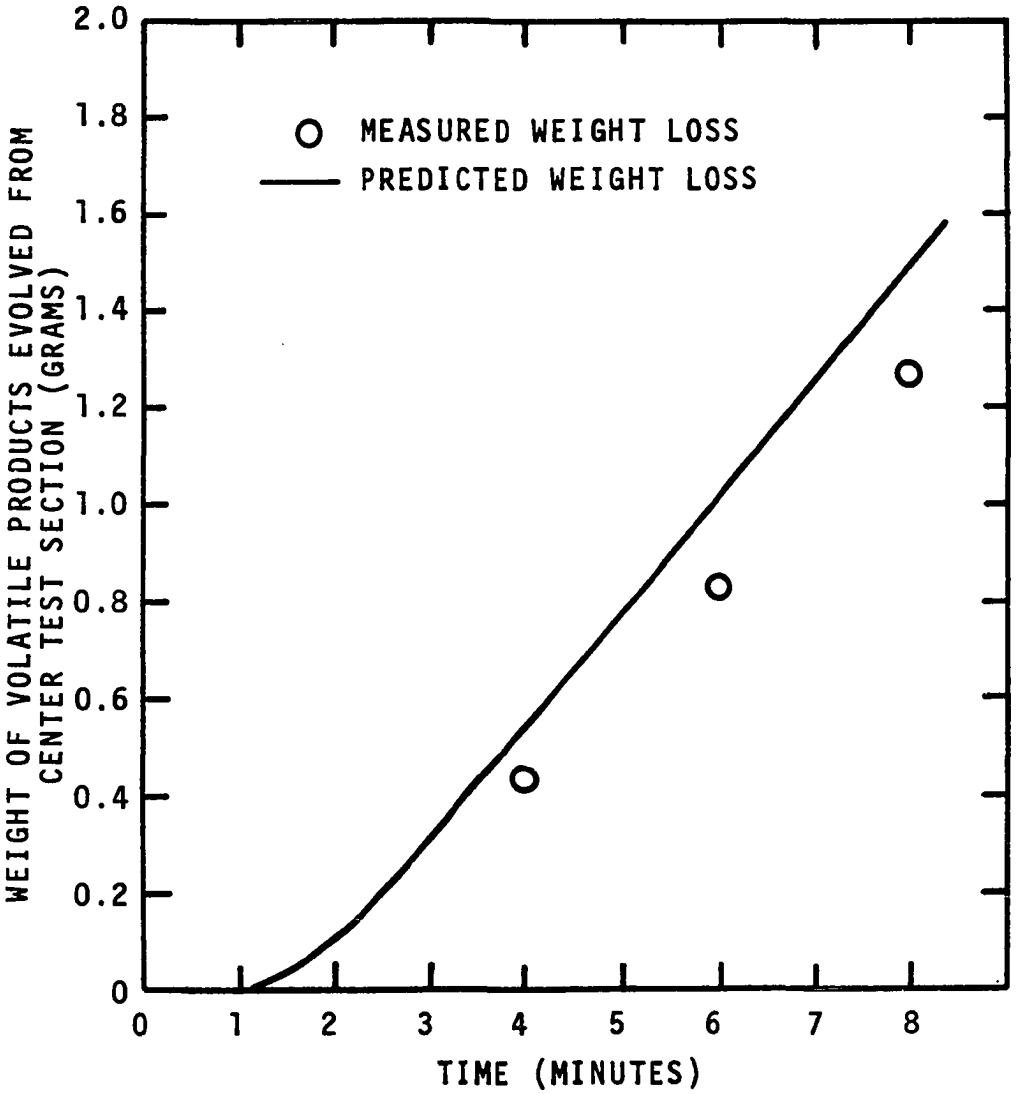

Figure II-28. Measured and Predicted Weight Loss of Pine Test Section as Given by Havens (16).

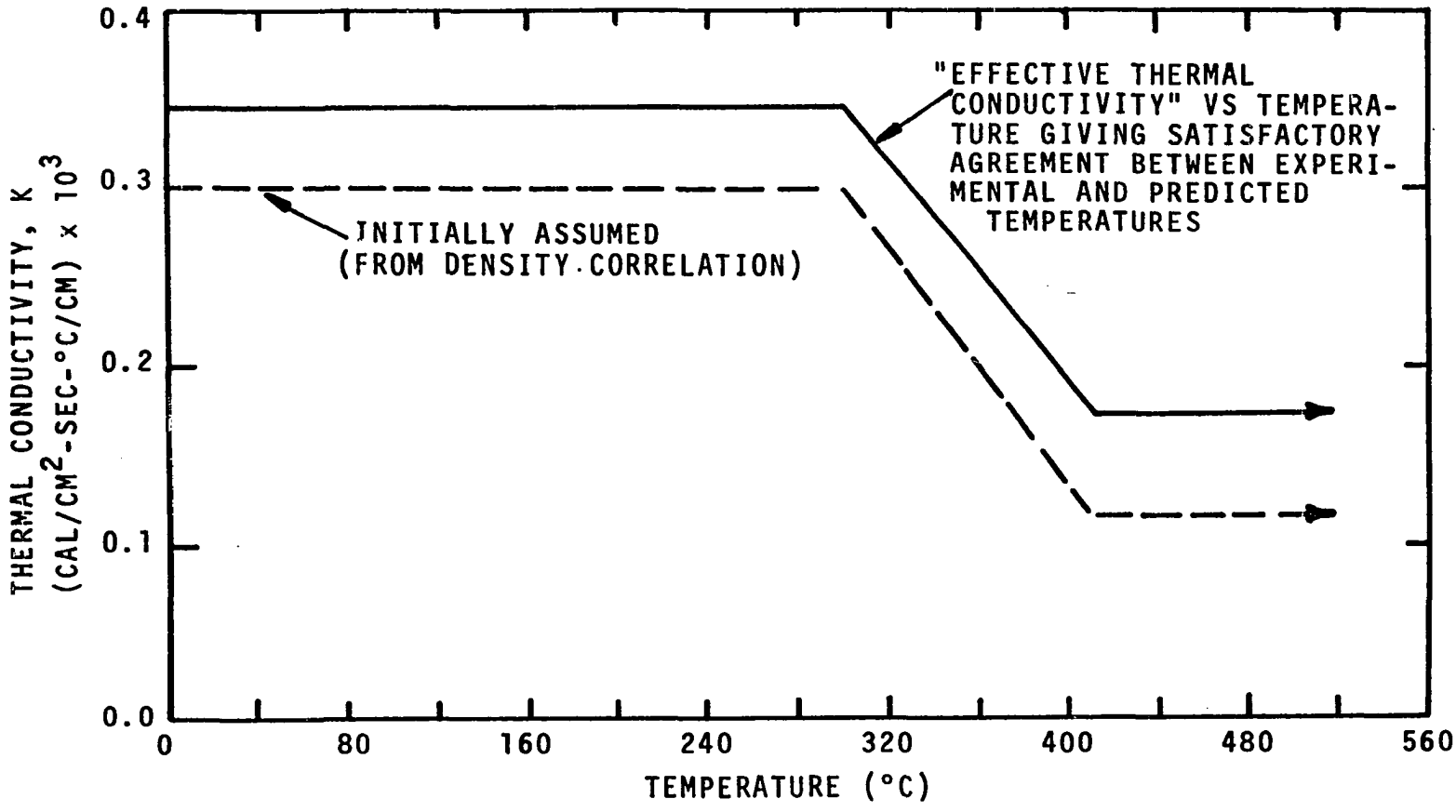

Figure II-29. Adjusted Thermal Conductivity Profile as Given by Havens (16).

TABLE II-11

SUMMARY OF MATHEMATICAL ANALOGS

Investigators	Mathematical Analog	Experimental Studies	Results and Conclusions
Bamford, Crank and Malan (4)	Model based on Fourier law of heat conduction with source term to account for heat of pyrolysis. Solved using finite difference method.	Exposed front and back surfaces of wood slab to flame. Measured time temperature profile at center of wood slab.	Compared center of wood to that predicted by model assuming wood thermal properties were constant during pyrolysis.
Weatherford and Sheppard (43)	Heat conduction model with internal energy balance. Heat of pyrolysis assumed to be a single value. Solved using finite difference method.	Measured time to ignition for wood slabs heated by convection.	Developed ignition criterion by comparing predicted temperature and ignition data. Neglect property changes in model.
Panton and Rittman (32)	Model based on Fourier law of heat conduction with internal heat balance. Accounts for the variation in thermal conductivity with pyrolysis. Solved using integral techniques.	None. Parametric study of the effect of hypothetical reaction schemes on predicted temperature profiles.	Present graphs of dimensionless time with temperature. Parameters of heat of pyrolysis, activation energies, etc.
Kanury (18) Kung (24)	Model based on Fourier law of heat conduction with source term for heat of pyrolysis considered effects of property changes and bulk flow. Solved using finite difference method.	Made kinetic calculations for pyrolyzing wood cylinders. Data not used in model.	Present graphs of dimensionless time with temperature and weight. Values for unknown properties were assumed and parametric plots prepared demonstrating the potential effect of these variables.
Havens (16)	Heat conduction model with internal energy balance. Heat of pyrolysis assume to be multivalued. Solved using predictor corrector technique.	Measure heat of pyrolysis and weight loss by independent means. These data used to compute temperature profiles in pyrolyzing wood cylinders.	Computed results were compared to experimental temperature profiles. Good agreement was obtained by adjusting the thermal conduction of wood and char.

CHAPTER III

EXPERIMENTAL PROCEDURES AND RESULTS

The experimental portion of this study was designed to provide the data needed to solve the mathematical analogs described in Chapter II. Experiments were undertaken to identify the reaction kinetics of wood pyrolysis, to measure the energy of pyrolysis, and to measure the thermal conductivity of wood char. Additionally transient temperature profiles in pyrolyzing wood were obtained for use in the modeling portion of this study.

Kinetics of Wood Pyrolysis at High Heating Rates

It is well known that at sample heating rates up to 10°C/min the pyrolysis mechanism for polymeric materials is usually independent of heating rate (heat history). At heating rates greater than 10°C/min it is generally found that the pyrolysis mechanism is altered and becomes heating rate dependent. The piloted wood ignition studies of Wesson (45) and Koohyar (23) have shown that a minimum surface heating rate of 30-40°C/min is required to ignite wood slabs. Surface heating rates in real fires of up to 1500°C/min are not uncommon. Akita has demonstrated that at heating rates up to

2°C/min the pyrolysis of wood is independent of heating rate. At higher heating rates the only data available are those of Havens who assumed that the pyrolysis reactions are independent of heating rate. Obviously, if this assumption is not true the "energy capacity" data of Havens obtained at 20°C/min does not necessarily represent the energy capacity of wood pyrolyzed at other heating rates. The applicability of "energy capacity" data obtained at 20°C/min to the heating rates at which ignition occurs can be partially deduced by demonstrating the dependence or independence of pyrolysis kinetics on heating rate.

Equipment

Weight loss data required for kinetic analysis were obtained using the Perkin-Elmer TGS-1 Thermobalance and UU-1 Temperature Control Unit shown in Figure III-1. The Perkin-Elmer TGS-1 sample holder, furnace, and weight assemblies are schematically shown in Figure III-2. The weight mechanism is a Cahn-RG Electrobalance and is located inside the glass vacuum bottle seen in Figure III-1. The Electrobalance is of the null-counter balance type and is designed for weight measurements from 0.1 to 200 mg. The Electrobalance generates a continuous signal proportional to weight during a test run which can be recorded as weight or can be internally differentiated with respect to time and then recorded. The recorder used in this study was a Texas Instrument Servowriter-II.

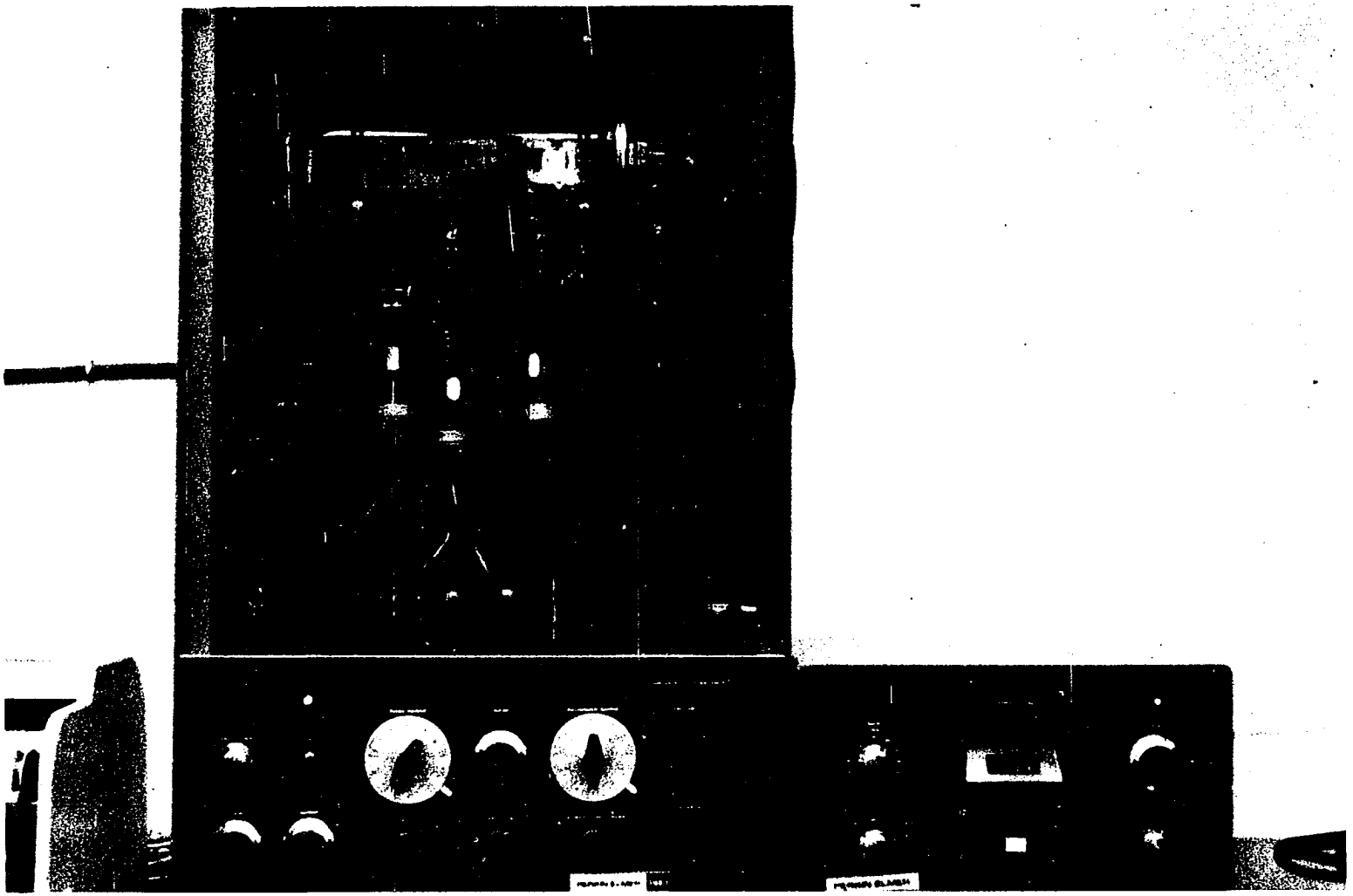

Figure III-1. Perkin-Elmer TGS-1 Thermobalance and UU-1 Temperature Controller.

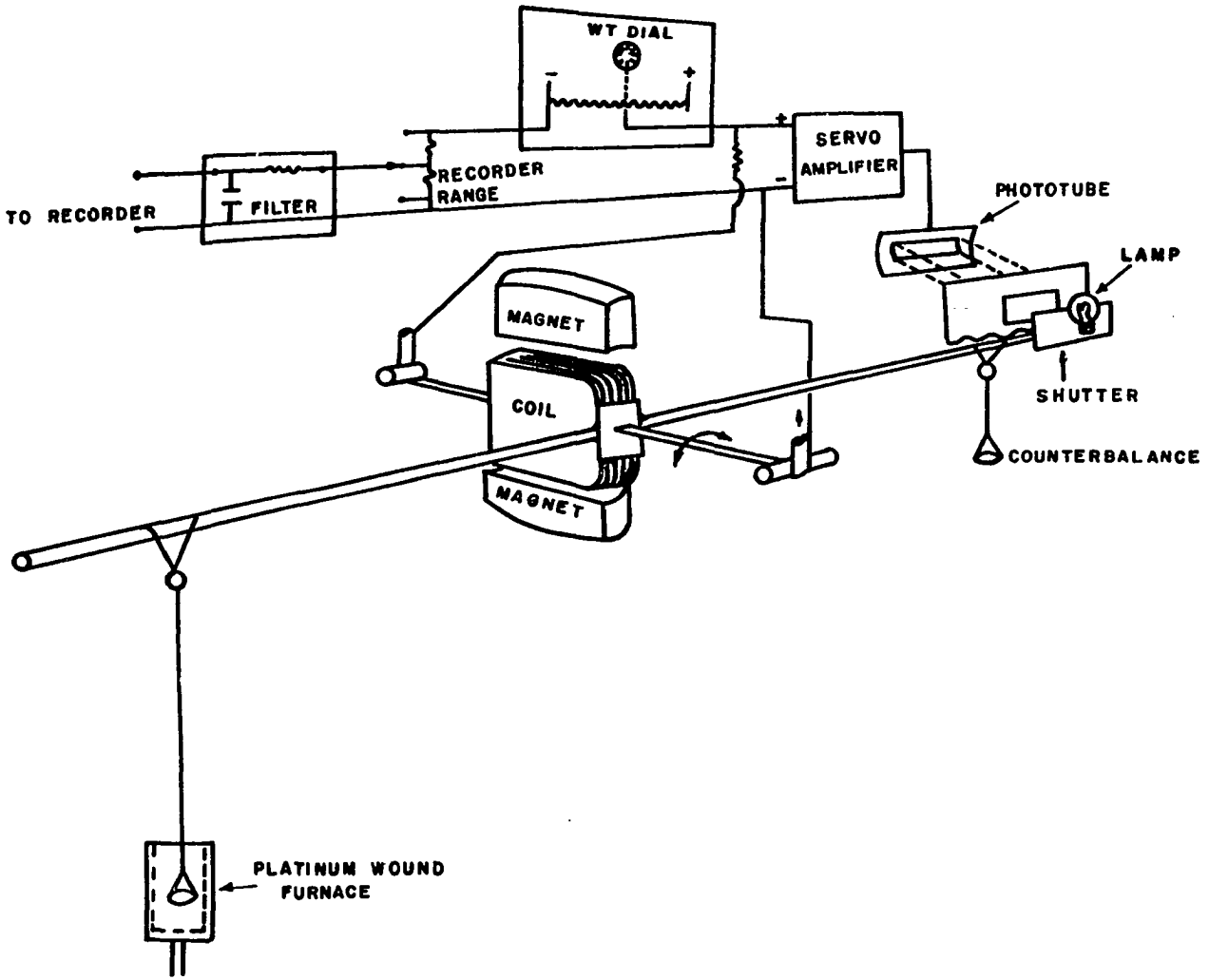

Figure III-2. Schematic of Perkin-Elmer TGS-1 Furnace and Weigh Assembly.

One of several unique features of the Perkin-Elmer TG system is that the sample is suspended from the Electrobalance weighing arm by a "hang-down" wire sufficiently long to permit complete insertion of the sample pan into the furnace. Other thermobalance manufacturers use the Cahn-Electrobalance; however, they insert both the sample and weighing arm directly into the furnace. With respect to this practice the Cahn-Electrobalance instruction manual of September 1, 1965 states "...The universal experience of other microbalance builders has been that even a minute amount of stray radiation can cause significant error, especially when it falls unsymmetrically on the two halves of the balance beam.... It seems extremely courageous to insert deliberately one-half of a balance beam into a furnace, whose temperature not only varies but may vary as much as 1,000°C during a run..."

The Perkin-Elmer TG furnace is called a microfurnace to distinguish it from the massive block furnaces used in other TG systems. The size of the microfurnace minimizes inertial heating effects and allows for heating rates of up to eight times faster than block heaters. The furnace is heated by a platinum wire wound around the furnace such that the wire acts as both a heating element and a thermometer for control of furnace temperature. Other TG systems have a thermocouple located in the sample with lead wires running from the sample pan to a junction. Special care must be taken when using this method to avoid interfering with the weighing mechanism.

The platinum wires wound around the furnace are coated with a thin film of insulating material. It was found in this work that the insulation failed after several heating cycles; when pyrolysis products were evolved from the furnace, they condensed on the platinum wires causing a short where the insulation failed. The Perkin-Elmer Corporation made available a modified furnace having a ceramic collar fitted over the furnace as shown in Figure III-3a. It was found that this furnace also failed after only a few tests due to the flow patterns in the test cell as shown in Figure III-3b. It was found at this laboratory that by placing a quartz wool plug around the base of the furnace and inside the collar the flow of volatiles under the collar and onto furnace heating elements was blocked. This modification increased furnace operational life from approximately 20 to 90 heating cycles.

The furnace temperature and heating rate were controlled with a Perkin-Elmer UU-1 Temperature Control Unit. This programmer permits selection of heating rates from 0.3 to 160°C/min. The selector switch also has a 320°C/min position; however, the power supply to the furnace is not sufficient to maintain that heating rate. The programmer is equipped with a digital temperature indicator; it also actuates a temperature marker on the weight recorder.

The unique heat transfer characteristics of a microfurnace require that each furnace be temperature calibrated.

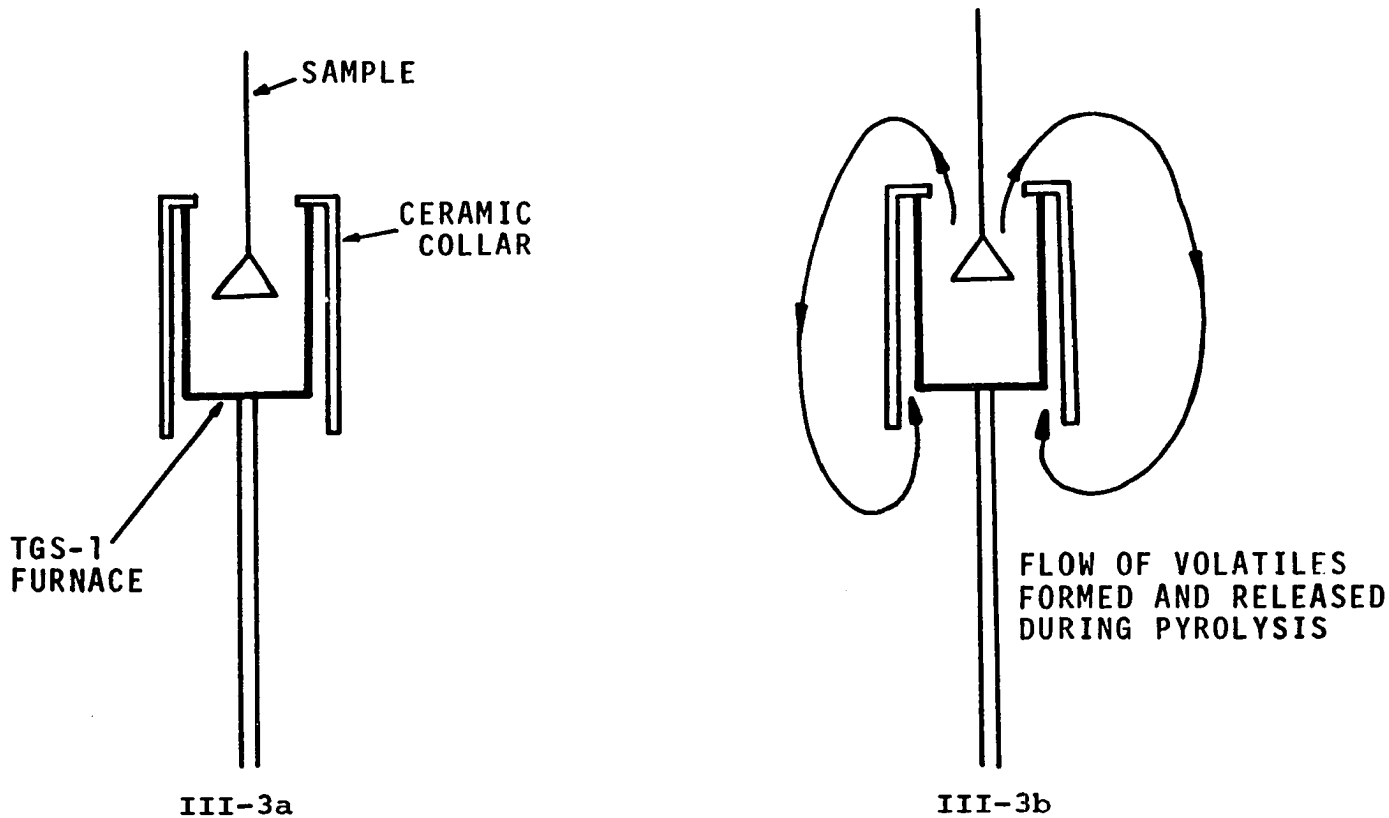

Figure III-3. Modified Thermobalance Furnace.

Perkin-Elmer has developed a furnace calibration method based on the use of reversible magnetic transitions in ferromagnetic alloys. In this technique small samples of several ferromagnetic elements and alloys are placed in a sample pan along with a small amount of aluminum oxide (Al_2O_3). A magnet is positioned around the sample hang-down tube at a level below the pan as shown in Figure III-4. The ferromagnetic standard samples exert a downward component of magnetic force on the sample pan, and this force will register as an apparent weight. As the furnace temperature is programmed upward, each of the ferromagnetic materials loses its ferromagnetism at a repeatable temperature called the magnetic transition temperature. The furnace can be temperature calibrated by comparing the known magnetic transition temperatures against the programmer digital output.

A set of magnetic standards are available for temperature calibration of the TGS-1b furnace over the full operating range of the unit. These metals are listed in Table III-1 along with their respective "Curie transition" and "magnetic" transition temperatures. The Curie point temperatures shown in Table III-1 are those originally published by Perkin-Elmer for the metals shown. Based upon careful reexamination of the magnetic transition temperature for these metals, Perkin-Elmer published a revised set of Curie point temperatures which they entitled magnetic transition temperatures.

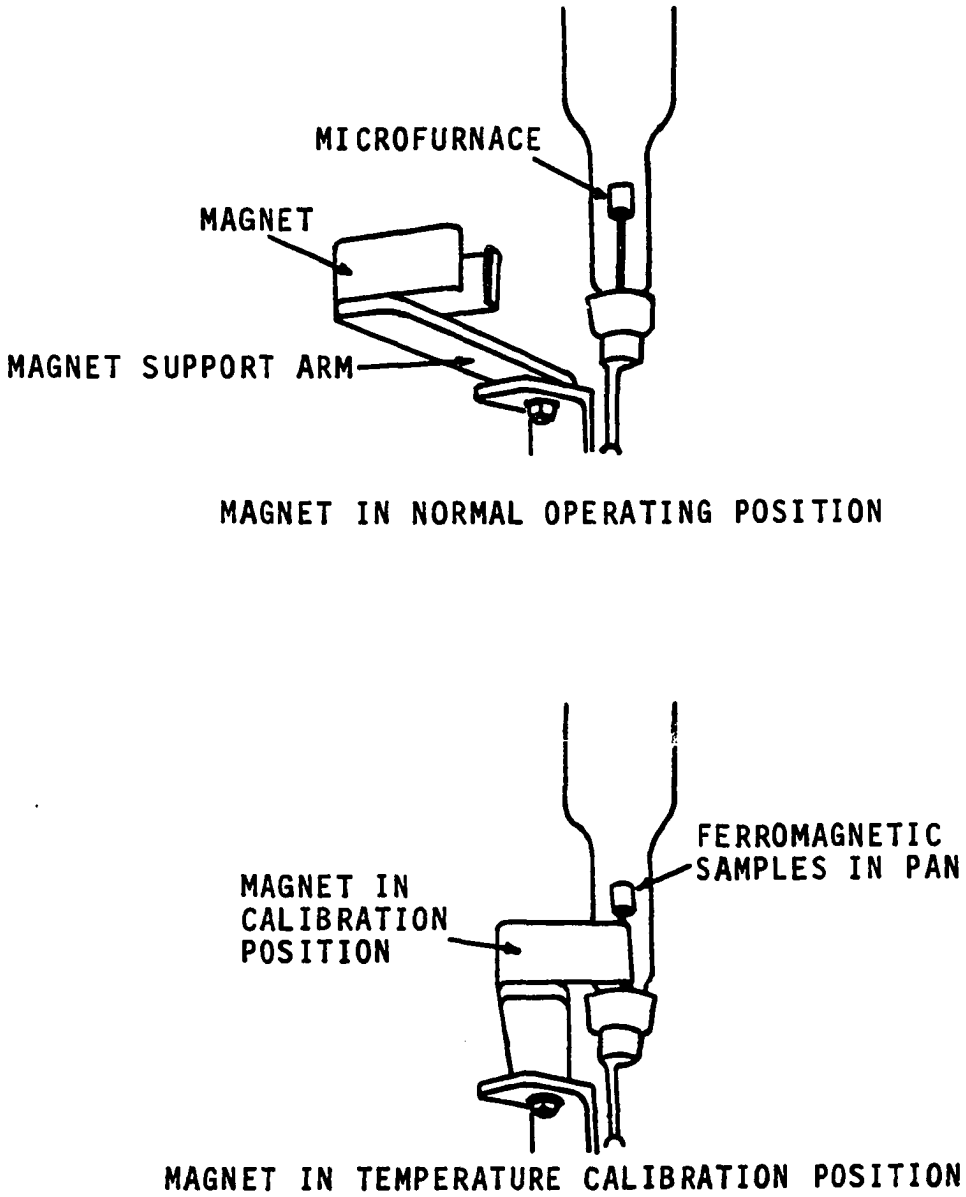

Figure III-4. Schematic of TGS-1 Temperature Calibration System.

TABLE III-1

MAGNETIC STANDARDS FOR TGS-1B FURNACE CALIBRATION

Metal	Curie Point Temperature °C	Magnetic Transition Temperature
Monel	65	65
Alumel	158	163
Nickel	358	354
Numetal	390	393
Nicoseal	445	438
Perkalloy	598	596
Iron	786	780
Hi-Sat 50	994	1000

Ideally the programmer-furnace temperature calibration should be linear over the range from 25°C to 1,000°C. The manufacturer claims that at a programmed heating rate of 20°C per minute a calibration can be obtained having a maximum error of ± 10°C over the instrument's full temperature range. In this study it was found that the instrument could be calibrated well within the temperature range of interest, 25°C to 700°C. (Note that the programmer used in this study is not the same as that used by Havens.) Instrument calibration was done at a programmed heating rate of 40°C/min using alumel, nickel, nicoseal and Perkalloy. Temperature calibration curves for all the heating rates studied are shown in Figure III-5.

Experimental Procedure and Data

Weight loss data for the pyrolysis of white pine and oak woods were obtained at programmed heating rates of 10, 20,

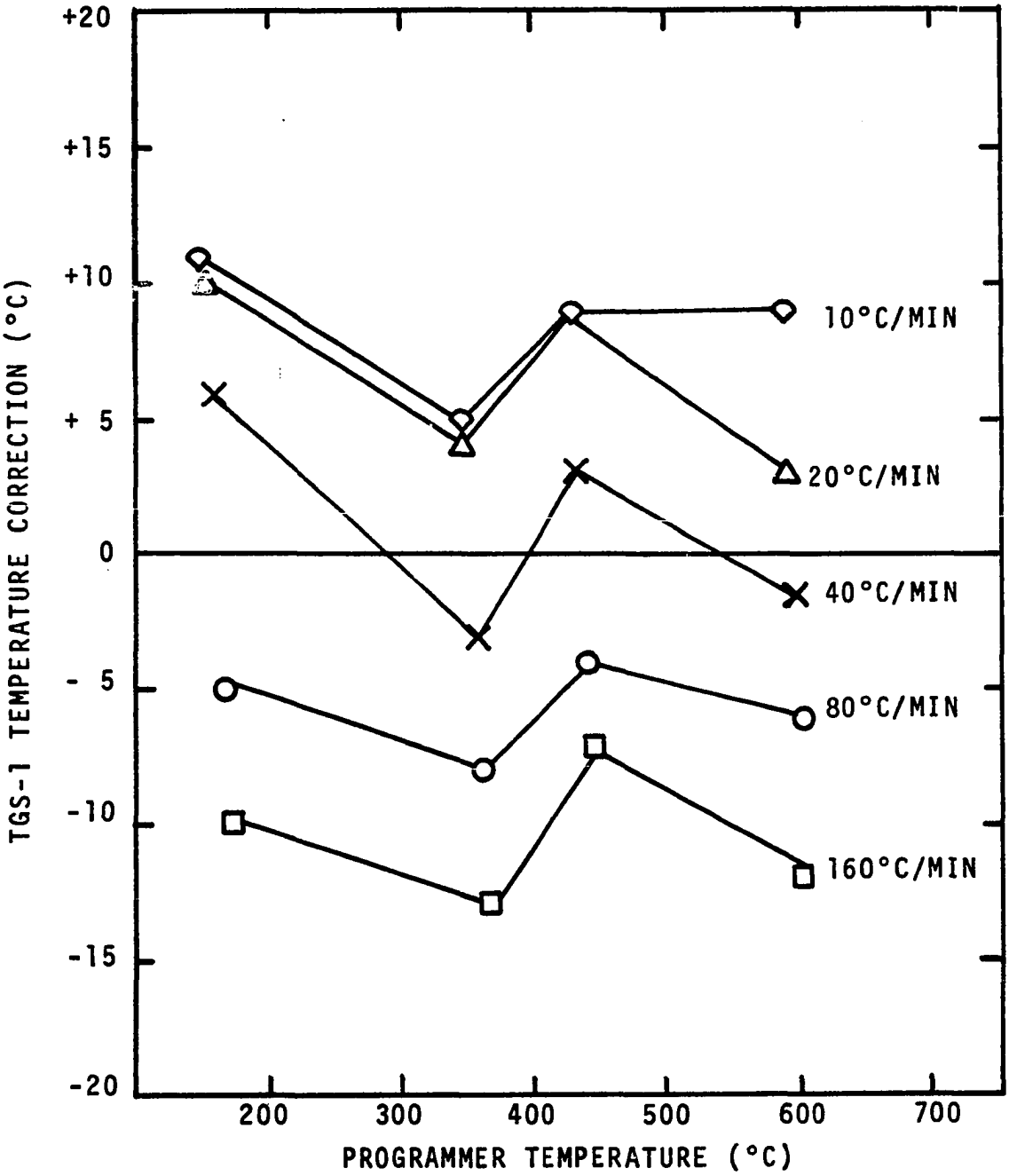

Figure III-5. Temperature Calibration Curves for TGS-1 Furnace.

40, 80 and 160°C/min. The samples used were cut from knot-free boards, were milled and were passed through a 40 mesh screen before being pyrolyzed.

At the beginning of each day the Cahn-Electrobalance was calibrated using calibration weights. Then, a furnace temperature calibration was made at the heating rate of interest. After temperature calibration, a sawdust sample 2-5 mg in size was placed in a platinum pan and suspended on the hang-down wire. The furnace was centered around the sample and the system was purged with nitrogen to remove all oxygen from the vacuum bottle. After five minutes purging, the nitrogen flow rate was adjusted to 40 ml/min and the temperature programmer actuated. At the completion of each run the furnace temperature was held at 700°C, and air was allowed to flow into the bottle to oxidize carbon deposits on the furnace. At each heating rate and for each wood at least five runs were made. The first and fifth runs consisted of obtaining and duplicating the furnace temperature calibration using the magnetic standards. Weight loss thermograms for wood pyrolysis were obtained in the second and fourth runs. In the third run the Cahn-Electrobalance was placed in the differential mode and a wood pyrolysis rate of weight loss thermogram was obtained.

Weight loss data and the derivative of weight loss with respect to time for pine are shown in Figures III-6 through III-10 and for oak in Figures III-11 through III-15.

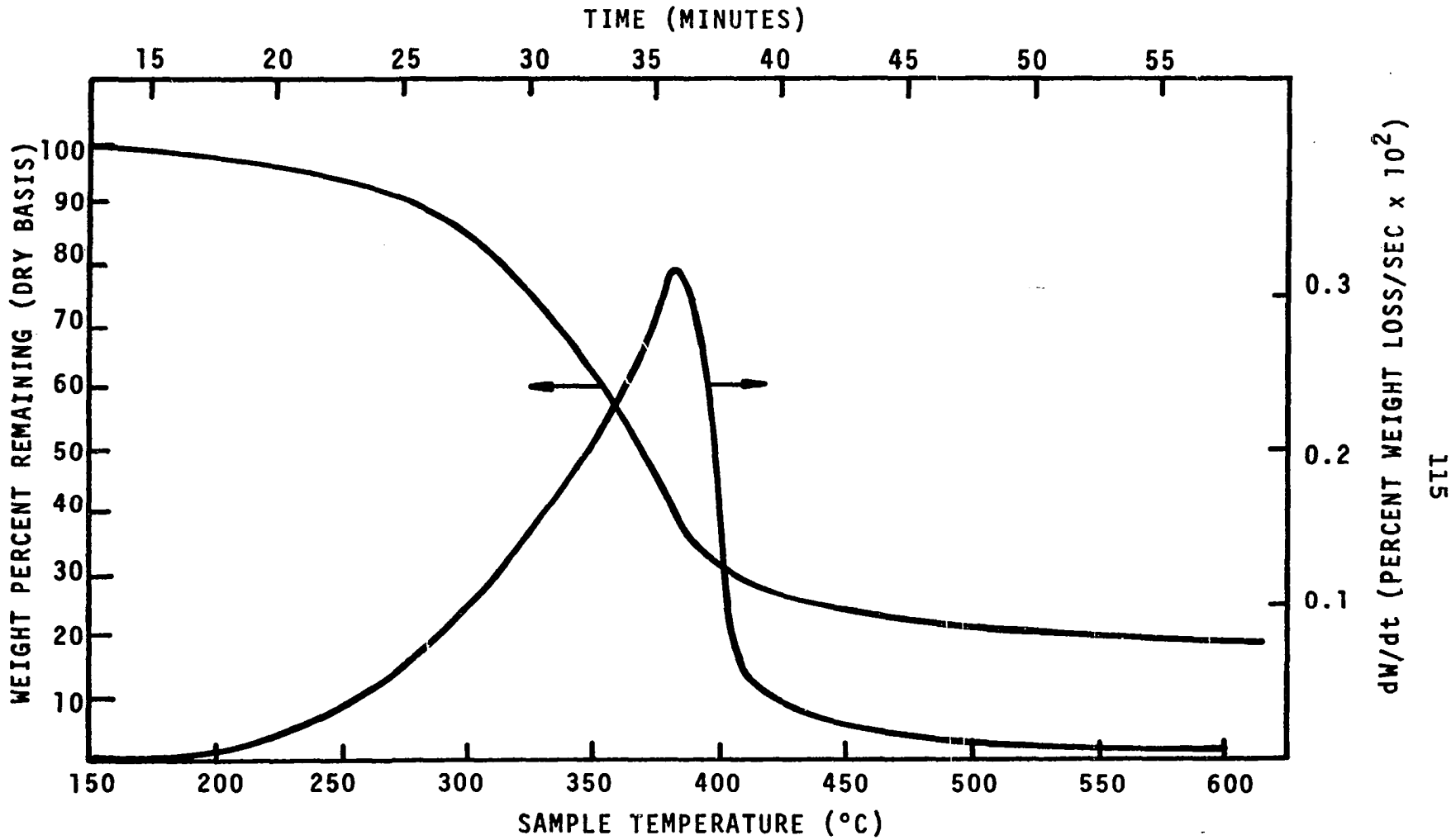

Figure III-6. TG and DTG Curves for White Pine at a Nominal Heating Rate of 10°C/min.

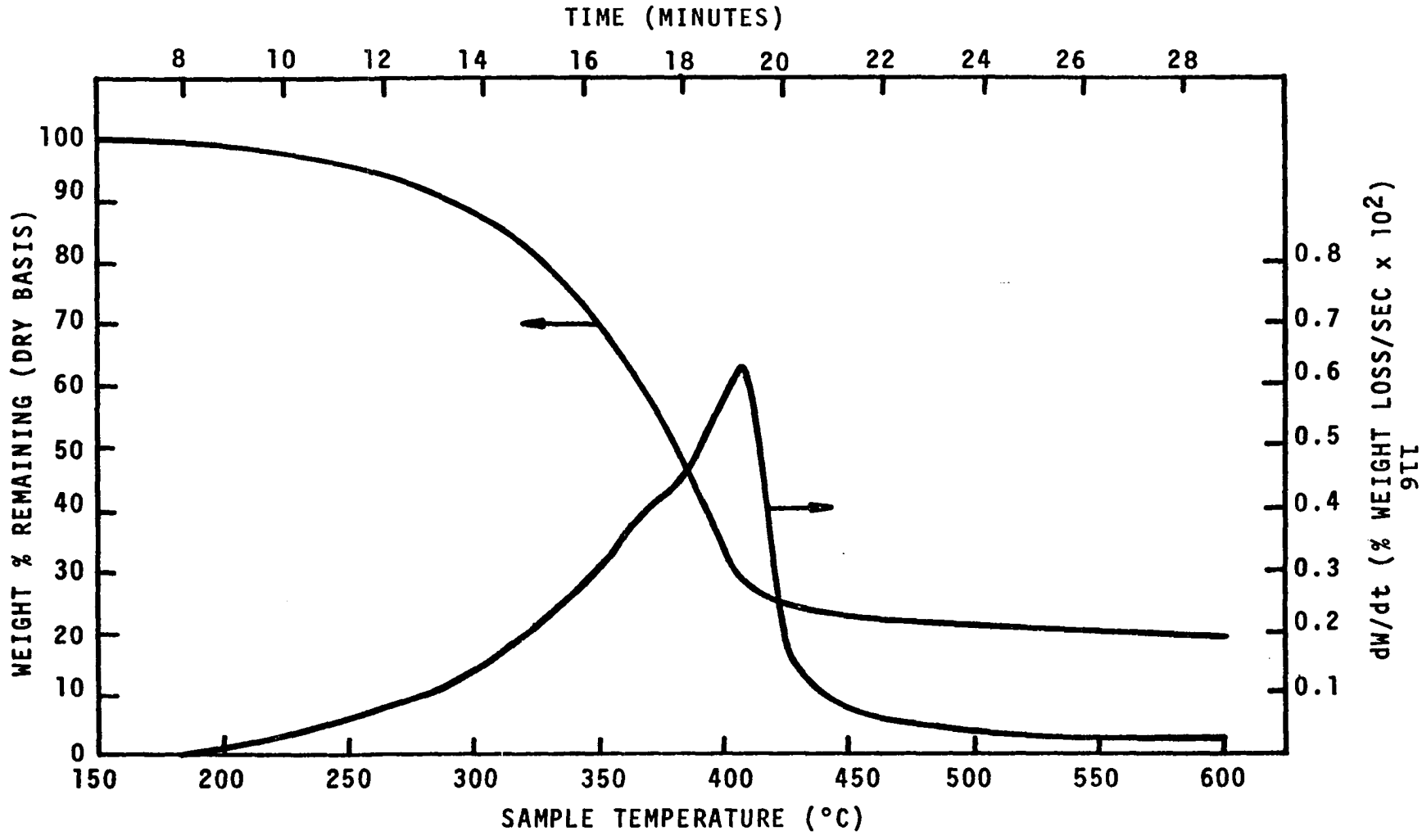

Figure III-7. TG and DTG Curves for White Pine at a Nominal Heating Rate of 20°C/min.

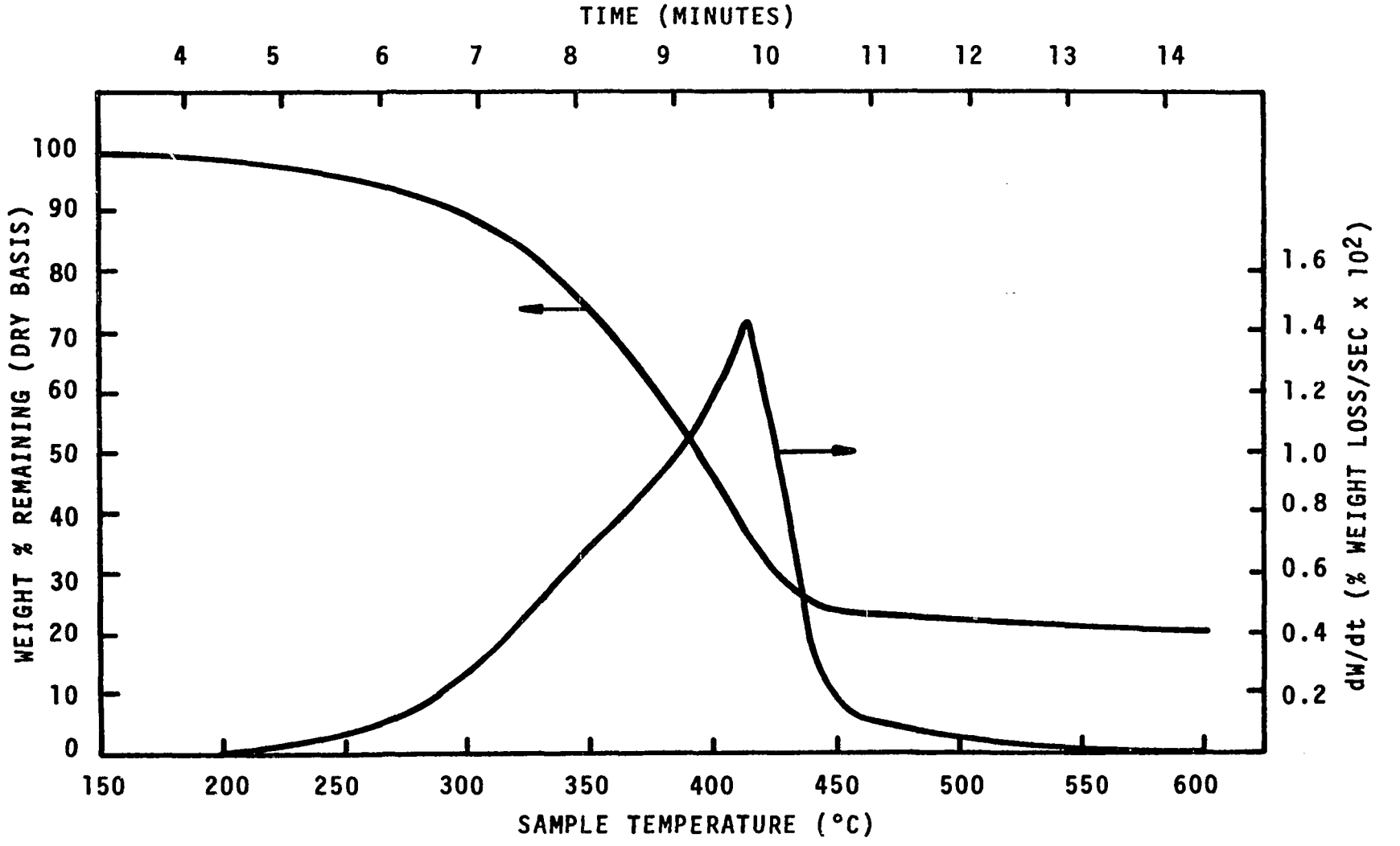

Figure III-8. TG and DTG Curves for White Pine at a Nominal Heating Rate of 40°C/min.

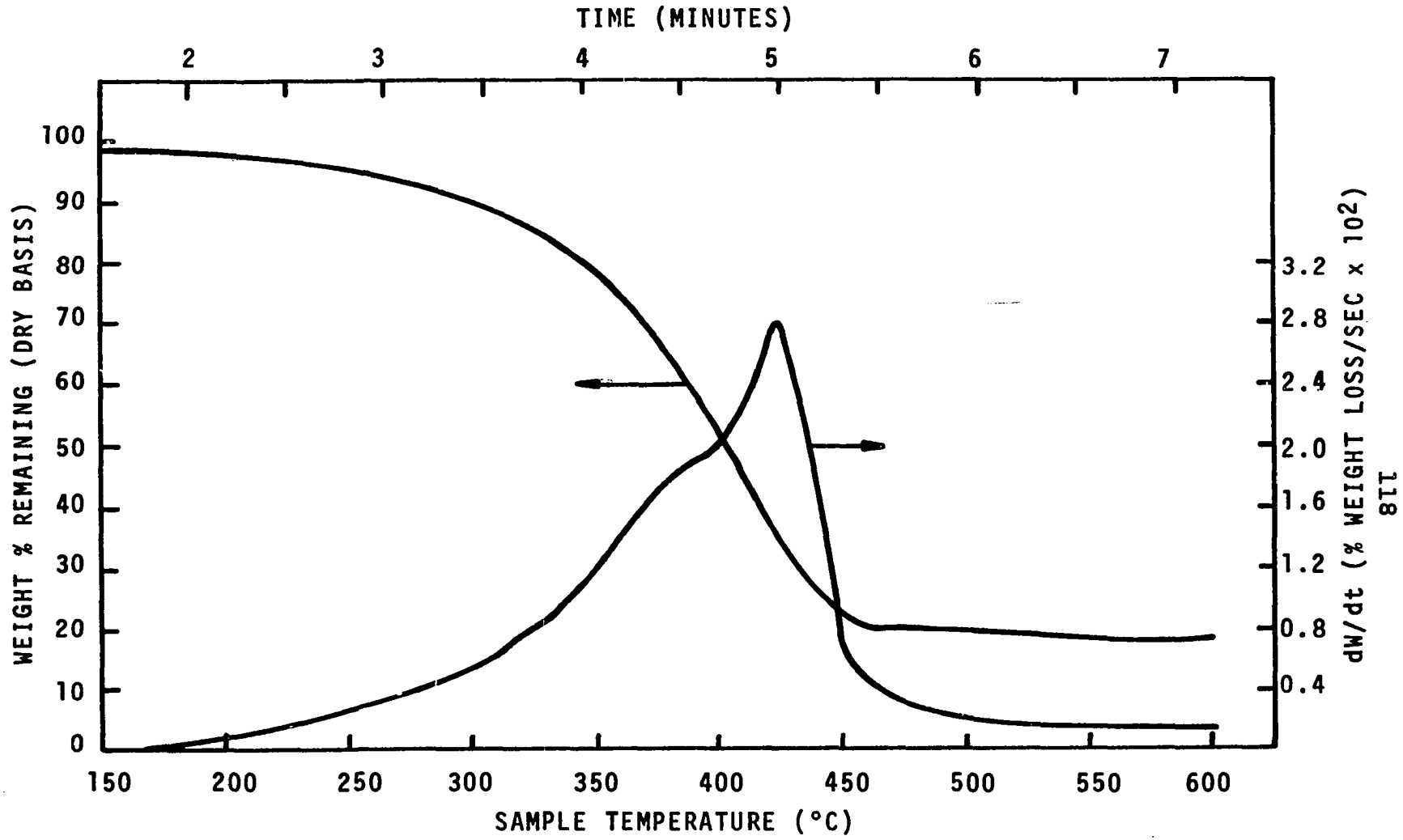

Figure III-9. TG and DTG Curves for White Pine at a Nomianl Heating Rate of 80°C/min.

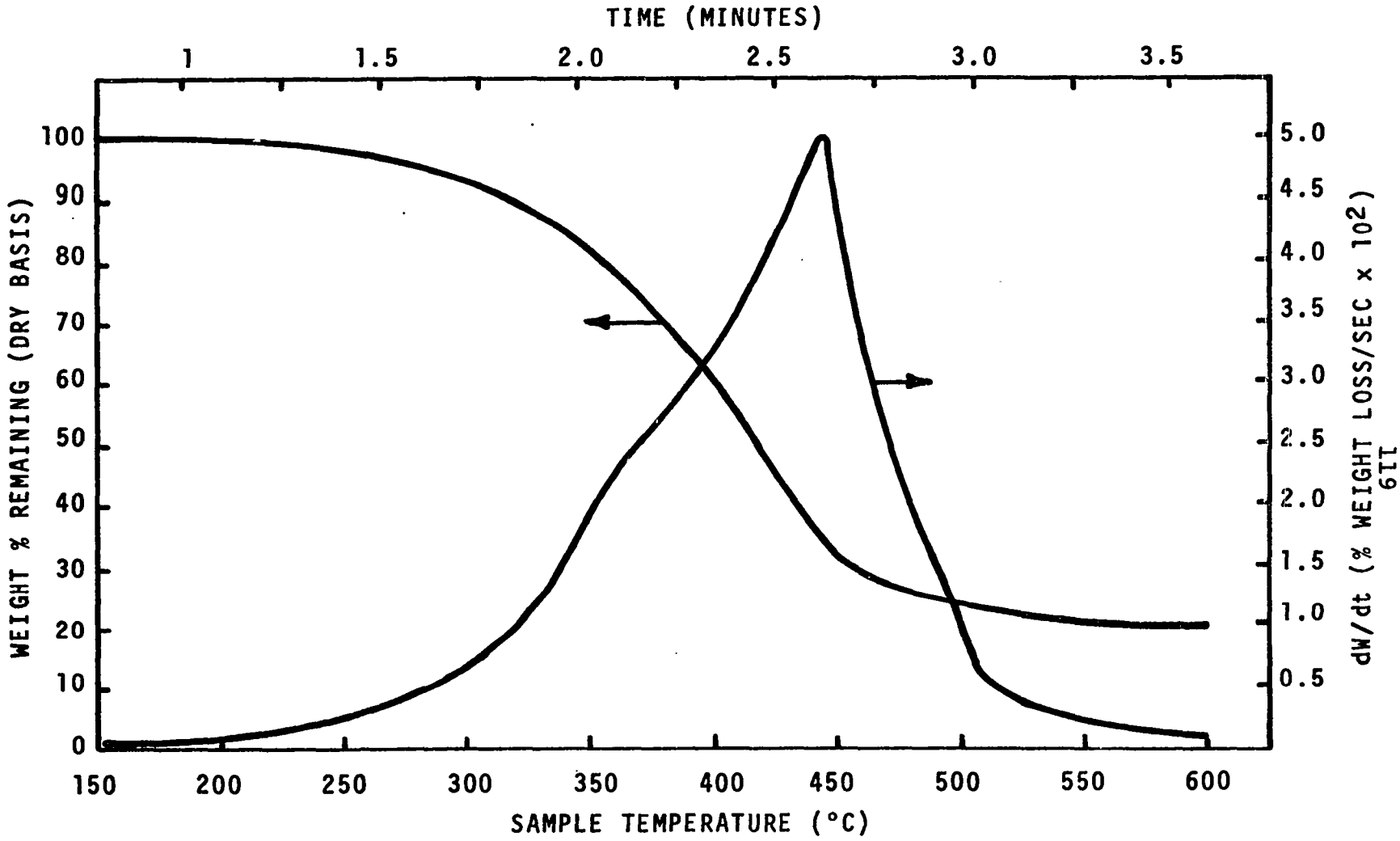

Figure III-10. TG and DTG Curves for White Pine at a Nominal Heating Rate of 160°C/min.

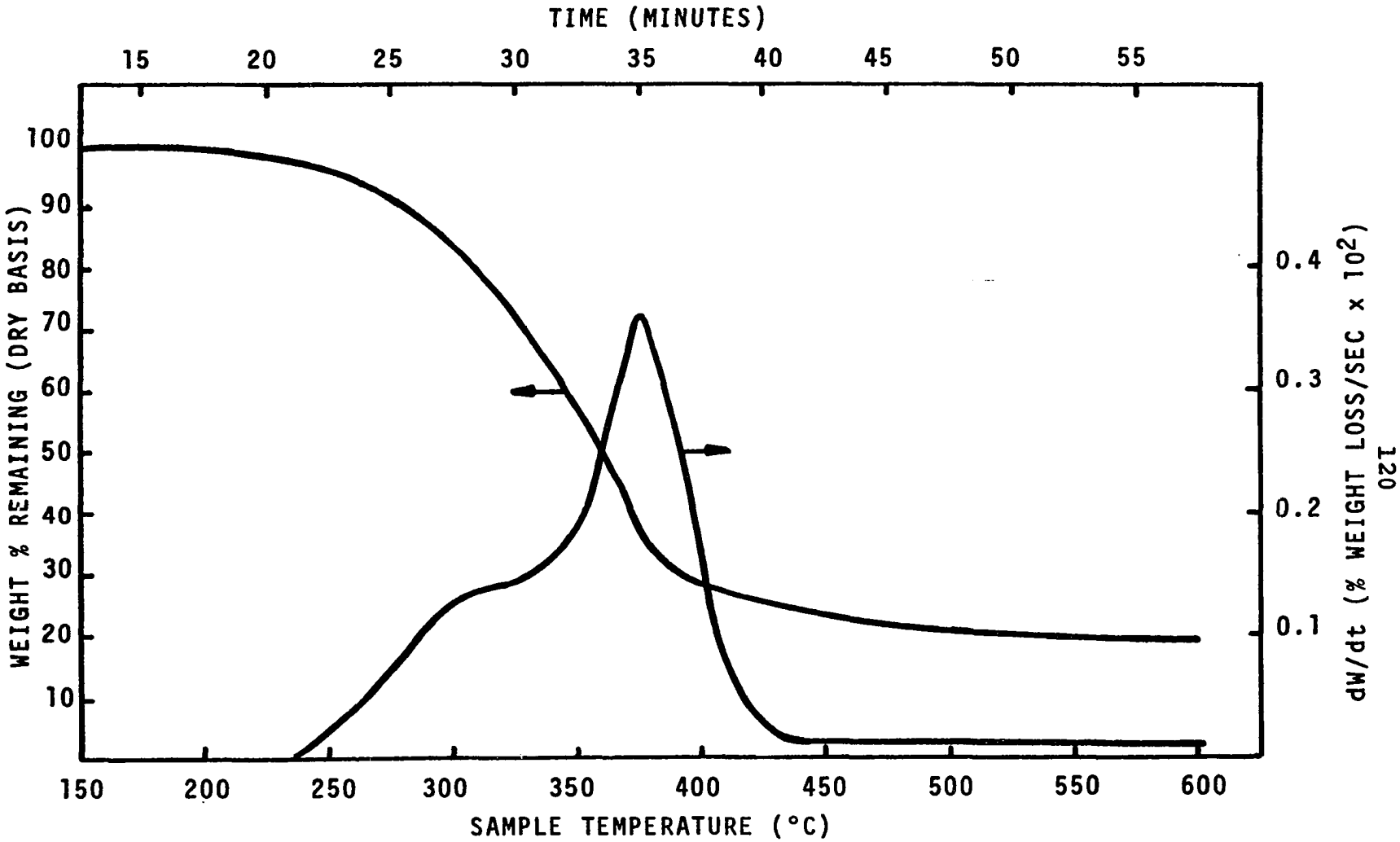

Figure III-11. TG and DTG Curves for Oak at a Nominal Heating Rate of 10°C/min.

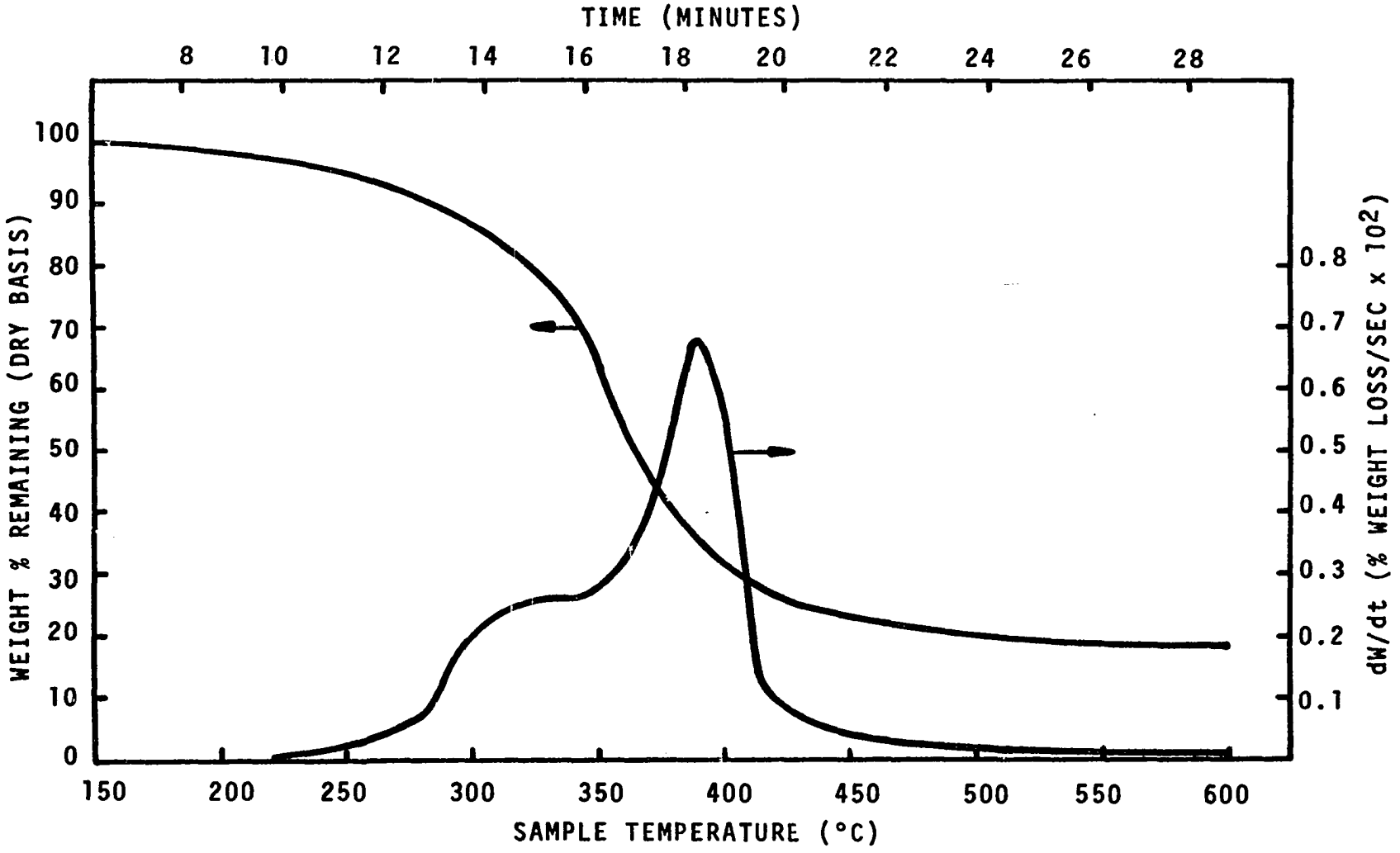

Figure III-12. TG and DTG Curves for Oak at a Nominal Heating Rate of 20°C/min.

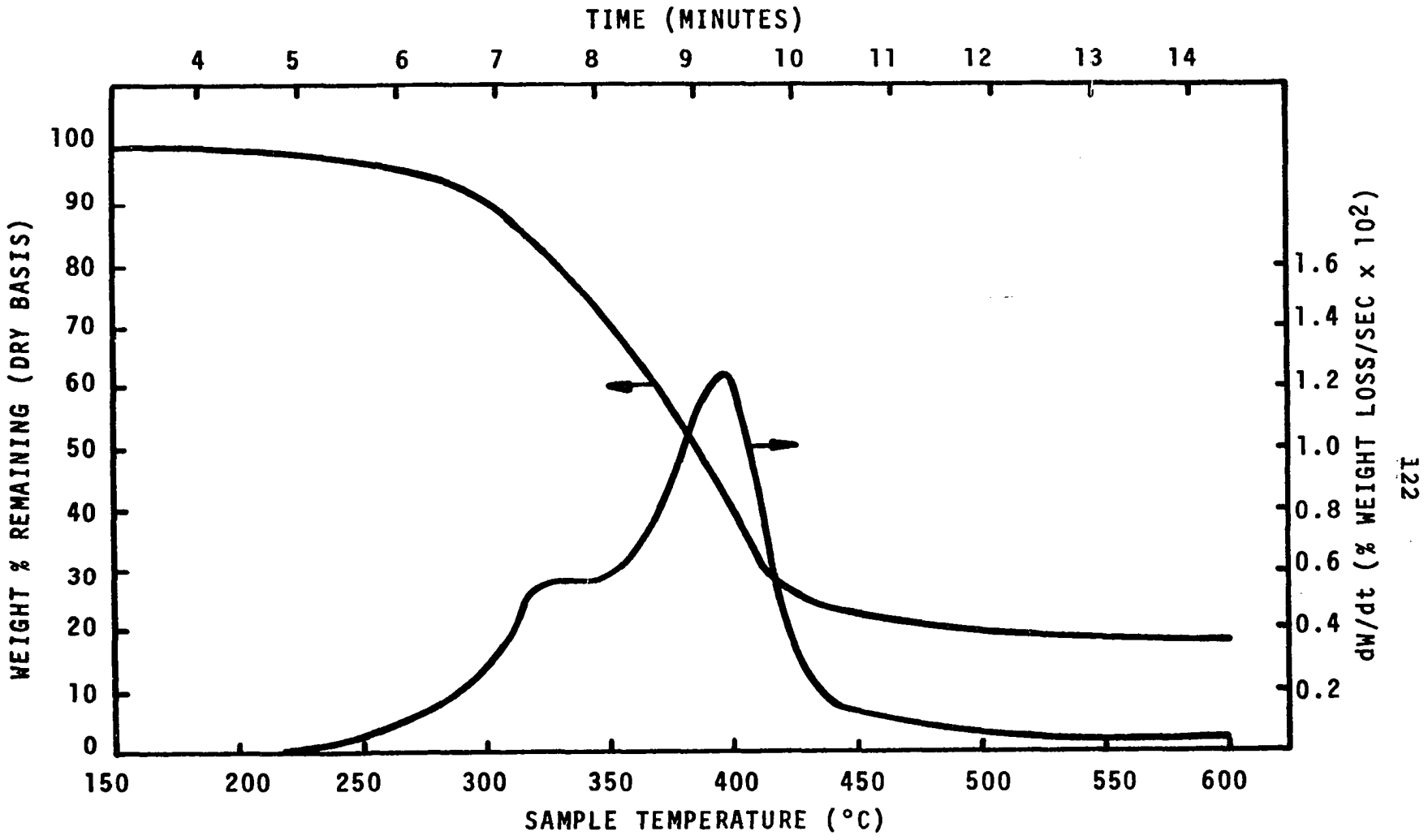

Figure III-13. TG and DTG Curves for Oak at a Nominal Heating Rate of 40°C/min.

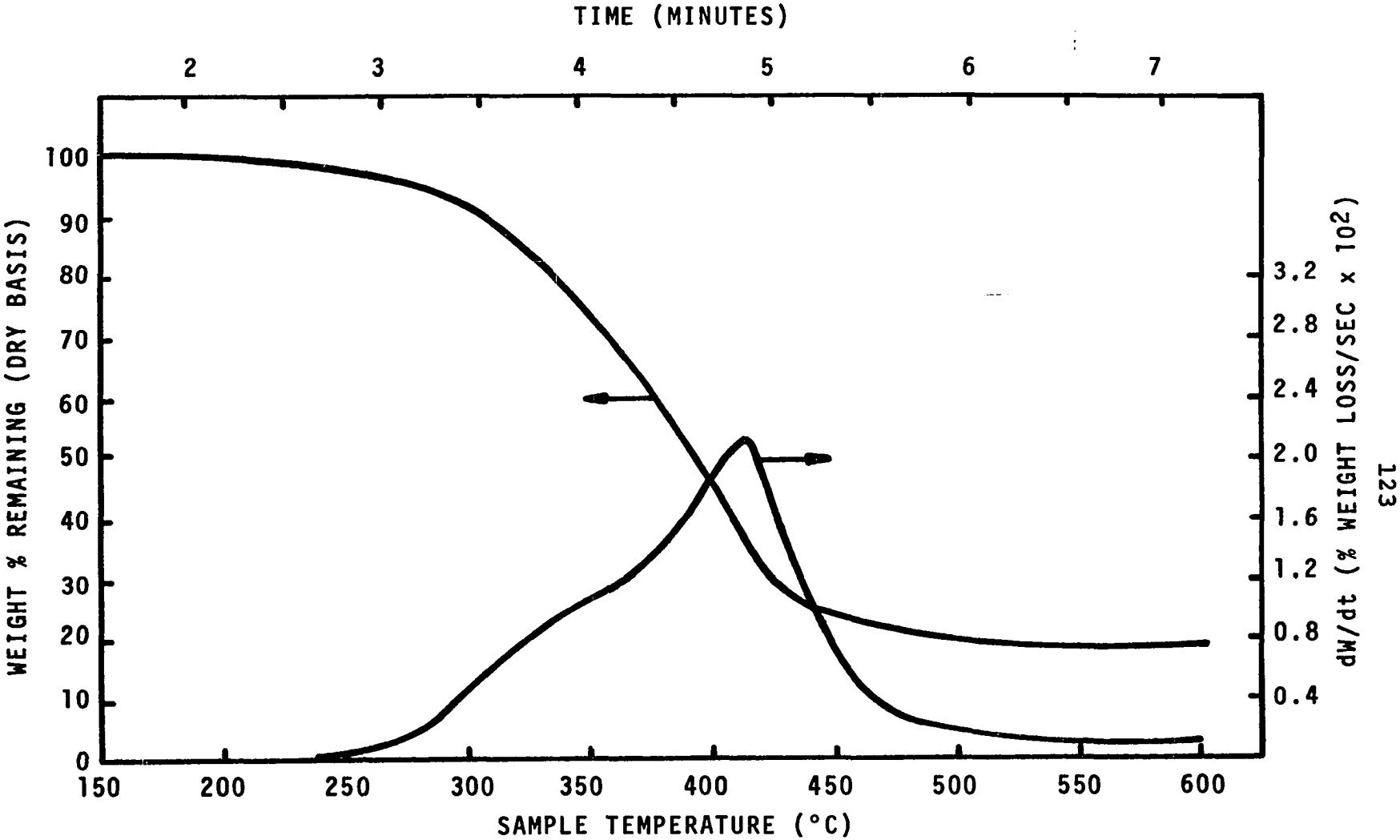

Figure III-14. TG and DTG Curves for Oak at a Nominal Heating Rate of 80°C/min.

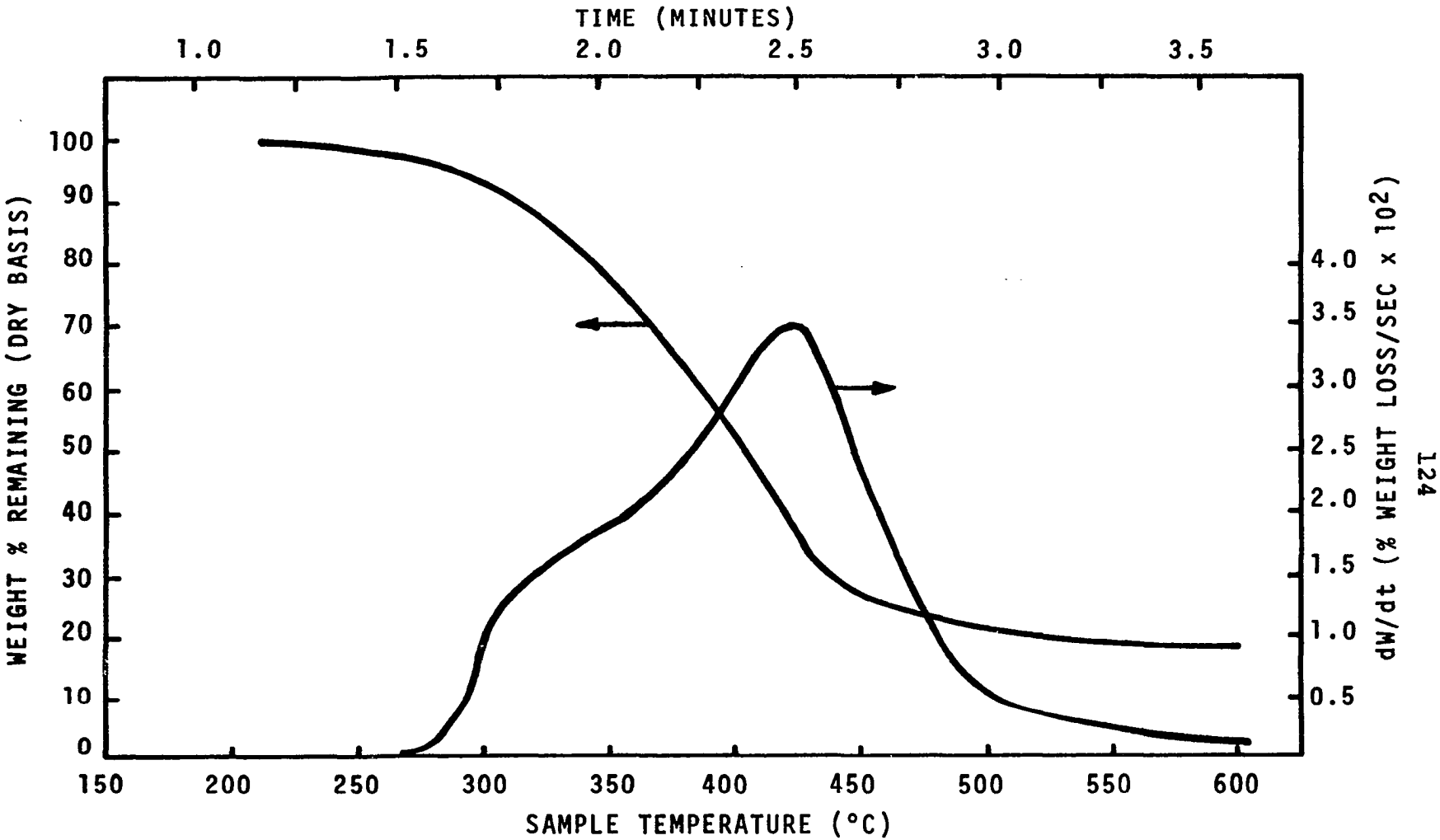

Figure III-15. TG and DTG Curves for Oak at a Nominal Heating Rate of 160°C/min.

The data are nearly identical to that obtained by Havens both with respect to the form of the curves and their location. It is of interest to note that the value for final weight remaining is dependent on the quantity of air in the vacuum bottle. As an example, Figure III-16 shows the weight loss curve for a white pine sample pyrolyzed in air at 20°C/min. A comparison of weight loss curves for pyrolysis of wood in air and in pure nitrogen indicates that the weight loss thermograms are similar until approximately 20 weight percent of the sample remains, at which time the char beings to oxidize in the air atmosphere. Figures III-17 and III-18 show that as heating rate is increased the TG curves are displaced to higher temperatures.

Analysis of Data

Goldfarb, McGuchan, and Meeks (13) have proposed a new technique for extraction of kinetic parameters from TG data obtained at multiple heating rates. The technique is developed assuming the decomposition obeys a rate law of the form given in Equation III-1.

$$\frac{1}{(W_o - W_f)} \frac{dW}{dt} = k_o e^{-E/RT} F(W) \qquad \text{III-1}$$

where W = sample weight (mg)

W_o = initial sample weight (mg)

W_f = final sample weight (mg)

t = time (sec)

k_o = frequency factor (sec^{-1})

E = activation energy (cal/gmole)

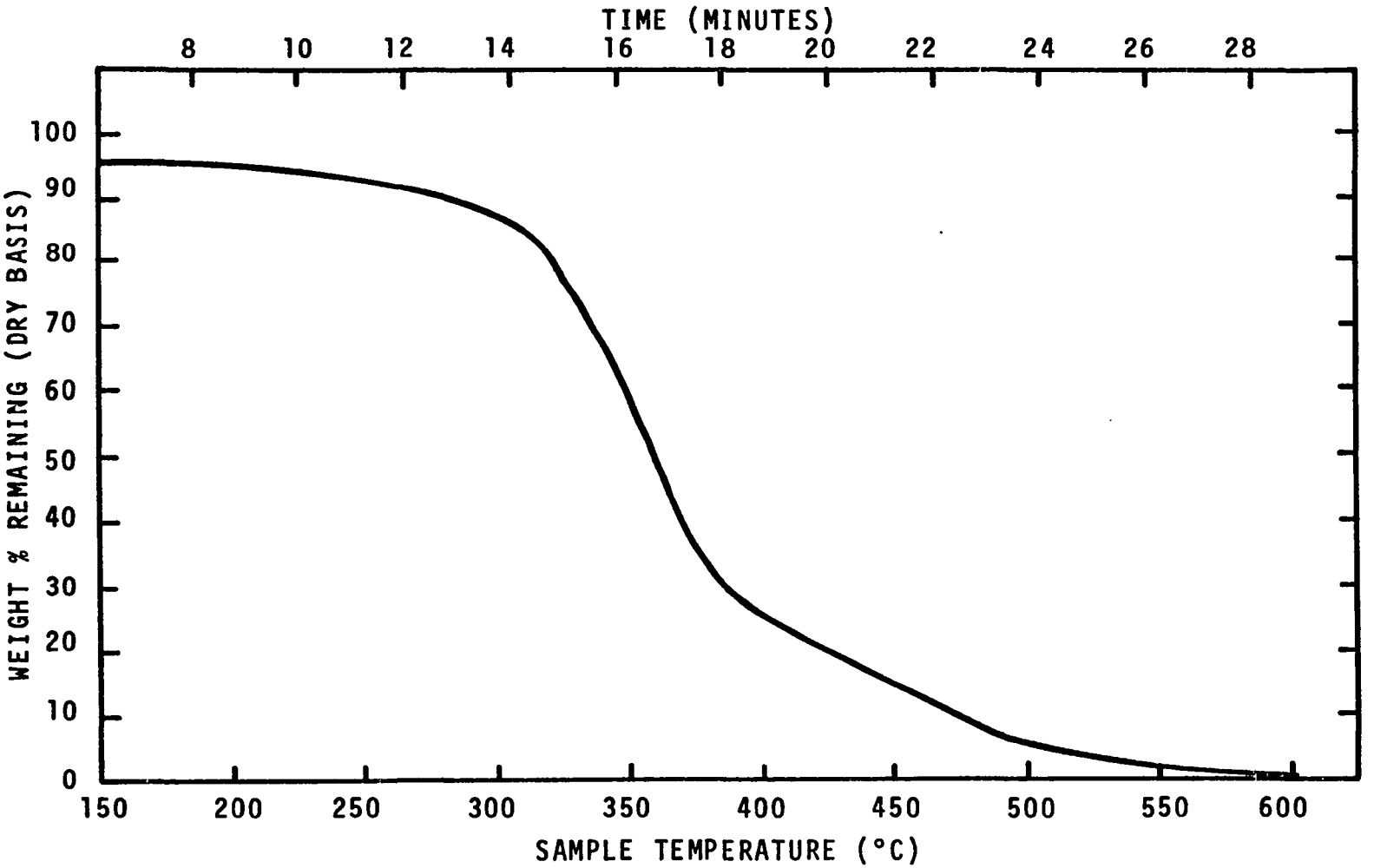

Figure III-16. TG Curve for White Pine in an Air Atmosphere at a Nominal Heating Rate of 20°C/min.

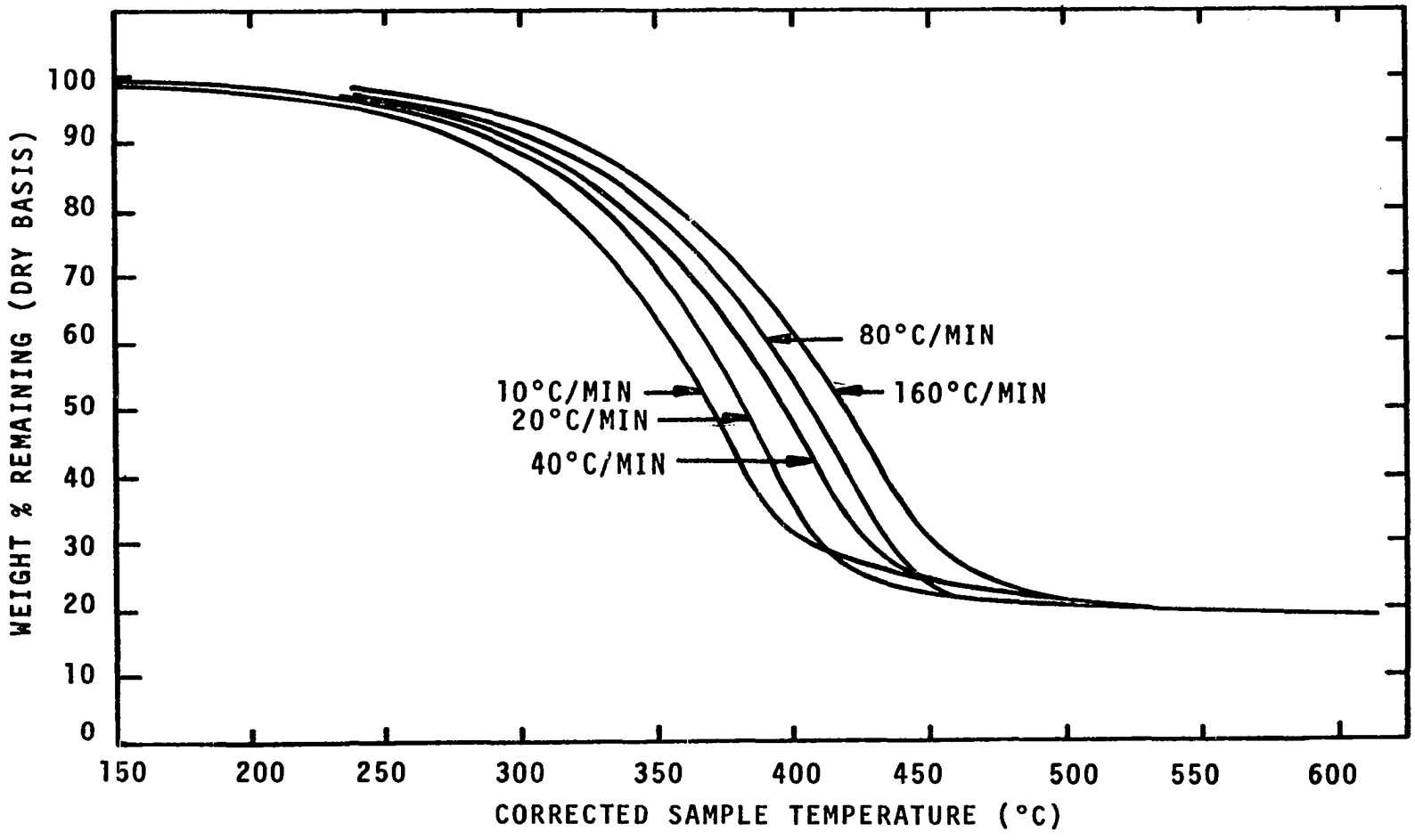

Figure III-17. Summary of TG Curve for White Pine in a Nitrogen Atmosphere.

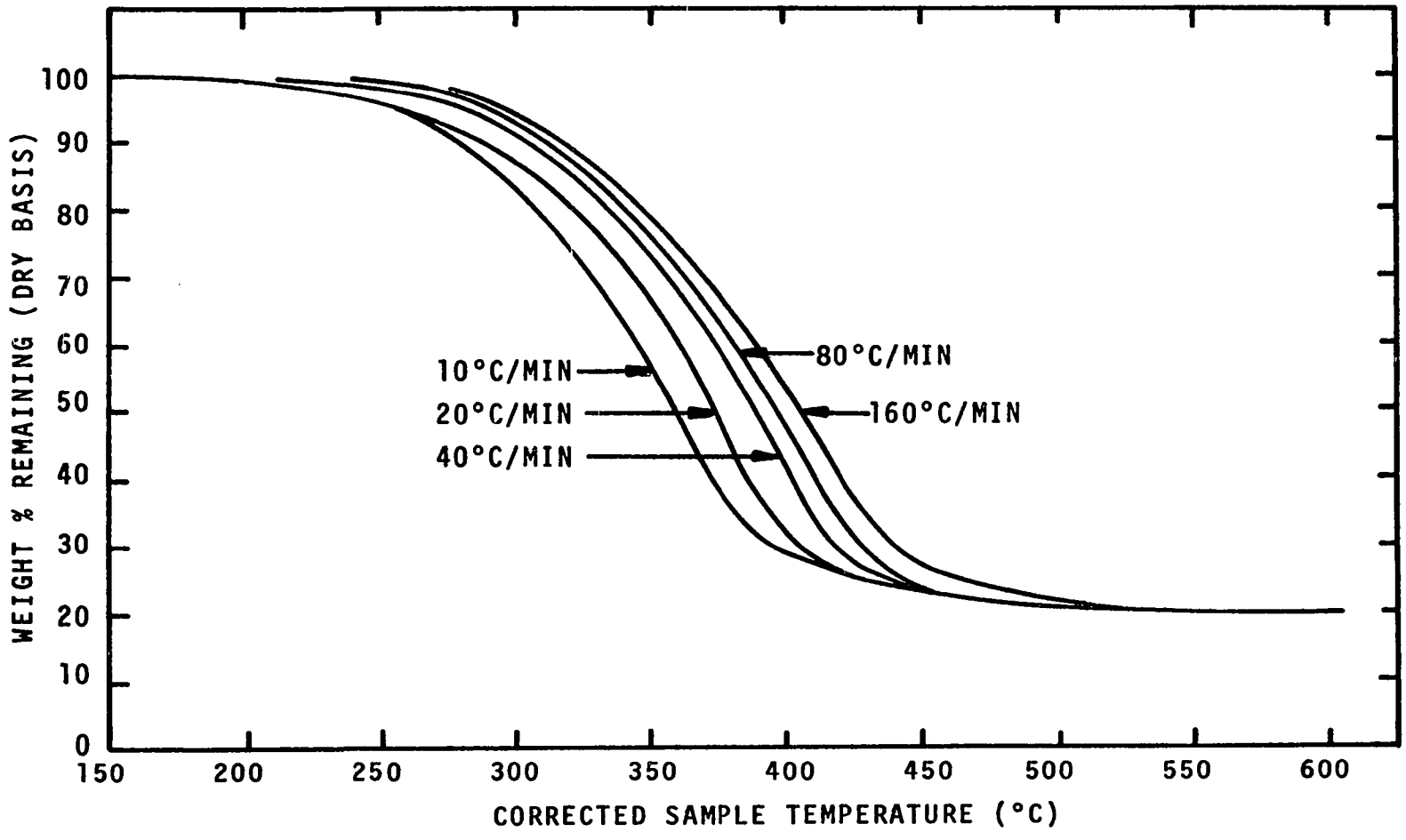

Figure III-18. Summary of TG Curves for Oak in a Nitrogen Atmosphere.

R = gas constant (1.986 cal/gmole-°K)

T = temperature (°K)

F(W) = an undefined function of weight

If data are obtained at a series of heating rates, the values of dW/dt and T at individual values of conversion are dependent on heating rate, symbolized by $[1/(W_o-W_f) \times dW/dt]_H$ and T_H in Equation III-2.

$$\log \left[\frac{1}{W_o - W_f} \frac{dW}{dt}\right]_H = \log k_o + \log F(W) - \frac{E}{2.303R\, T_H} \qquad \text{III-2}$$

If the chemistry of pyrolysis is independent of heating rate, then for TG data obtained at several heating rates, plots of log rate versus $1/T_H$ with parameters of constant conversion should yield straight lines of slope -E/2.303R. These plots are shown in Figures III-19 and III-20 for white pine and oak. As can be seen, parallel straight lines are obtained at all conversions down to about 30 weight percent remaining. Between 20 and 30 weight percent remaining there is a small amount of scatter in the data. An activation energy of 49,400 cal/gmole was obtained for white pine and 57,000 cal/gmole for oak. These values are in good agreement with those obtained by Akita and Kase (2) for α-cellulose. More importantly, the overall chemistry of pyrolysis is independent of heating rate.

The form of F(W) and the frequency factor can be determined by reference to the following equation:

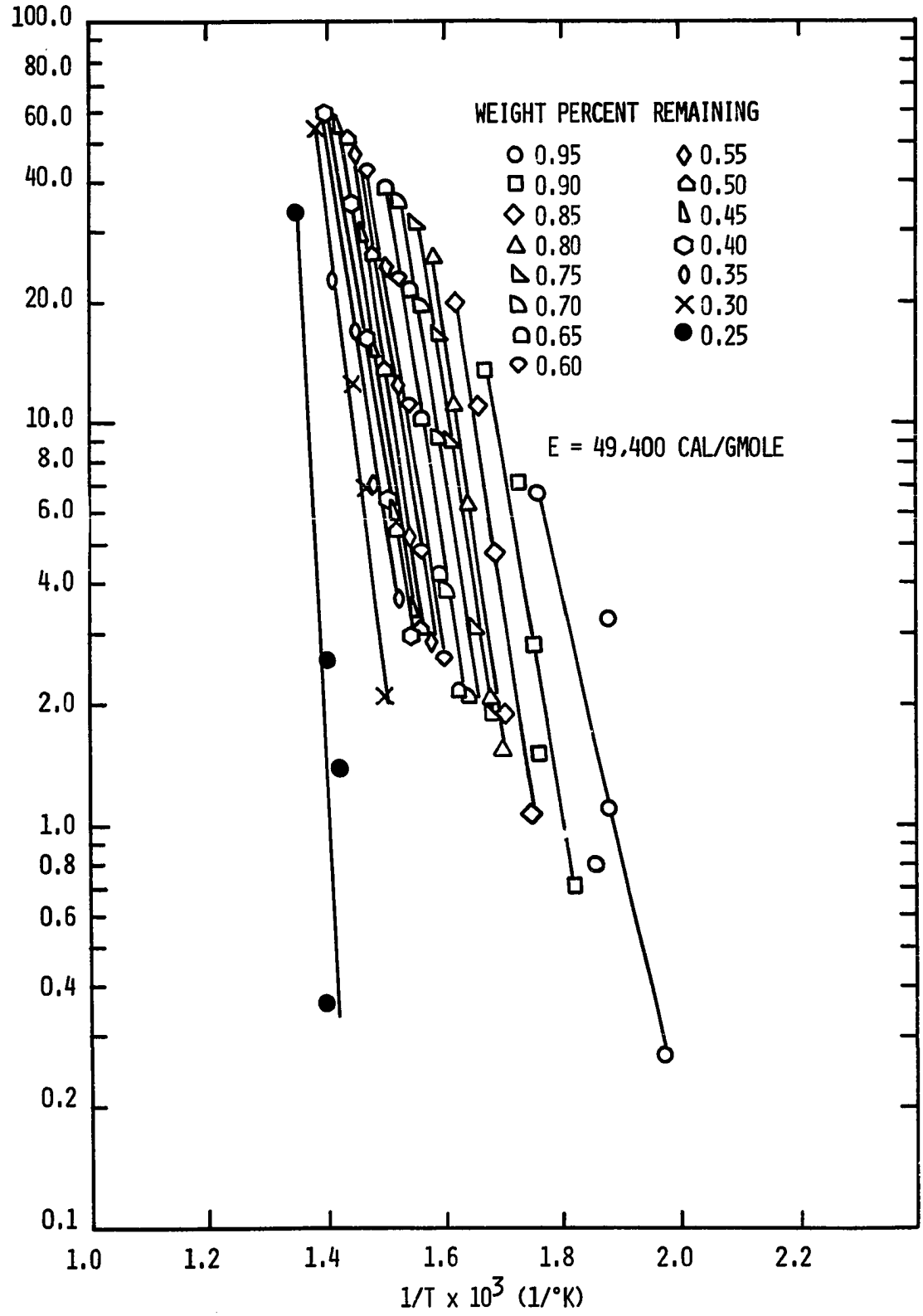

Figure III-19. Log Rate as Dependent on Reciprocal Temperature for White Pine.

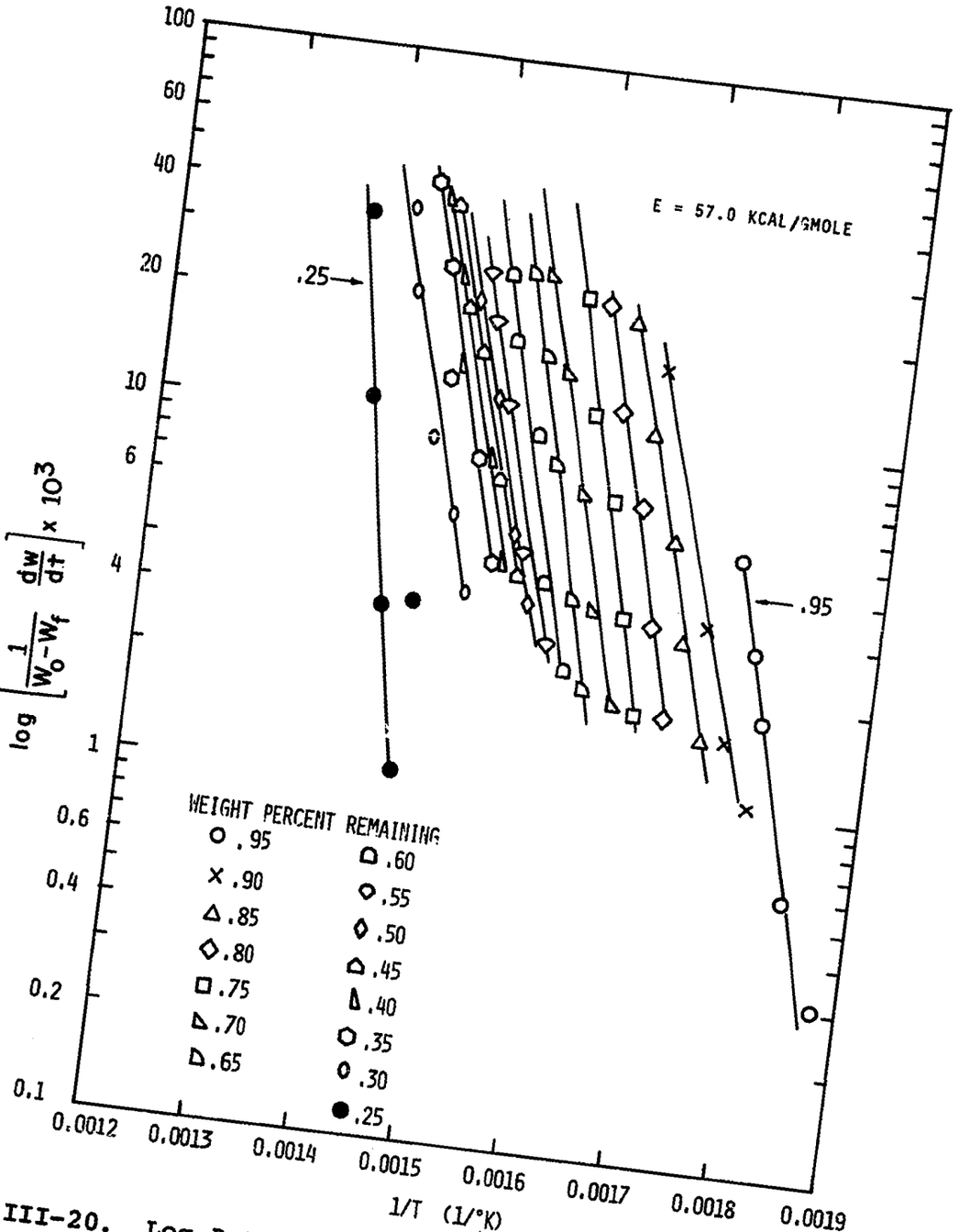

Figure III-20. Log Rate as Dependent on Reciprocal Temperature for Oak.

$$\log k_o F(W) = \log k_o + \log F(W) = \log \left[\frac{1}{W_o - W_f} \frac{dW}{dt}\right]_H + \frac{E}{2.303R\ T_H} \qquad \text{III-3}$$

The right hand side of Equation III-3 can be computed directly. If it is assumed that F(W) is the form $[(W_o - W)/(W_o - W_f)]^n$, a plot of $(W_o - W)/(W_o - W_f)$ versus $\log [1/(W_o - W_f) \times dW/dt]_H + E/2.303R\ T_H$ of Equation III-3 should yield a straight line of slope n. These calculations were made, and the results are shown in Figure III-21 for both woods. The results for oak can be described by two straight lines, one resulting in an order 2.1, the second in an order of 1.7. The white pine results below 50 percent decomposable material remaining can be approximated by an order of 1.7. Between 50 and 90 percent weight remaining a line resulting in a first order reaction has been drawn. The data above 90 percent weight remaining is not fitted to any reaction order.

It should be noted that at each value of conversion, $\log [1/W_o - W_f \times dW/dt]_H + E/2.303RT_H$ should have the same value regardless of the rate of heating. Goldfarb et al. stated that due to experimental error inherent in the measurements, some scatter should be expected in the values of $\log [1/W_o - W_f \times dW/dt]_H + E/2.303RT_H$ at each conversion. They suggested that the scatter be accounted for by averaging over $\log [1/W_o - W_f \times dW/dt]_H + E/2.303RT_H$ at each conversion before preparing plots of the type shown in Figure III-21. As can be seen in Figure III-21, this averaging step was not necessary

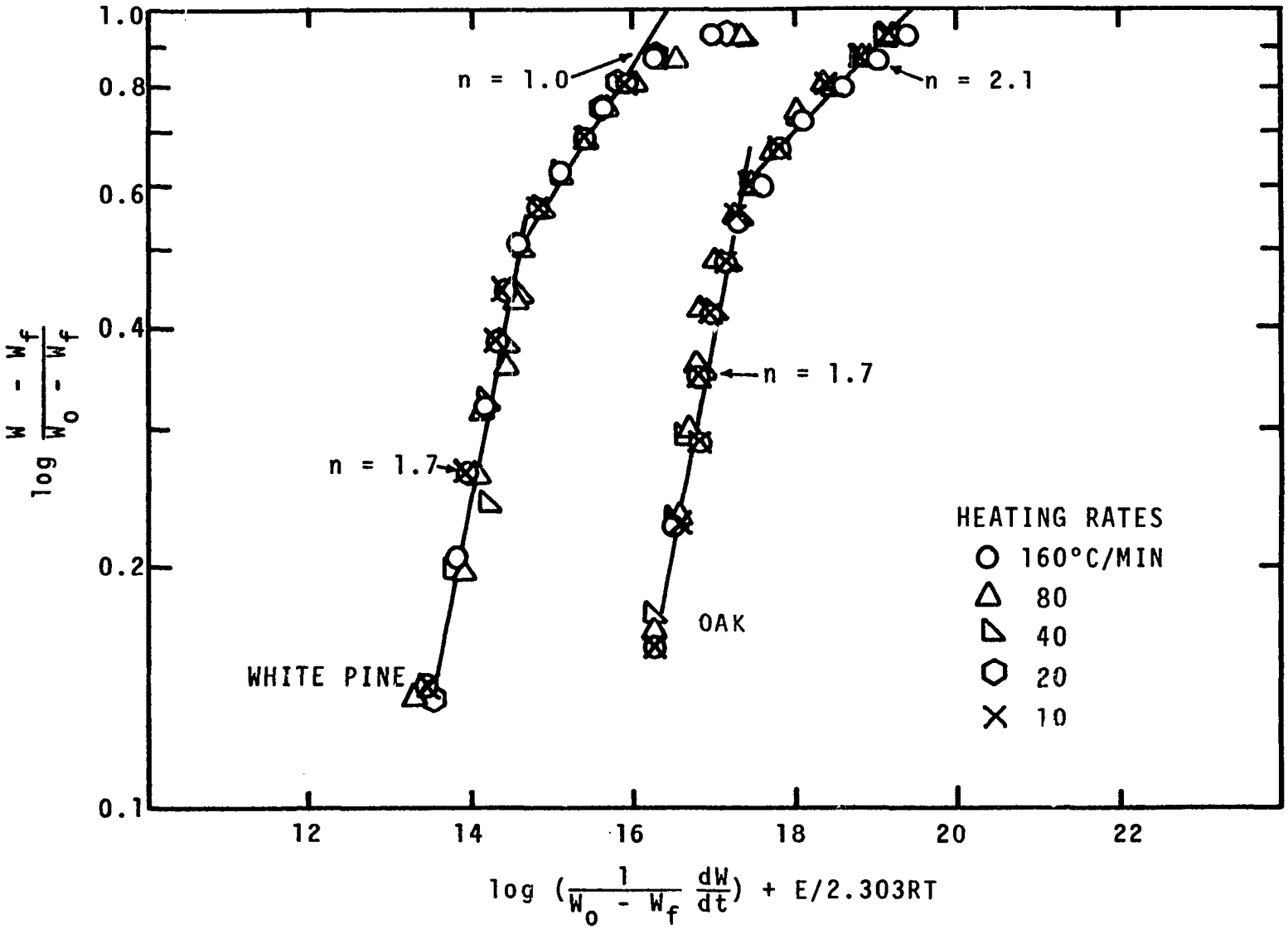

Figure III-21. Determination of the Order of Reaction and Frequency Factors for White Pine and Oak.

in this work, thus providing additional confirmation that the TG data are reliable and that the overall chemistry of pyrolysis is independent of heating rate. The kinetic parameters--activation energy, order, and frequency factor--for the pyrolysis of white pine and oak are summarized in Table III-2.

TABLE III-2

KINETIC PARAMETERS FOR PYROLYSIS OF WHITE PINE AND OAK

Wood	Weight % Decomposable Material Remaining	n	k_o (sec^{-1})
White Pine	90 - 100	-	
E = 49,400 cal/gmole	50 - 90	1.0	7.94×10^{15}
	0 - 50	1.7	10^{13}
Oak	60 - 100	2.1	5.14×10^{18}
E = 57,000 cal/gmole	0 - 60	1.7	2.69×10^{16}

Heat of Pyrolysis

It was shown in the previous section of this chapter that at heating rates up to 160°C/min the overall pyrolysis chemistry for white pine and oak is independent of heating rate. The only effect of heating rate is to displace the weight loss curve. Thus the DSC energy capacity data of Havens can be extended from 20°C/min to higher heating rates. Although the energy capacity data for white pine and oak are available, it was decided to remeasure these quantities for the following reasons:

1. The DSC energy capacity technique was developed by Havens. Additional data are needed to demonstrate the usefulness and repeatability of the technique.
2. Havens found that changes in the radiative heat transfer properties of the sample cell resulted in a number of runs of little value.

The DSC used in this study is the Perkin-Elmer DSC-1b shown in Figure III-22.

It is well known that the radiative heat transfer properties of solids are dependent on their color and surface roughness. Wood sawdust when pyrolyzed changes in color from a light brown to black, and its surface characteristics change due to shrinkage. The effect of changes in wood radiative heat transfer properties on DSC measurements is eliminated by covering the sample pan and contents with a thin aluminum disc. Volatiles escape through four small holes in the disc but the sample can also radiate directly through these holes. Therefore, the DSC sample cup and pan were covered with an aluminum radiation dome which has one small vent hole near its center.

A more troublesome radiative heat transfer problem is that due to condensation of volatiles on the radiation dome and on the bottom of the sample cup. The sensitivity of DSC (and in fact DTA) measurements due to changes in radiative heat transfer properties can be demonstrated by a hypothetical heat capacity test. Suppose that a 10 mg sample of pine is



Figure III-22. Perkin-Elmer DSC-16.

heated at 20°C/min in a DSC. Assuming that the specific heat of the wood is 0.35 cal/gm-°C, the differential heat that must be supplied to offset the effect of heat capacity is

$$\frac{dq}{dt} = 100 \text{ mg } (0.35 \text{ mcal/mg-°C})(0.333 \text{ °C/sec})$$
$$= 1.166 \text{ mcal/sec} \qquad \text{III-4}$$

The surface area of the radiation dome is slightly greater than 1 cm^2, and if during a run the emissivity of the surface changes by 0.1 at 400°C, the differential heat which must be supplied to counteract the change in surface emissivity is:

$$\frac{dq}{dt} = 0.1 \sigma A T^4$$

where σ = the Stephan-Boltzmann constant 1.355×10^{-9} (mcal/sec-cm^2-°K)

A = area of the radiation dome (cm^2)

T = temperature (°K)

$dq/dt = (0.1)(1.355 \times 10^{-9})(1)(673)^4 = 27$ mcal/sec

Obviously a small change in surface emissivity would become the dominant factor during a wood heat capacity measurement. Havens found it necessary to modify the DSC and the manufacturer's suggested experimental procedure to avoid this problem.

Havens observed that the heat transfer characteristic of the test cell cover plate varied from run to run, such that the no-sample base line could not be duplicated on two

successive runs over a wide temperature range. Although this plate protects uninsulated sample and reference pan lead wires, it was removed and the problem was eliminated. In this study even with a new test cell it was found that to obtain reproducible no-sample base lines the cover plate must be removed.

Heat loss from an isothermal DSC sample head is dependent on its radiative properties, temperature, and flow rate of purge gas and is independent of cell content if no reaction is occurring. Recognizing this fact enables one to check the heat loss characteristics of the no-sample base line against a sample run at the initial and final temperatures of the run. If these two points agree, one can reasonably assume that the heat loss characteristics during the base line and sample run are the same. The importance of this check should not be underestimated because even a small difference between the check points, when integrated over a long time internal, can result in significant error.

The sample head purge gas system, as shown in Figure III-23, is designed to bring gas in just below the sample cups. The gas sweeps through the cell, picking up volatiles, and exits through a port just behind the inlet port. It has been observed that with this flow pattern and at Perkin-Elmer's suggested purge gas flow rate, volatiles condensed on the radiation dome, making it impossible to reproduce the high temperature isothermal heat losses.

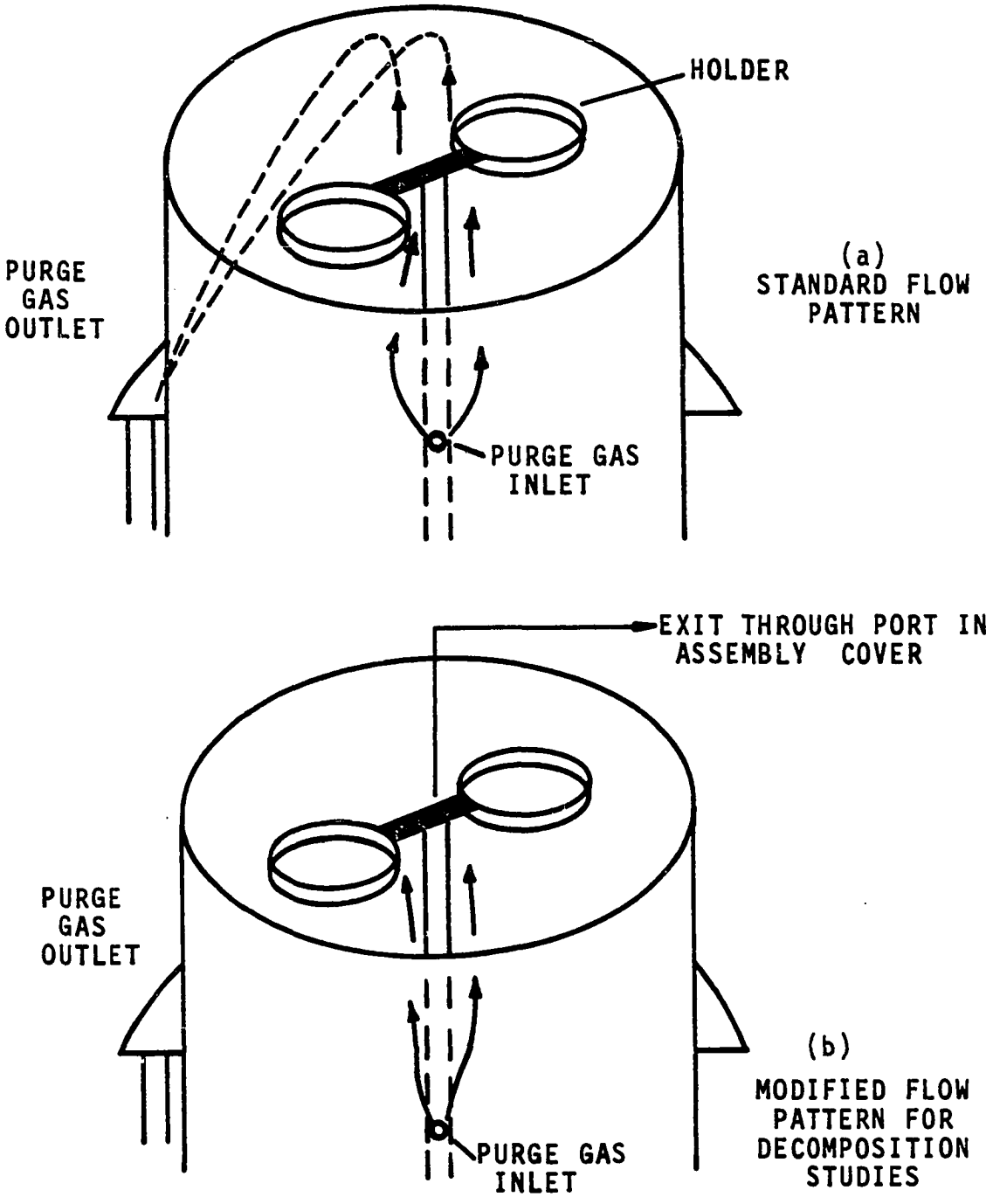

Figure III-23. Purge Gas Flow Pattern in Differential Scanning Calorimeter Sample Head.

However, it has been found that by redirecting the purge gas flow to discharge through a port in the sample head cover and increasing the purge gas flow rate from 40 to 100 ml/min, data with acceptible heat loss characteristics could be obtained.

Even though Havens could obtain reliable DSC data, the changes in radiative properties of the sample cell from base-line to sample run caused up to 60 percent of the thermograms obtained to be of little quantitative value. An attempt was made as part of this study to improve the DSC experimental procedure of Havens. The primary objective was to reduce the number of runs in which radiative heat transfer becomes the dominant factor.

It was observed that the purge gas rotatometer-flow controller tended to fluctuate a small amount during a run. A Brook's Flow Controller valve was installed in the purge gas line to dampen out these fluctuations. Although the purge gas fluctuations were dampened out, no noticable improvement in reproduction of isothermal heat losses was observed.

Since the purge gas enters the sample head at room temperature, it would be expected that the purge gas cools the volatiles. Since this cooling could contribute to the condensation problem, a purge gas heater was installed to keep the purge gas near the initial temperature of a run. Several types of controlled heaters were studied, but it was found

that the off-on cycling of the controller resulted in noise on the thermogram. After spending considerable time in examining various heating systems, it was decided to use the experimental procedures of Havens.

Three different calibration checks are suggested by Perkin-Elmer to insure that DSC experimental data are accurate. These are power, temperature, and programmer calibrations.

The area enclosed by a DSC no-sample base line and a sample thermogram represents the energy capacity of the material studied. The value of energy which each unit of area represents is obtained from a DSC calibration thermogram for the heat of fusion of indium. The Perkin-Elmer Corporation states that over the entire operating range of the instrument the heat of fusion calibration will result in an error of less than 5 percent. This error is said to be due to non-linearities in the temperature programmer.

The programmer control circuits and the platinum resistance temperature sensing element are both slightly non-linear, which results in a true temperature rise that deviates from that indicated by the programmer as shown in Figure III-24. The difference in true temperature and programmer temperature can be corrected by calibrating the programmer digital output against the melting temperature of several well-defined materials. For this study the metals used were indium (M.P. = 156.2°C), tin (231.9°C), and lead (327.3°C).

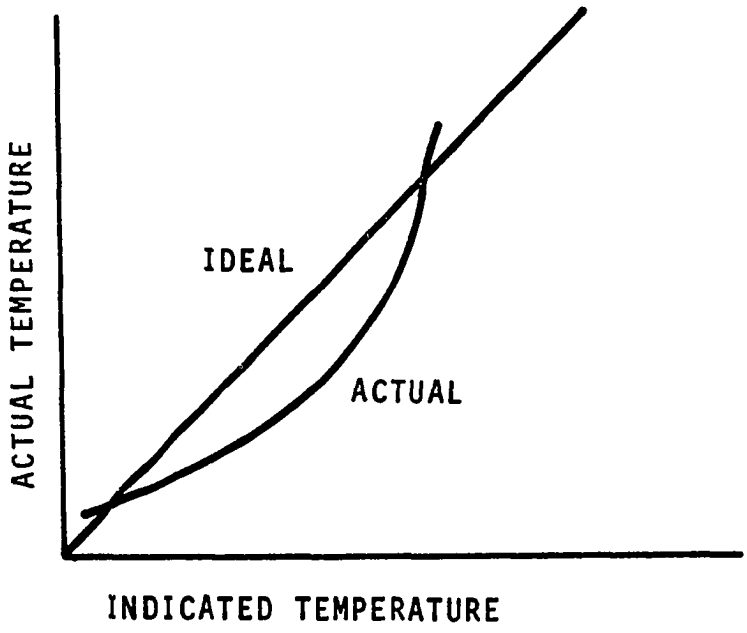

Figure III-24. Relation Between Programmed and Actual Temperatures in Perkin-Elmer DSC-1B Instrument.

The curvature of the temperature calibration curve shows that the true heating rate (dT/dt) is not a constant but varies slightly from point to point along the curve. The slight error caused by this curvature can be eliminated by performing a specific heat calibration. In this calibration the displacement of the instrument readout is measured from a no-sample base-line for an inert sample whose heat capacity as a function of temperature is accurately known. The displacement Y' is equal to

$$Y' = \frac{1}{k} \frac{dT}{dt} C'm' \qquad \text{III-6}$$

where Y' = pen deflection with standard material

k = calibration constant (cal/sec-cm)

dT/dt = nominal rate of heating (°C/sec)

C' = heat capacity of standard (cal/gm-°C)

m' = mass of standard material (gm)

Rearranging Equation III-6 a calibration factor k can be computed as a function of temperature as given below.

$$k = \frac{(dT/dt)\ C'm'}{Y'} \qquad \text{III-7}$$

This calibration was performed using a sapphire (Al_2O_3) heat capacity standard; the calibration curve is given in Figure III-25.

The energy capacity of wood can be obtained by solving Equation III-7 for C as shown in Equation III-8.

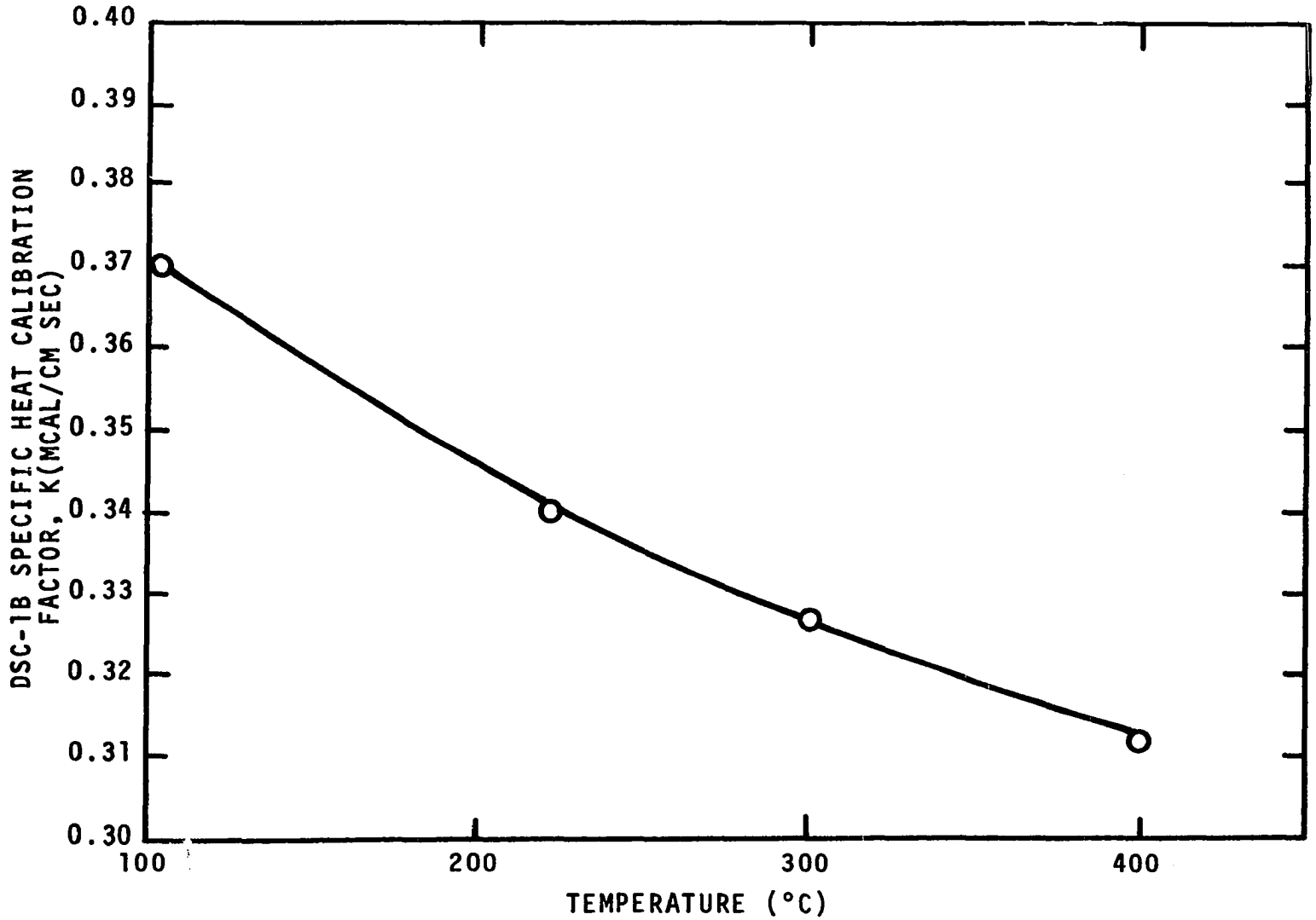

Figure III-25. Power Calibration for the Differential Scanning Calorimeter.

$$C = dE_s/dT = \frac{kY}{(dT/dt)m} \qquad \text{III-8}$$

where C = energy capacity (cal/mg-°C)

dE_s/dT = energy capacity (cal/mg-°C)

Y = pen displacement for wood

m = mass of wood (mg)

k = calibration constant

dT/dt = nominal heating rates (°C/min)

The power calibration using the specific heat of sapphire as a standard was made once during this study. The power calibration was regularly checked at 156°C by measuring the heat of fusion of a known quantity of indium. Although a specific heat calibration for each wood sample run would improve the reliability of the experimental data slightly, the time required to obtain this calibration cannot be justified in view of the negligible improvement in data accuracy.

The energy capacity data obtained in this study for white pine are shown in Figure III-26. The wood samples used were cut from knot-free boards and were ground in a Wiley intermediate model laboratory mill. The fraction of the wood sample passing a 40-mesh screen was analyzed. The samples were dried in the DSC for 5 minutes at 200°C. The measurements were made at a nominal heating rate of 20°C/min and a nitrogen purge flow of 100 ml/min.

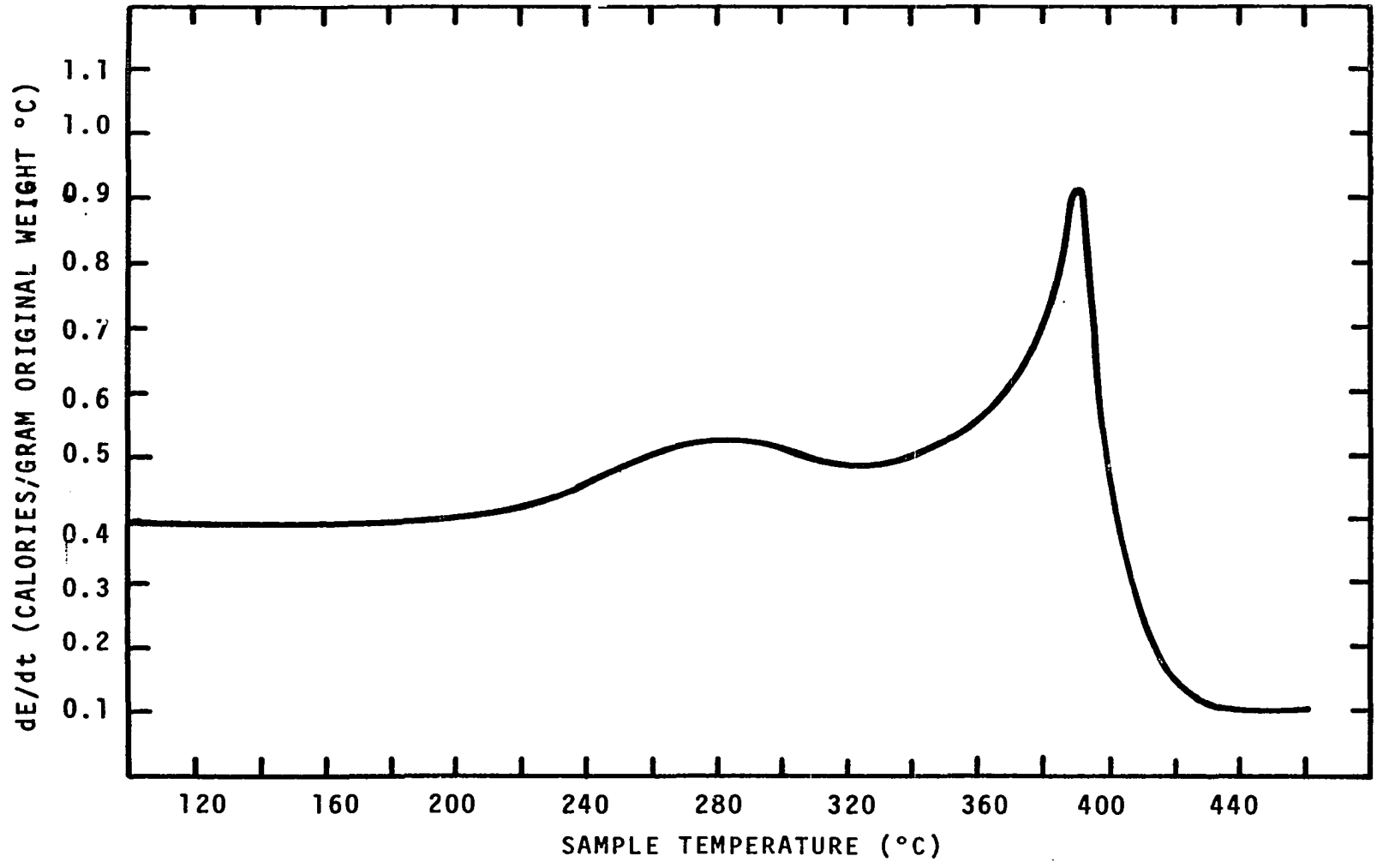

Figure III-26. Energy Capacity of White Pine Wood as a Function of Temperature in a Nitrogen Atmosphere (Based on Original, Non-Decomposed Weight).

It was found in this study, and noted by Perkin-Elmer, that it is all but impossible to reproduce no-sample and sample isothermal heat losses over a temperature range of much more than 200°C. The measurements in this study were made in two parts: first, the energy capacity from 220°C to 450°C was measured and then that from 100°C to 220°C. The TG data indicated that no decompositon occurred before 220°C and decomposition is complete before reaching 410°C.

The energy capacity data obtained for oak are shown in Figure III-27. The oak samples were prepared and the data were obtained identically to the pine procedure.

Measurement of Wood Char Thermal Conductivity

The char thermal conductivity of interest in this study is that for wood char at temperatures above 350°C, where the char is formed by pyrolyzing wood. The char consists of a carbon matrix whose weight is 20 percent of that of the original wood. Havens (16) postulated, based on the x-ray photographs of Blackshear and Kanury (5), that over the temperature range of interest the density of wood char is also 20 percent of the original density. However, Havens observed that when wood char is cooled or totally pyrolyzed, it loses its dimensional stability, shrinks and cracks, making it impossible to pyrolyze the wood first, to cool it, and then to measure the thermal conductivity. Based on these findings, it was decided that an in situ pyrolysis-thermal

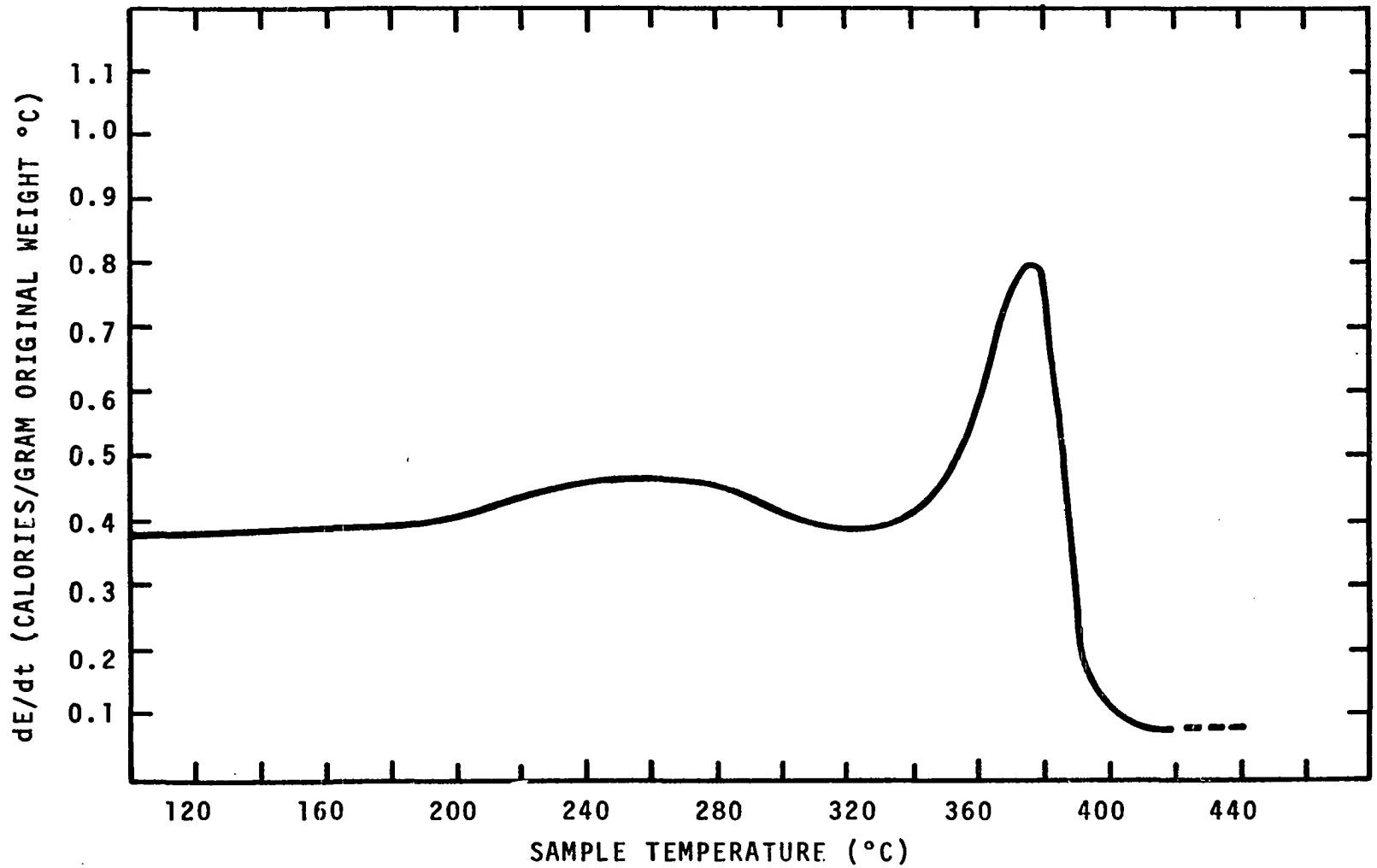

Figure III-27. Energy Capacity of Oak Wood as a Function of Temperature in Nitrogen Atmosphere (Based on Original, Non-Decomposed Weight).

conductivity experiment must be designed in which the wood was first partially pyrolyzed as shown in Figure II-1c, and the char thermal conductivity was then measured at pyrolysis equilibrium without cooling the sample.

Havens, in his model validation experiments discussed in Chapter 2, developed a pyrolysis experiment in which boundary conditions for pyrolyzing wood cylinders could be identified. For the present study it was felt that if the propagation of the char front approached an equilibrium state, the steady state temperatures in the char zone could be measured, in which case the thermal conductivity could be computed. Several questions regarding the applicability of this method had to be considered.

1. At the time this work was initiated, the estimates of char thermal conductivity in the literature were so low that only a thin char zone would be generated. With a thin char zone it might not be possible to locate thermocouples at two different radii within the potential char zone.
2. If the thermocouples were located in the wood before pyrolysis and then during pyrolysis the char shrank, the thermal conductivity could not be accurately determined since the location of the thermocouples would not be exactly known. Thus, dimensional stability of the sample during pyrolysis must be determined.

3. At the anticipated char temperatures, the insulation on the thermocouple wire would fail, resulting in multiple junctions along the thermocouple leads.

These questions could only be answered experimentally.

Preparation of the Samples

Rectangular samples 25 x 4-1/2 x 4-1/2 cm were cut from knot-free white pine board such that the grain ran along the longitidinal axis. A 0.635 cm diameter hole was center drilled through the full length of the sample, and the drill bit was left in the center hole. The sample was then machined to form a cylinder centered about the drill bit thus guaranteeing a true center for the cylinder with an outside diameter of about 4 cm. After machining, the cylinder was cut to a length of 15 cm and this section was then cut into three cylinders each 5 cm in length. Four small thermocouple holes were drilled through the center section parallel to the longitudinal axis. The drill bit used was a No. 60 aircraft extension drill approximately 4 inches long. Drill bits of this diameter and length usually do not have sufficient rigidity to hold a true center if the drill hole exceeds 1 cm in length. The variations in wood due to grain pattern magnify this problem to the extent that in several instances in this work, drill bit deflection of 0.5 cm occurred over a distance of 1 cm. It was found that by operating the drill bit at about 5500 RPM the holes could be sighted through.

The thermocouples used were constructed from 36 gauge Chromel-Alumel wire. The insulation on the section of each wire which was to be located inside the specimen was stripped off, and the wires were butt welded end to end using a small acetylene torch. The butt welded thermocouples were inserted in the thermocouple holes and the Chromel leads were brought out on one end of the center section and the Alumel on the other. The thermocouple holes were filled with white pine sawdust to minimize any temperature effect due to contact resistance. The location of each thermocouple was determined from an x-ray photograph, an example of which is shown in Figure III-28. The x-ray photographs were obtained using a General Electric D37G X-ray unit with Polaroid type 57 film

The center wood section and the two end covers were reassembled such that the wood grain lines matched at the boundary of each section. The sections were taped together at their intersection with Permacel PE 100 electrical tape. The thermocouple wires were brought out between the center section and the two end sections.

The instrumented sample was placed in the pyrolysis cell shown in Figure III-29. The resistance wire heater was centered in the specimen using lava end caps shown schematically in Figure III-30. The resistance wire heater was spring loaded to maintain its rigidity throughout each test. The pyrolysis cell is provided with a Plexiglas cover to permit evacuation of the cell and continuous purging.

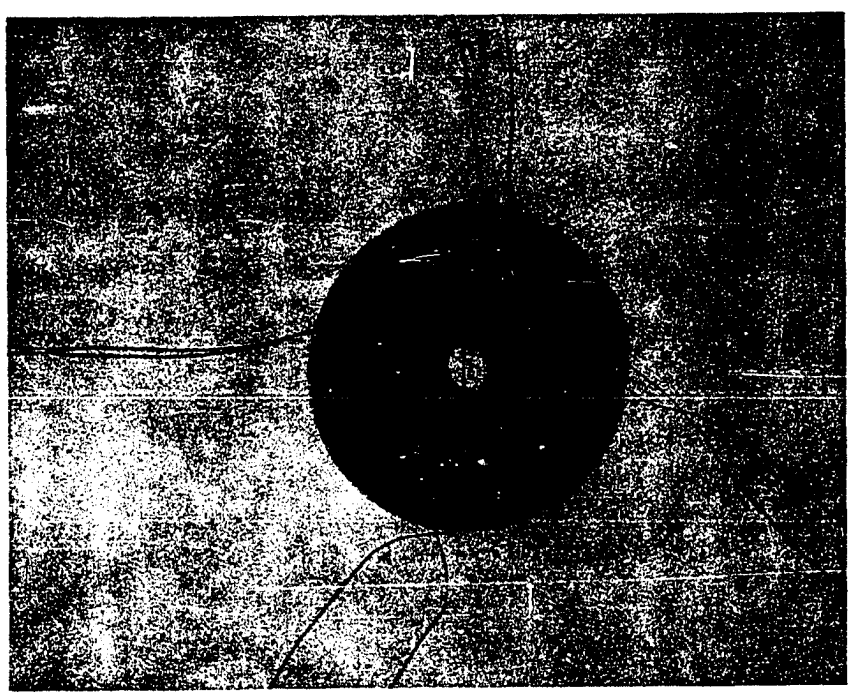

Figure III-28. Radial X-Ray of White Pine Cylinder Showing Thermocouple Bead Location.

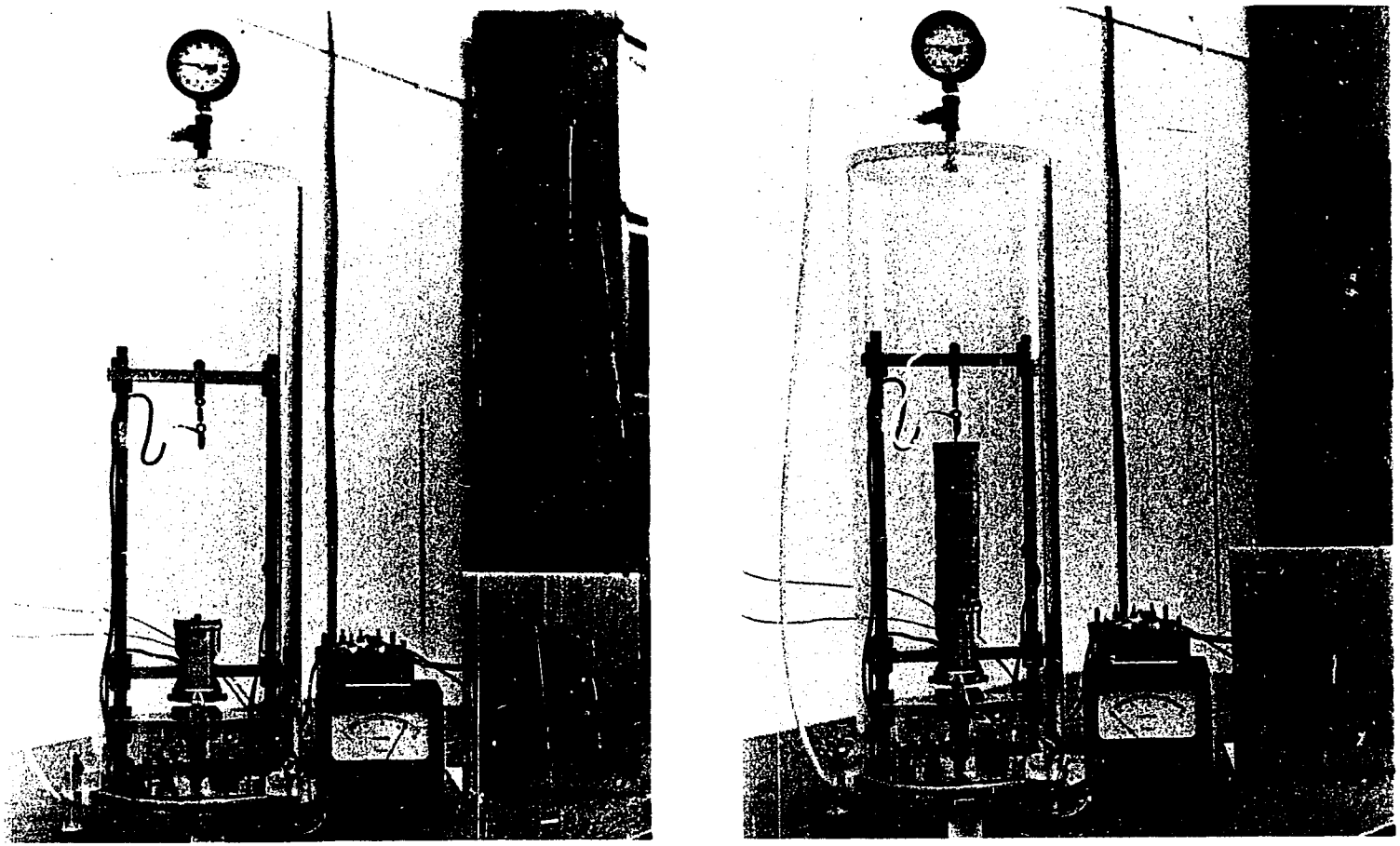

Figure III-29. Photograph of the Instrumented Wood Cylinder in Test Cell.

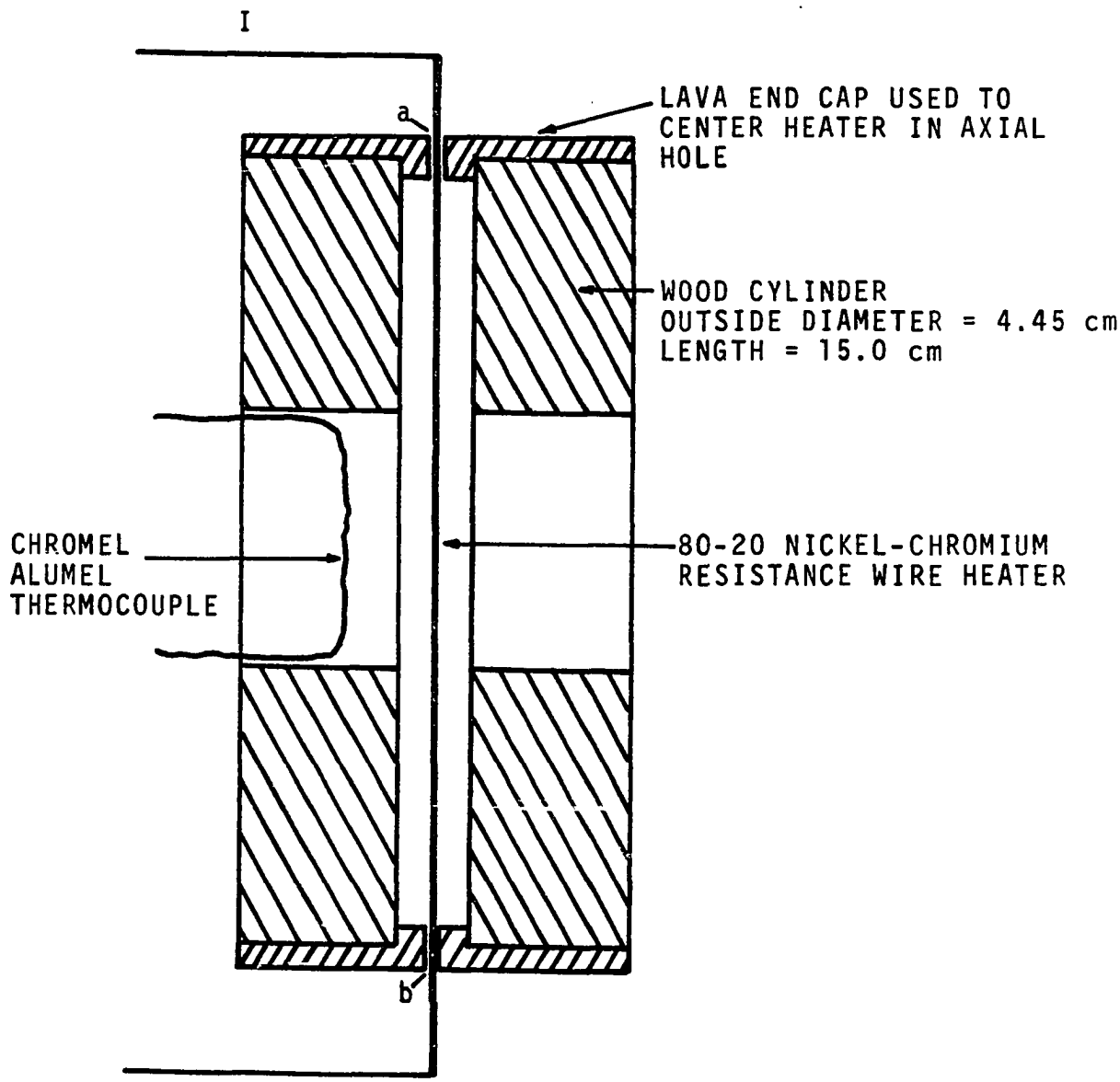

Figure III-30. Diagram of Instrumented Wood Cylinder.

The resistance heating wire used was Trophet A, a nominal 80-20 nickel chromium alloy containing traces of other metals. The temperature dependence of the wire resistivity with respect to its resistivity at 25°C is shown in Figure III-31. Over the wire temperature range from 500°C to 1,100°C the wire resistivity is equal to 1.06 times its 25°C value to within ± one percent. The wire temperatures of interest in this study are within this range; thus the temperature dependency of wire resistivity did not need to be considered. The heat leaving the wire could then be calculated as given below.

$$P = I^2R = (14.0)^2 (R_o) (1.06)$$

where R_o = resistance of wire at 25°C = 0.0135 ohm/cm of length

$P = 2.84$ watts/cm = 0.68 cal/sec-cm

Current to the heater was controlled using a variac, and the current was measured using a Simpson A.C. ammeter.

The thermocouple lead wires were passed through a small hole drilled in the base of the pyrolysis cell; the thermocouple was referenced to an ice bath. The thermocouple outputs during a run were continuously recorded.

Thermal Conductivity Test Run

After the sample was placed in the test cell, the thermocouple leads were connected to a reference block, a

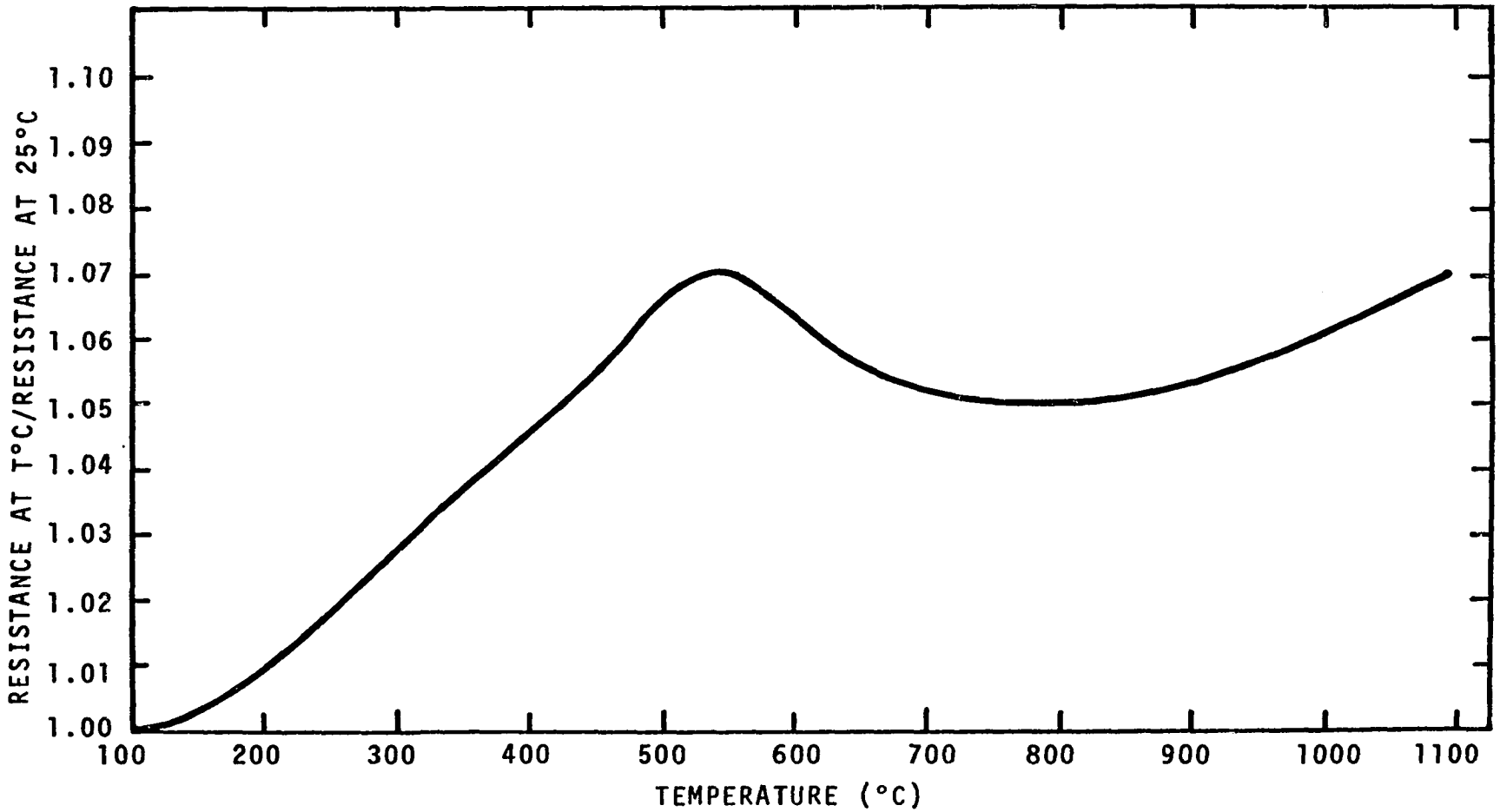

Figure III-31. Temperature Dependence of Electrical Resistance of Tophet A 80-20 Nickel-Chromium Wire.

plastic bell cover was placed over the cell and nitrogen was purged through the system for one hour. While purging with nitrogen x-ray photographs were taken perpendicular to the instrumented section of wood to locate again the position of the thermocouples. After one hour the nitrogen purge was reduced to a low flow rate and power to the heater was set at 14.8 amperes. Periodically during pyrolysis x-ray photographs were taken of the test sample. A typical series is shown in Figure III-32. As can be seen the thermocouple position remains constant, indicating that char maintains its dimensional stability during pyrolysis.

Treatment of the Data

At steady state the variations in radial temperature profile for a cylindrical sample exposed to a flux Q are given by

$$\frac{d}{dr}\left(r \frac{dT}{dr}\right) = 0 \qquad \text{III-9}$$

where r = radial position (cm)

T = temperature (°C)

Upon integration,

$$T_r = A \ln r + B \qquad \text{III-10}$$

where A and B are constants of integration. This equation shows that if radial heat transfer data are consistant, then a plot of ln r versus T should yield a straight line.

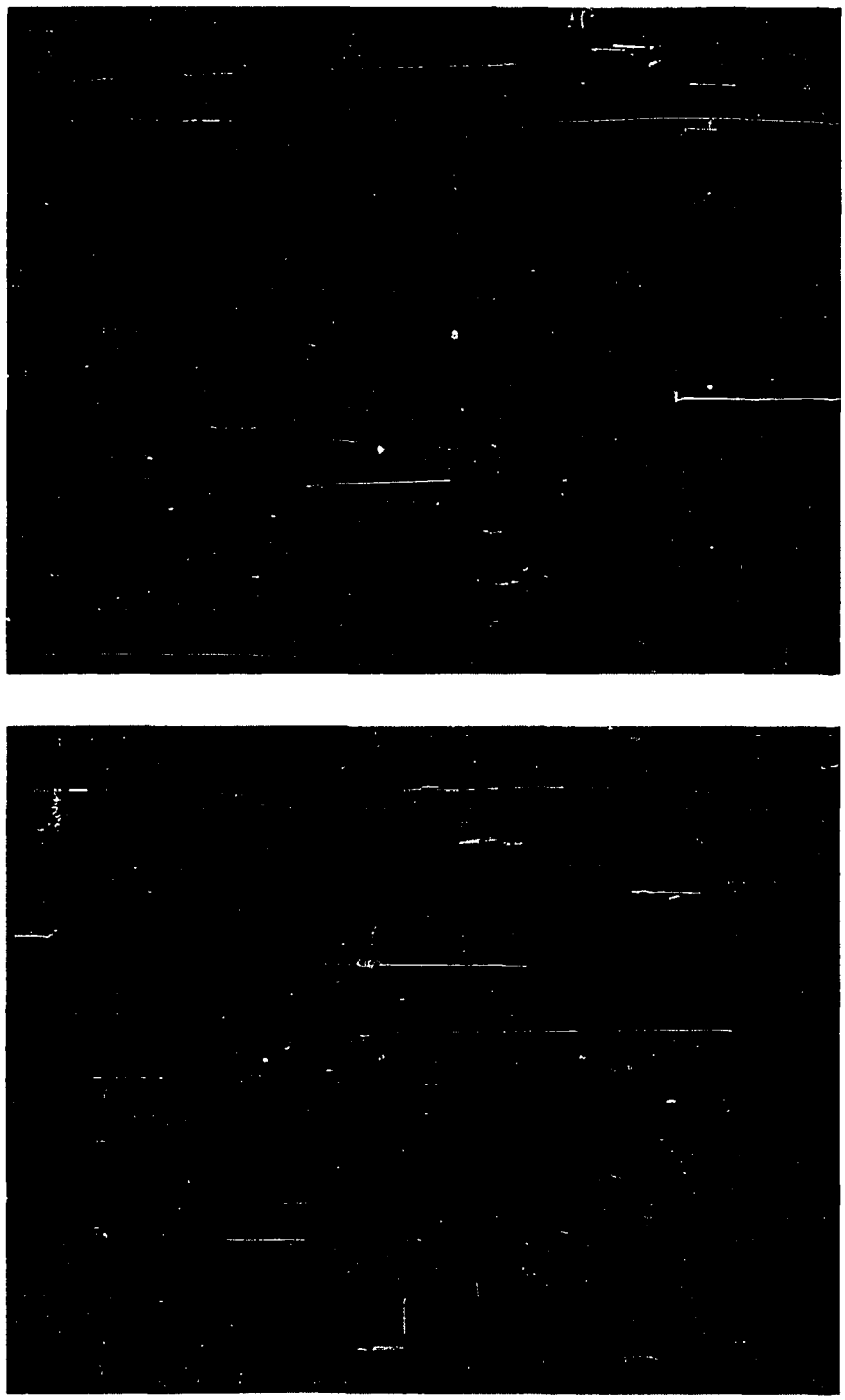

Figure III-32. X-Ray Photograph of Pyrolyzing Wood.

Figure III-33 shows this relation for one experimental run. The multiple curves shown are for different power levels.

If temperatures are measured at radial positions r_1 and r_2, the integration constants in Equation III-10 can be determined, resulting in Equation III-11.

$$T_r = \frac{(T_1 - T_2) \ln (r/r_2)}{\ln (r_1/r_2)} + T_2 \qquad \text{III-11}$$

Fourier's law of heat conduction can be used in Equation III-11 for the radial dependence of temperature to obtain

$$q = K \nabla_r T \qquad \text{III-12}$$

$$q = - K \frac{d}{dr} \left[\frac{(T_1 - T_2) \ln (r/r_2)}{\ln (r_1/r_2)} + T_2\right] \qquad \text{III-13}$$

Since lateral area of a cylinder of length ℓ is $2\pi r\ell$, the flux can be written as

$$q = P/2\pi r\ell \qquad \text{III-14}$$

Substituting Equation III-14 into Equation III-13 and solving for thermal conductivity yields

$$K = \frac{P \ln (r_2/r_1)}{2 \pi \ell (T_1 - T_2)} \qquad \text{III-15}$$

A total of five conductivity runs were made using the nickel chromium wire. The first two runs were used to develop

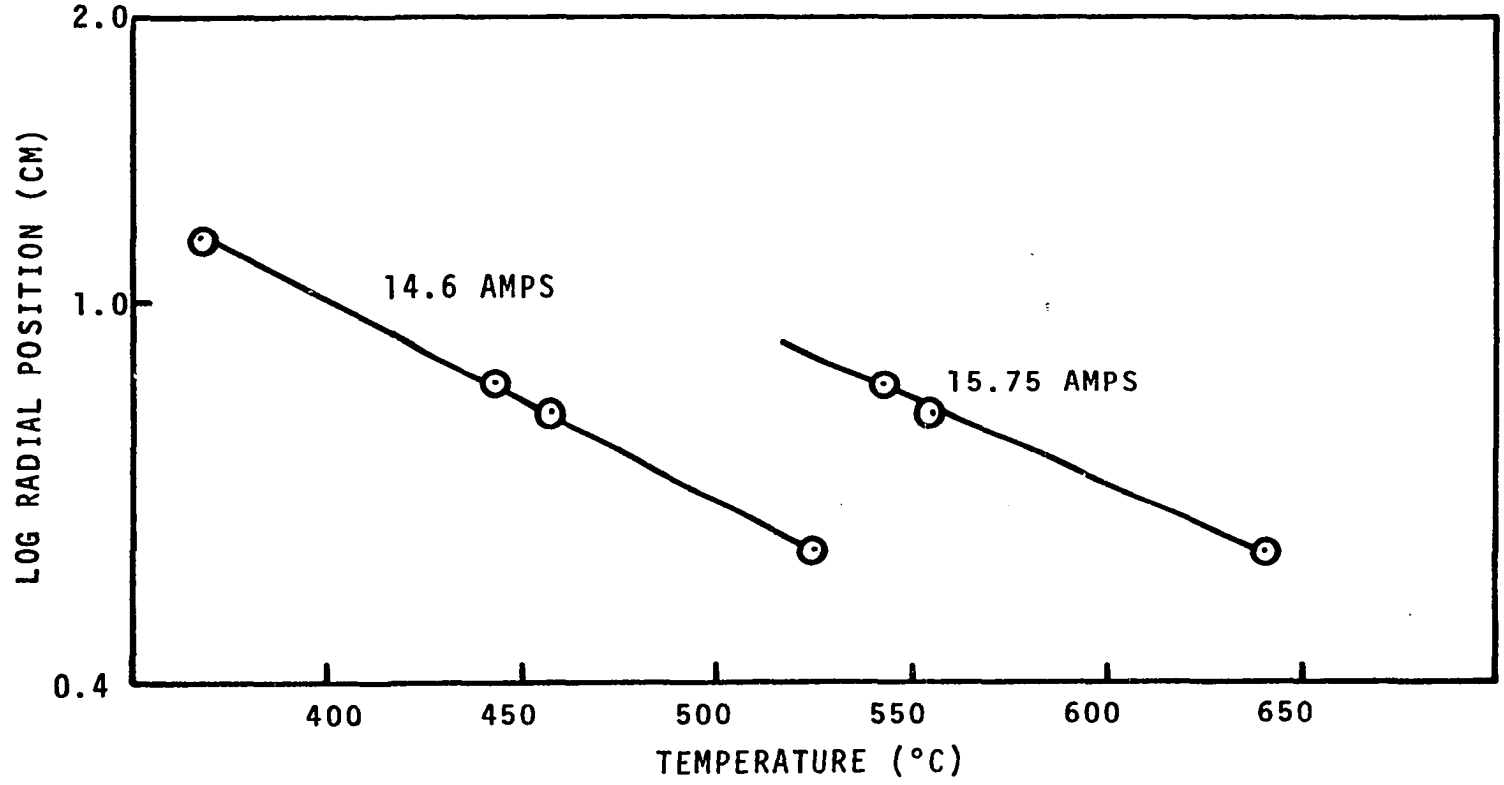

Figure III-33. Char Temperature as a Function of Thermocouple Position.

the technique. The results of the last three runs are shown in Table III-3.

TABLE III-3

EXPERIMENTAL VALUES OF CHAR THERMAL CONDUCTIVITY

Test	Temperature Range (°C)	Thermal Conductivity (cal/cm^2-sec-°C/cm)
3	345-650	0.00056
4	350-550	0.00052
5	350-550	0.00050
Average		0.000527

The above values of thermal conductivity are approximately three times greater than that predicted by the density correlation; in fact, they are nearly twice as high as that of white pine wood.

Transient Temperature Profiles

The validity of any mathematical model for predicting the transient temperature profiles in pyrolyzing wood can be demonstrated by comparing experimental temperature profiles with those predicted by a model. Experimental temperature profiles were available from the thermal conductivity experiments. The boundary conditions for the instrumented center wood section are shown in Figure III-34.

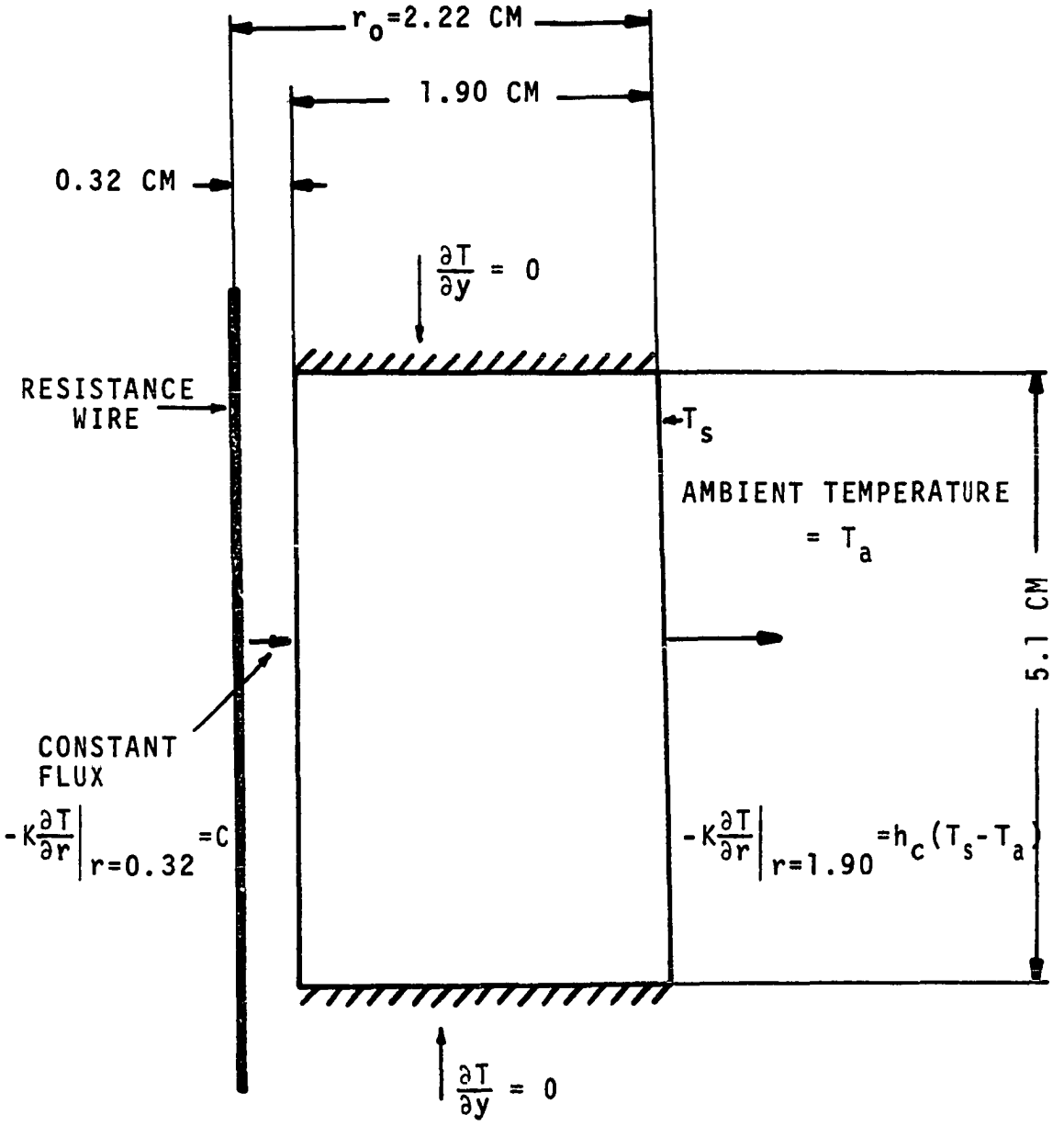

Figure III-34. Schematic of Section of Cylindrical Test Section Showing Boundary Conditions.

Over the sample length one would expect strong end effects due to heat transfer directly from the wire to the lava end caps and from the wood to the lava caps. The boundary conditions at the lava caps are difficult to define; however, by considering only the center wood section this problem is eliminated. If the flux generated by the wire heater along its length is uniform and constant, the heat flux at the inside surface of the wood cylinder can be defined. In such a case a boundary condition of no heat flux can be made at the top and bottom of the 5.0 cm center section of the wood sample. Heat transfer from the surface of the cylinder to the surroundings can be assumed to follow Newton's law of cooling.

$$- K \left.\frac{\partial T}{\partial r}\right|_{r_o = \text{outside radius}} = h_c (T_s - T_a)$$

where K = thermal conductivity (cal/cm^2-sec-°C/cm)

h_c = heat transfer coefficient (cal/cm^2-sec-°C)

T_s = temperature of outside surface (°C)

T_a = ambient temperature (°C)

The heat transfer coefficient was calculated using the Saunders and Weise correlation (27) given below.

$$\frac{h_c L}{K_f} = 0.59 \left[\left(\frac{L^3 \rho_f^3 g B_f \Delta T}{\mu_f^2} \right) \left(\frac{C_p \mu}{K} \right)_f \right]^{0.25} \qquad \text{III-16}$$

where ρ_f = density (0.00108 gm/cm^3)

μ_f = viscosity (0.00019 gm/cm-sec)

C_p = specific heat (0.25 cal/gm-°C)

K_f = thermal conductivity (0.0000691 cal/cm^2-sec-°C/cm)

B_f = coefficient of volumetric expansion (0.00367)

L = length of cylinder (15.3 cm)

T = temperature driving force assumed (67°C)

h_c = heat transfer coefficient (cal/cm^2-sec-°C)

Using the above physical property data, h_c was found to be 0.00021 cal/cm^2-sec-°C.

The wire operating temperature is such that the wave length of the energy leaving the wire is totally absorbed by the wood. The transient data obtained are shown in Chapter IV.

CHAPTER IV

MATHEMATICAL MODEL

An energy balance for a dry wood specimen can be written, neglecting potential energy effects, as follows:

$$\frac{\partial}{\partial t}\left(\rho\bar{E} + 1/2\ \rho v^2\right) = -\nabla\cdot\vec{q} - \nabla\cdot\vec{m}_f\ \left(\bar{H}_f + 1/2\ v_f^2\right) \qquad \text{IV-1}$$

where ρ = density of wood specimen (gm/cm^3)

$\bar{E}$ = specific internal energy of wood specimen (cal/gm)

v = local velocity of the solid wood (cm/sec)

v_f = local velocity of all fluids in the wood (cm/sec)

$\vec{q}$ = heat flux vector ($cal/sec\text{-}cm^2$)

$\vec{m}_g$ = mass flux vector for fluid ($gm/cm^2\text{-}sec$)

$\bar{H}_f$ = specific enthalpy of fluids (cal/gm)

At temperatures at which pyrolysis occurs the internal energy of the wood is sufficiently high that kinetic energy effects due to bulk flow may be neglected. The continuity of mass for a differential element requires that

$$\nabla\cdot\vec{m}_f = -\ \partial\rho/\partial t \qquad \text{IV-2}$$

Equation IV-1 may now be written as

$$\left[\rho\ \left(\frac{\partial\bar{E}}{\partial t}\right)_x + \left(\bar{E} - \bar{H}_f\right)\left(\frac{\partial\rho}{\partial t}\right)_x\right] = -\nabla\cdot\vec{q} - \vec{m}_f\nabla\cdot\bar{H}_f \qquad \text{IV-3}$$

where x denotes the position vector.

It has been shown in Figures III-17 and III-18 that weight loss is a function of both temperature and rate of heating. Assuming that over the time period of interest the sample maintains dimensional stability, then sample density is a function of both temperature and heating rate. The density dependence on time can be written,

$$\frac{\partial \rho}{\partial t} = \left[\left(\frac{\partial \rho}{\partial T}\right)_{\phi} + \left(\frac{\partial \rho}{\partial \phi}\right)_{T}\left(\frac{\partial \phi}{\partial T}\right)\right]_{x} \frac{\partial T}{\partial t} \qquad \text{IV-4}$$

where ϕ = rate of temperature increase (°K/min)

x = position vector

Similarly if the internal energy is a function of both temperature and heating rate its dependence on time may be expressed,

$$\frac{\partial \bar{E}}{\partial t} = \left[\left(\frac{\partial \bar{E}}{\partial T}\right)_{\phi} + \left(\frac{\partial \bar{E}}{\partial \phi}\right)_{T}\left(\frac{\partial \phi}{\partial T}\right)\right]_{x} \frac{\partial T}{\partial t} \qquad \text{IV-5}$$

Substituting Equations IV-4 and IV-5 into IV-3,

$$\left\{\rho\left[\left(\frac{\partial \bar{E}}{\partial T}\right)_{\phi} + \left(\frac{\partial \bar{E}}{\partial \phi}\right)_{T}\left(\frac{\partial \phi}{\partial T}\right)\right]_{x} + (\bar{E}-\bar{H}_f)\left[\left(\frac{\partial \rho}{\partial T}\right)_{\phi} + \left(\frac{\partial \rho}{\partial \phi}\right)_{T}\left(\frac{\partial \phi}{\partial T}\right)\right]_{x}\right\} \frac{\partial T}{\partial t}$$

$$= -\nabla\cdot\vec{q} - \vec{m}_f \nabla\cdot\bar{H}_f \qquad \text{IV-6}$$

If it is assumed that the effects of heating rate and bulk flow of gases are negligible then Equation IV-6 simplifies to

$$\left[\rho\left(\frac{\partial \bar{E}}{\partial T}\right)_{x} + (\bar{E}-\bar{H}_f)\left(\frac{\partial \rho}{\partial T}\right)_{x}\right] \frac{\partial T}{\partial t} = -\nabla\cdot\vec{q} \qquad \text{IV-7}$$

Equation IV-7 is exact for very small samples where temperature and density are uniform throughout the sample. The DSC measurements made in this study satisfy these criteria. Dividing Equation IV-7 by the initial mass of the sample, $m_o = \rho_o v_o$, and integrating over volume, Equation IV-7 becomes

$$\left[\frac{\rho}{\rho_o}\left(\frac{\partial \bar{E}}{\partial T}\right) + (\bar{E}-\bar{H}_f)\,\frac{\partial(\rho/\rho_o)}{\partial T}\right]\frac{dT}{dt} = \left(-\int_v \nabla\cdot\vec{q}\,\frac{dv}{\rho_o v_o}\right) \qquad \text{IV-8}$$

where m_o = initial mass (gm)

ρ_o = initial density (gm/cm^3)

v_o = initial volume (cm^3)

The left hand side of Equation IV-8 accounts for the energy required to raise the temperature of the solid ($\rho/\rho_o \cdot \partial\bar{E}/\partial T$), and the energy required to volatilize the solid $[(\bar{E}-\bar{H}_f) \cdot \partial(\rho/\rho_o)/\partial T]$. If a small DSC test specimen is used such that temperature gradients within the sample are eliminated then the energy capacity measured using DSC is identical to the quantity represented by Equation IV-8.

The energy capacity measured using DSC can be applied to heat conduction in pyrolyzing wood as follows:

$$\left[\frac{\partial E^*}{\partial T}\,\frac{\partial T}{\partial t}\right]_y = \nabla\cdot k\nabla T \qquad \text{IV-9}$$

where $\partial E^*/\partial T = [\rho/\rho_o\ \partial\bar{E}/\partial T + (\bar{E}-\bar{H}_f)\ \partial(\rho/\rho_o)/\partial T]$

y = over the small element represented by the position vector y

Equation IV-9 must be solved numerically for decomposing wood since both the energy capacity and thermal conductivity are non-linear functions of time. This expression is identical to that solved by Havens (16) who assumed values of thermal conductivity. In this present study the first objective was to determine whether the mathematical model proposed by Havens was applicable when experimental data for wood char thermal conductivity were used to predict transient temperature profiles in pyrolyzing wood.

The dependency of thermal conductivity on temperature shown in Figure IV-1 was used in the numerical solution of the model. It was developed based on the TG weight loss data obtained at a heating rate of 20°C/min. Thus at temperatures up to 280°C and above 420°C the thermal conductivity is the thermal conductivity for undecomposed and charred wood respectively. For the thermal conductivity of pyrolyzing wood a linear approximation has been made between the thermal conductivity of charred and uncharred wood and is shown as the dashed line between 280° and 420°C.

Effects of Heating Rate and Bulk Flow Neglected

The first set of computations were undertaken to determine the applicability of the mathematical model to the present problem when experimental values for all physical properties were used in the model. These results are shown as the solid lines in Figure IV-2 along with the experimental

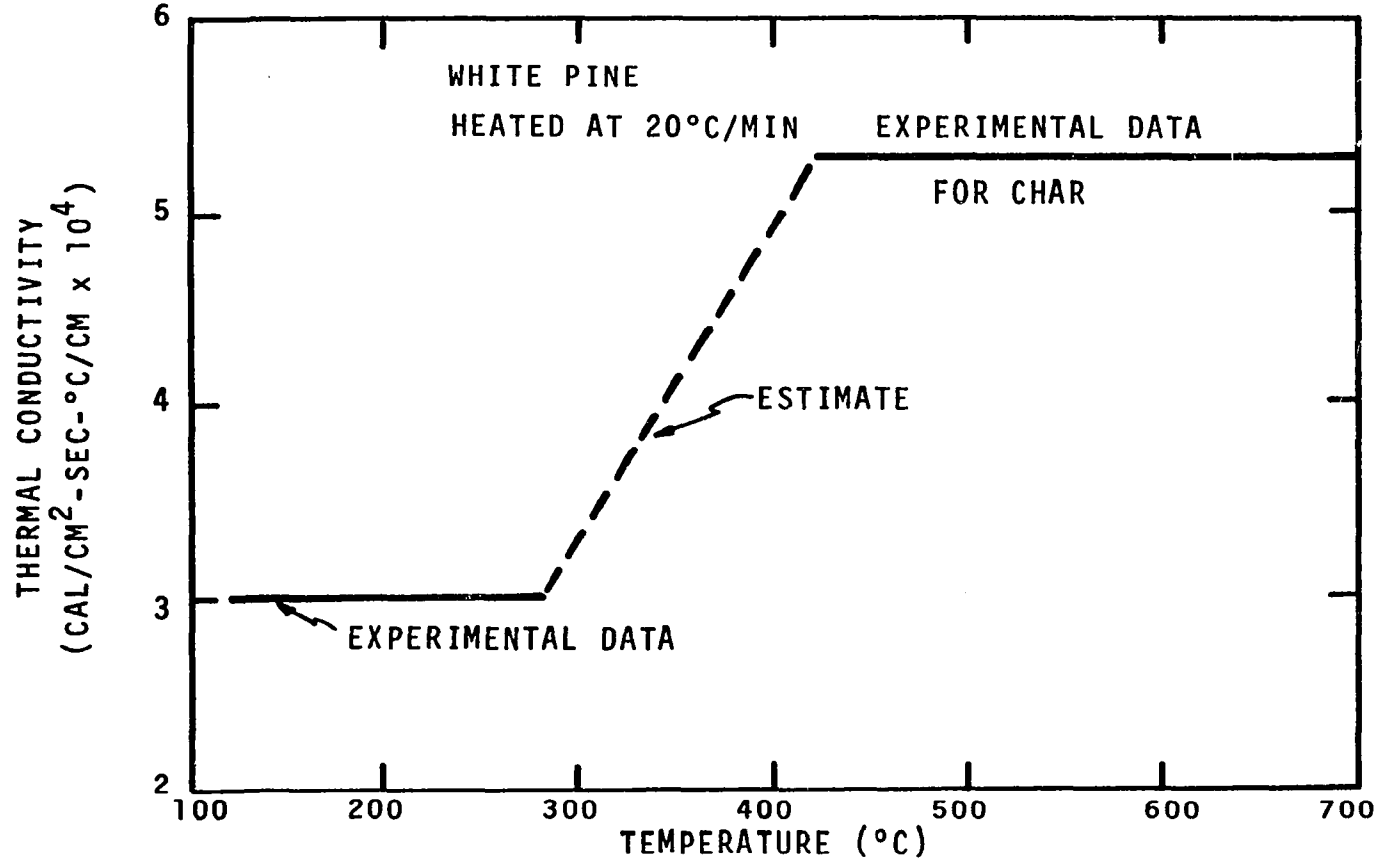

Figure IV-1. Thermal Conductivity of White Pine as a Function of Temperature.

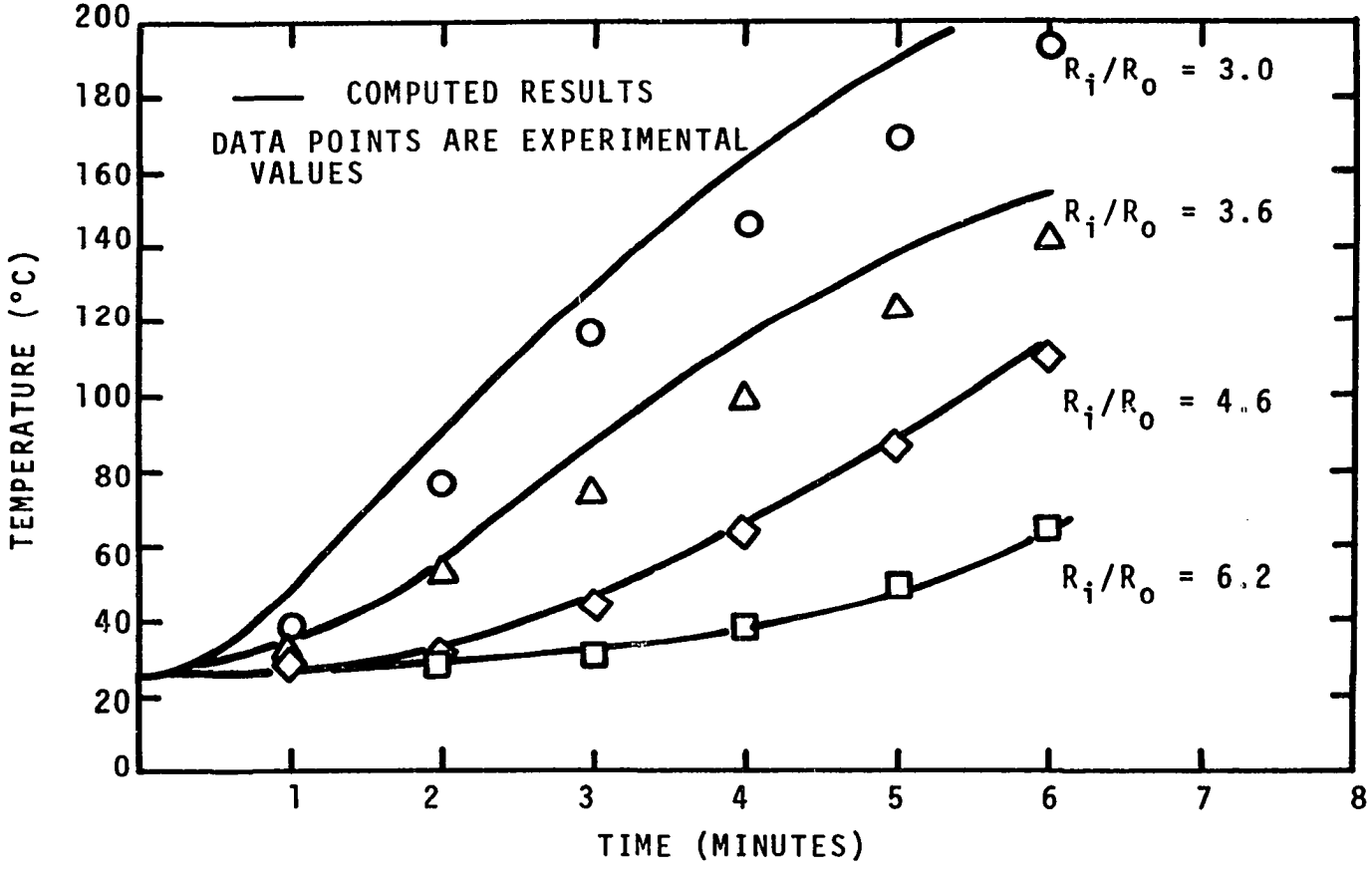

Figure IV-2. Comparison of Computed and Experimental Temperature Profiles for White Pine (Model of Havens).

data of Havens which were discussed in Chapter II. As can be seen the computed results for the present study predict a higher temperature profile than that measured, by about 15 percent in the worst case. As one moves further away from the char front, at dimensionless radii of 4.6 and 6.2, the computed temperature profiles are in good agreement with the experimental results.

Both heating rate and bulk flow act as heat sinks for the pyrolysis of wood. Thus neglecting these effects in the mathematical model should result in predicted temperatures which are higher than those obtained experimentally.

Inclusion of the Effect of Heating Rate

The effect of heating rate on weight loss at heating rates up to 160°C/min was incorporated into the mathematical model utilizing the experimental weight loss data discussed in Chapter III. The similarity of the weight loss curves obtained at each heating rate suggested the possibility of using the weight loss curve obtained at 20°C/min as a reference and of applying a temperature correction to that data to define the weight loss data at other heating rates. This procedure was accomplished by comparing the temperatures at 30, 60, 45 and 90 percent weight remaining at each heating rate to their corresponding temperature at 20°C/min. The four values of temperature difference were average at each heating rate to obtain the correction factor shown in Table IV-1.

TABLE IV-1

TEMPERATURE CORRECTION FACTORS

Heating Rate, °C/min	Temperature Correction, °C
10	-12
20	0
40	+ 8
80	+24
160	+32

The temperature correction factor was applied to the numerical computations by computing an average heating rate for each mesh point at a temperature of approximately 200°C and by applying the corresponding temperature correction factor during pyrolysis. The 200°C temperature was chosen to obtain a heating rate before the onset of pyrolysis.

It has been demonstrated that the overall chemistry of pyrolysis for white pine and oak is independent of heating rate up to 160°C/min. Assuming that the detailed chemical mechanism for wood pyrolysis is also independent of heating rate, the dependence of energy capacity on heating rate is given by

$$\left\{\frac{\rho}{\rho_o}\left[\left(\frac{\partial \bar{E}}{\partial T}\right)_\phi + \left(\frac{\partial \bar{E}}{\partial \phi}\right)_T \left(\frac{\partial \phi}{\partial T}\right)\right] + \left(\frac{\bar{E}-\bar{H}_f}{\rho_o v_o}\right)\left[\left(\frac{\partial \rho}{\partial T}\right)_\phi + \left(\frac{\partial \rho}{\partial \phi}\right)_T \left(\frac{\partial \phi}{\partial T}\right)\right]\right\}\frac{dT}{dt}$$

$$= -\int_V \nabla\cdot\vec{q}\,\frac{dv}{\rho_o v_o} \qquad \text{IV-10}$$

Ideally it should be possible to measure the effect of heating rate on the energy capacity using DSC. Unfortunately at the higher heating rates required, it has not as yet been possible to reproduce isothermal heat loss. However, the effect of heating rate on the energy capacity curve can be deduced from Equation IV-10.

The left hand side of Equation IV-10 consists of two terms; the first represents the sensible energy required to raise the temperature of the wood; the second represents the energy required to pyrolyze the wood to a fluid of enthalpy $\bar{H}_f$. The only heating rate dependence in this second term is that associated with density, i.e., weight loss for a solid of constant volume. Thus the energy of pyrolysis is associated with weight loss regardless of the rate of heating.

The $(\partial\bar{E}/\partial T)_\phi$ in Equation IV-10 represents the sensible heat required to raise the temperature of a material at a constant rate of heating ϕ (the heat capacity). The $(\partial\bar{E}/\partial\phi)_T \cdot (\partial\phi/\partial T)$ is the sensible energy associated with a change in heating rate ϕ. The magnitude of these terms can be estimated recognizing that if the chemistry of pyrolysis does not change with heating rate then the energy required to raise the temperature where the wood is totally charred is the same regardless of the path by which the heating was accomplished.

Figure IV-3 shows the total energy required to raise the temperature of wood from 25°C to 460°C with parameters of heating rate. At each heating rate both sensible and pyrolysis

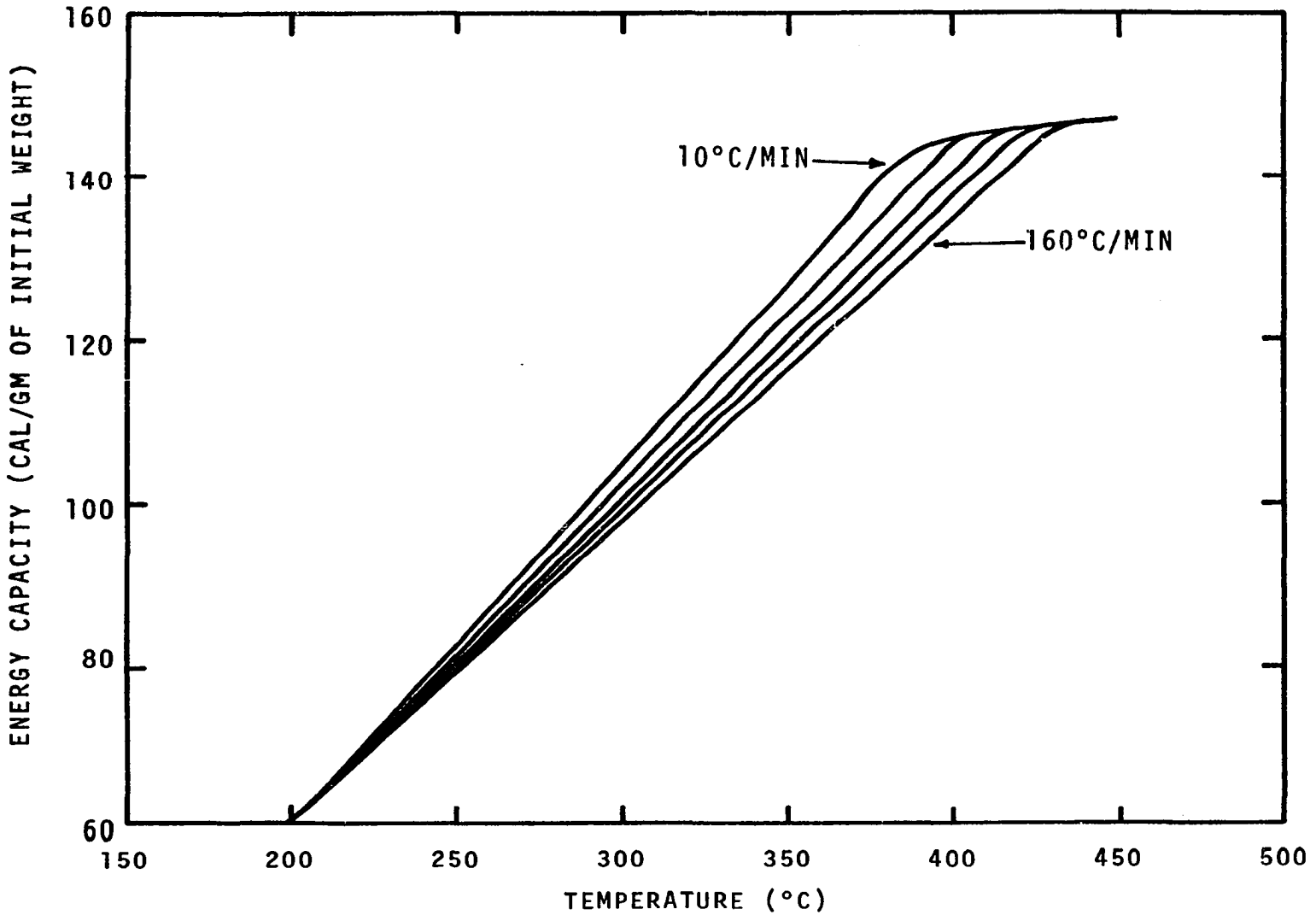

Figure IV-3. Estimate of Effect of Heating Rate on Heat of Pyrolysis for White Pine.

heat effects are assumed to follow their respective weight loss curves. From Figure IV-3 cross plots of energy against heating rate can be prepared with parameters of constant temperature; one such plot is shown in Figure IV-4. The $(\partial\bar{E}/\partial\phi)_T$ at 390°C has a value of approximately 0.1 cal-sec/gm-°C at a heating rate of 10°C/min and approaches zero at a heating rate of 160°C/min.

Values for $\partial\phi/\partial T$ can be determined from the experimental temperature profiles shown in Figure IV-2 or IV-6. For example, in Figure IV-6 the heating rate at 300°C is 23°C min, at 390°C the heating rate is 19°C/min. Thus

$$\frac{\partial\phi}{\partial T} = \frac{23-19}{300-390} = \frac{4}{90} \simeq 0.04 \text{ °C/sec-°C}$$

The magnitude of the $(\partial\bar{E}/\partial\phi)_T(\partial\phi/\partial T)_x$ can be computed and at heating rates of interest its value is less than 0.01 cal/gm-°C, which is negligible in comparison to the heat capacity, about 0.5 cal/gm-°C. Thus the only adjustment required in the energy capacity curve is to account for the effect of heating rate on weight loss.

The computer program was modified to account for the effect of heating rate on energy capacity, weight loss and thermal conductivity. (At heating rates other than 20°C/min the temperature dependence for thermal conductivity in Figure IV-1 was adjusted for heating rate by applying the perperature correction factors in Table IV-1.) The temperature profiles shown in Figure IV-2 were recomputed, and the results are

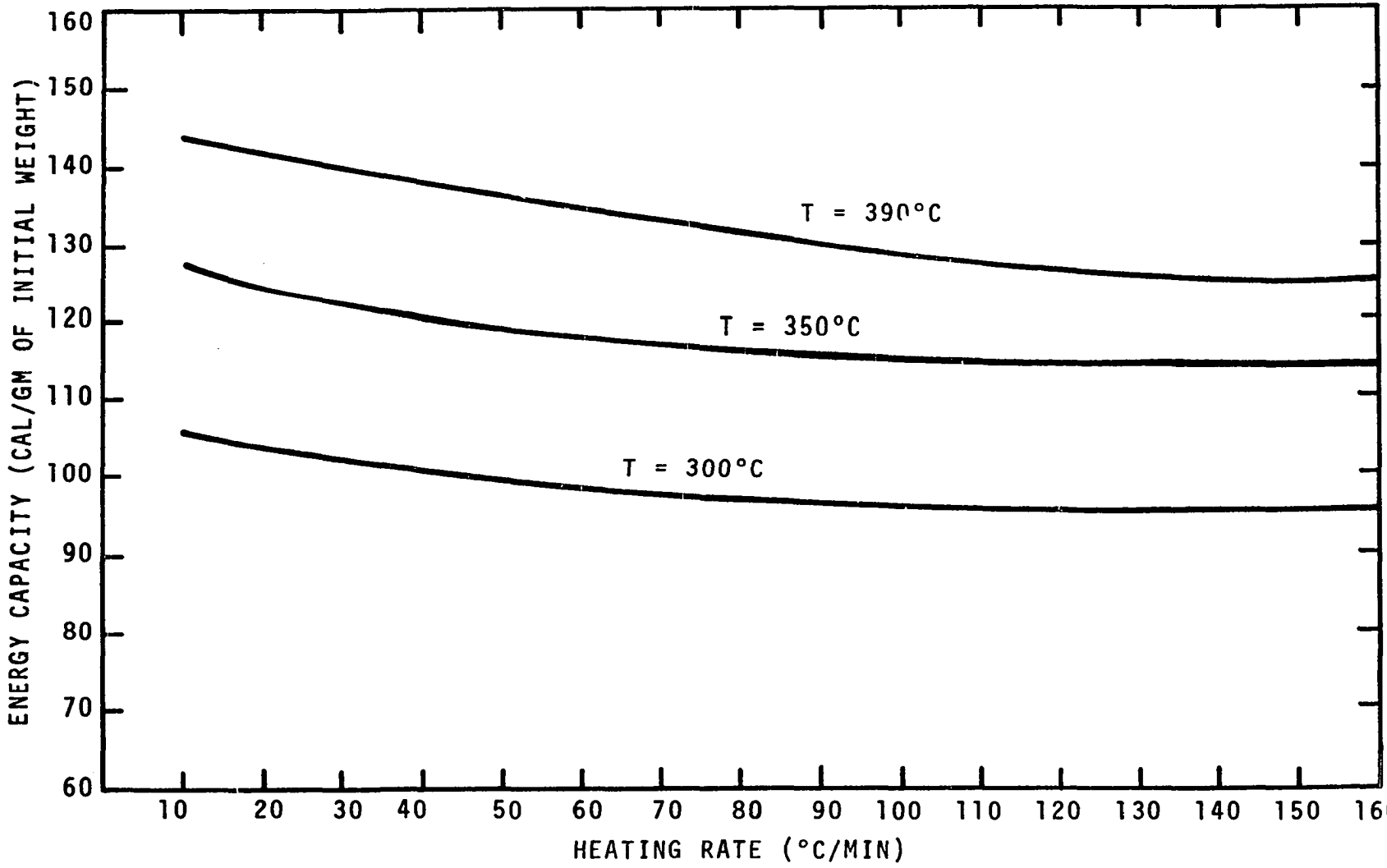

Figure IV-4. Energy Capacity as a Function of Heating Rate for White Pine.

shown in Figure IV-5. As can be seen the computer profiles are about 8 percent high at worst.

The experimental temperature profiles shown in Figures IV-2 and IV-5 are for material that has not pyrolyzed. An experimental temperature profile for pyrolyzing wood is presented in Figure IV-6 along with the predicted temperature profile. At worst the computed temperatures are again 8 percent high.

Effect of Bulk Flow

The heat sink associated with the heating of volatiles as they flow through the char zone was accounted for by assuming the volatiles to be in thermal equilibrium with the solid. The rate of mass flow was obtained from the data of Havens, and the heat capacity of the gases was assumed to be 0.25 cal/gm-°C of gas. Inclusion of this effect into the model brought the computed and experimental results to within 5 percent at worst. At both the high temperature and low temperature ends, the agreement was almost exact as shown in Figure IV-7.

Mass Loss

Computed and experimental mass losses are presented in Figure IV-8. The results are about 8 percent high. These results are within the experimental accuracy of the data.

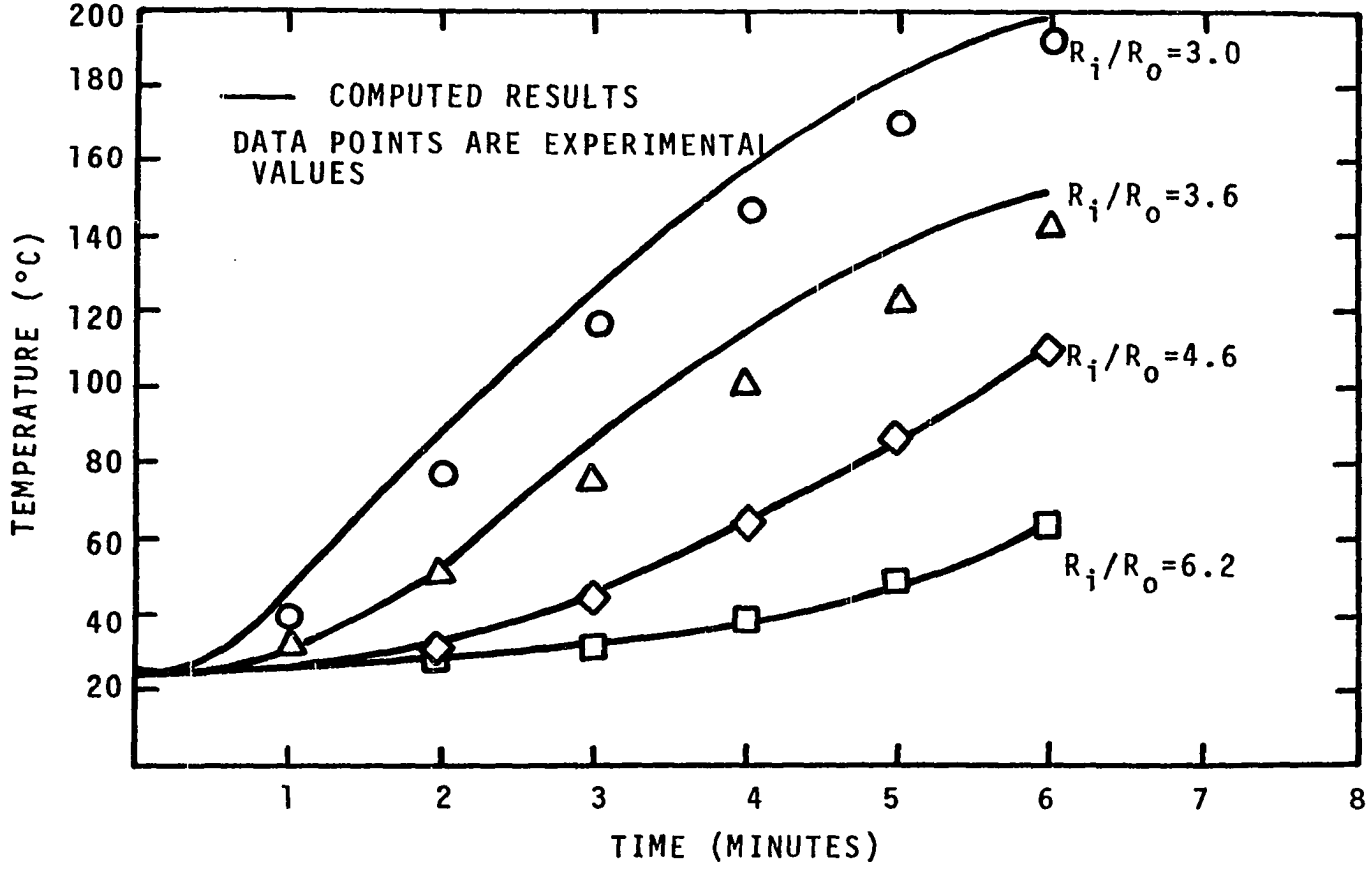

Figure IV-5. Computed and Experimental Temperature Profiles for White Pine. Computed Results Include Effect of Heating Rate.

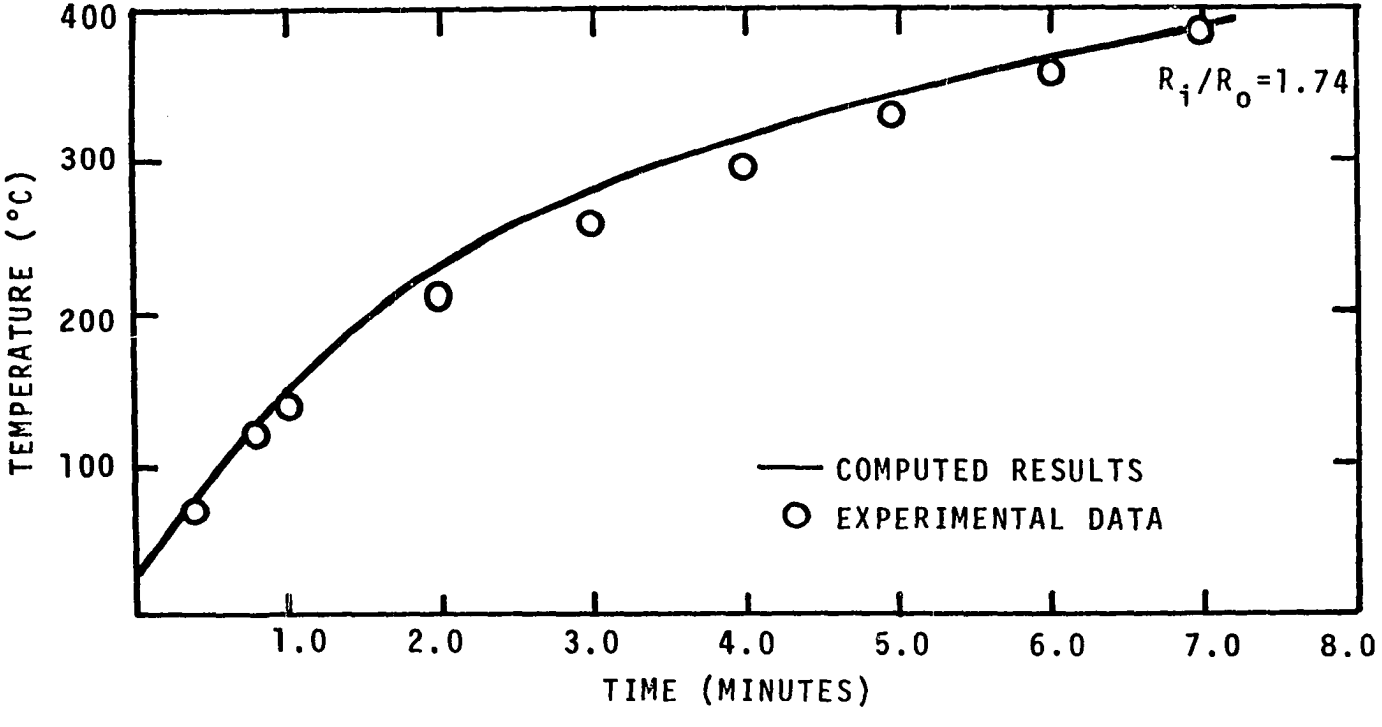

Figure IV-6. Experimental and Computed Temperature Profile for White Pine. Model Includes Effect of Heating Rate.

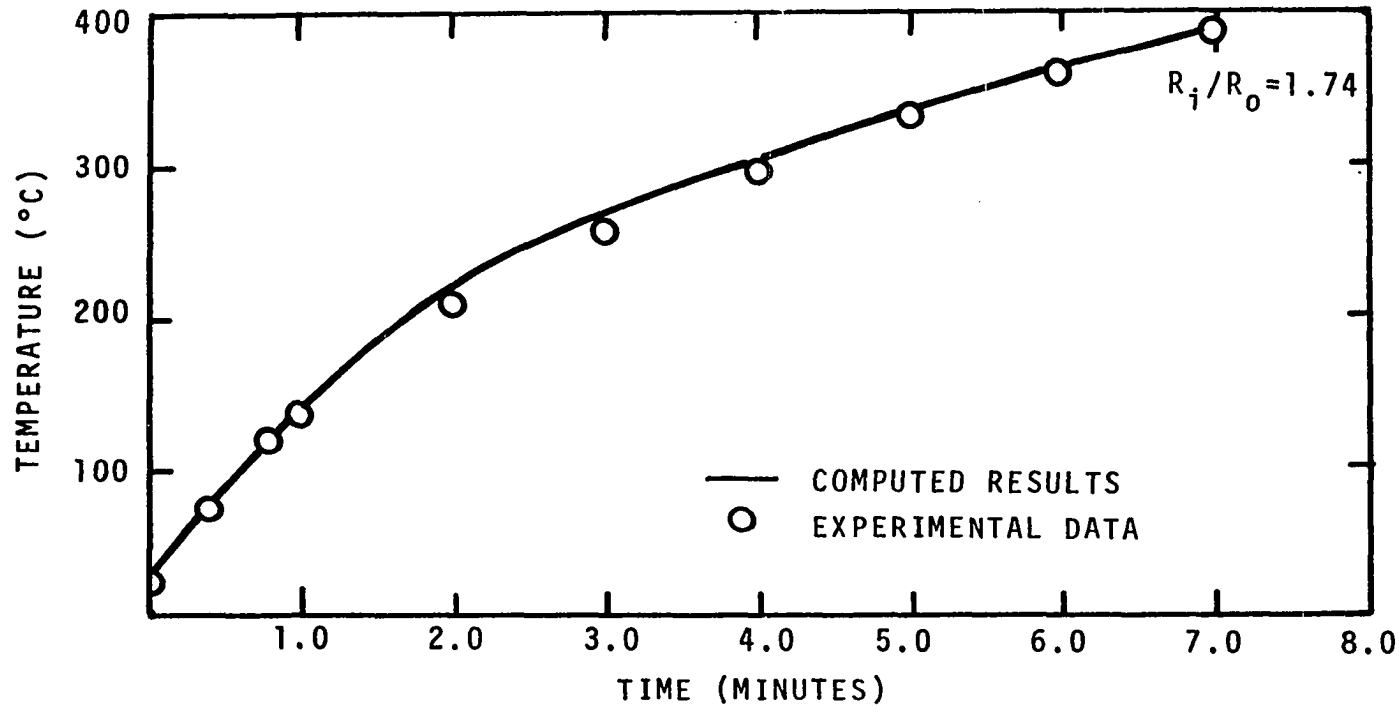

Figure IV-7. Experimental and Computed Temperature Profile for White Pine. Model Includes Heating Rate and Bulk Flow Effects.

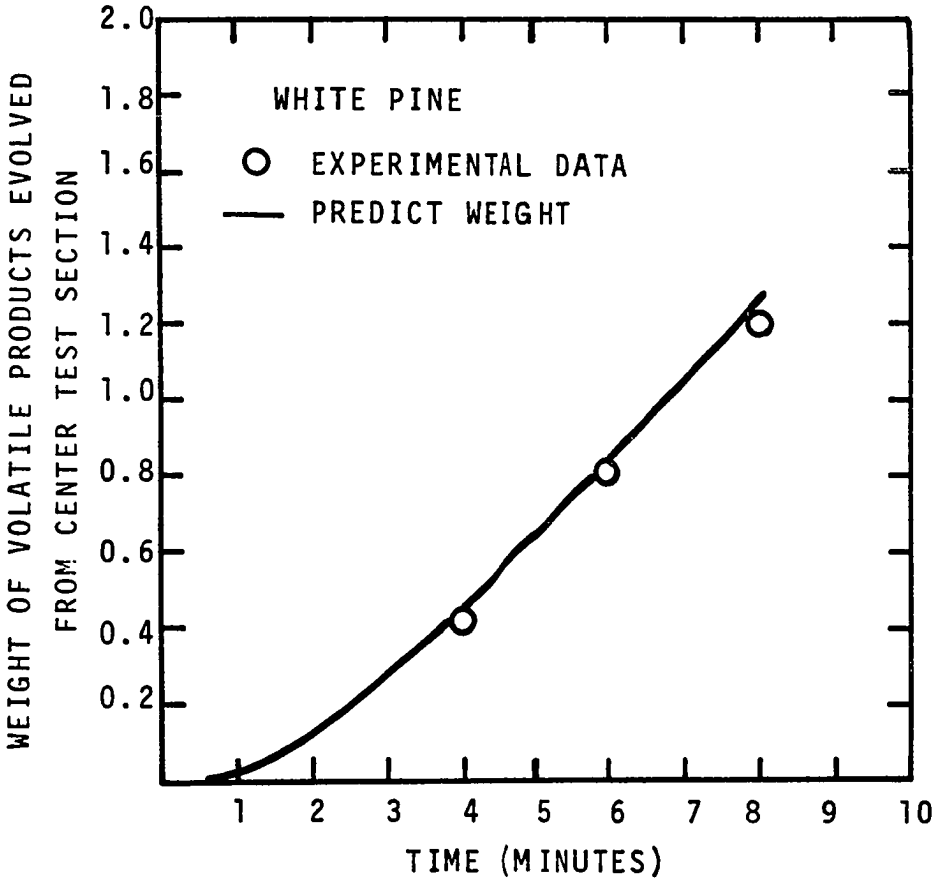

Figure IV-8. Computed and Experimental Weight Loss Profiles for White Pine.

CHAPTER V

DISCUSSION OF RESULTS

The experimental energy capacity, thermogravimetric and thermal conductivity data described in Chapter III were obtained from individual experiments without reference to the pyrolysis model developed in Chapter IV.

The DSC and TG measurements were made on very small sawdust samples to minimize sample geometry and heat transfer effects on the experimental results. Thus, the experimental data should represent the physical and thermal properties of the woods studied.

The energy capacity data shown in Figure III-26 and III-27 provide a complete accounting for the energy required to heat white pine and oak sawdust from 25°C to 450°C. Both sensible and decomposition heat effects are included in these data. One objective of this study is to compare the DSC data obtained in this study and those of Havens described in Chapter II. The white pine data for the two studies are very similar. For oak the large peak shown in Figure III-27 is broader and reaches a lower maximum value than that reported by Havens.

The energy capacity curve can be separated into its two components by assuming that pyrolysis occurs at temperatures from 200°C to 420°C and that within this temperature range the sensible heat effect decreases in proportion to sample weight. The shaded areas in Figure V-1 and V-2 represent the heat of pyrolysis for white pine and oak respectively. Below 230°C and above 430°C the energy capacity curves represent sensible heat effects.

Integration over the shaded area in Figure V-1 and V-2 yields a heat of pyrolysis of 43.2 cal/gm of original weight endothermic and 27.0 cal/gm of original weight, for white pine and oak respectively. The value for heat of pyrolysis of white pine is 8 percent lower, and for oak it is 2 percent higher than those reported by Havens. Tang reported a heat of pyrolysis for α-cellulose of 88±3.6 cal/gm, endothermic.

The heat capacity of the charred residue can be computed from the portion of the DSC curve above 420°C. Based on the actual weight of the residue, a value of 0.36 cal/gm-°C was obtained which is in good agreement with the specific heat data for charcoal reported by Widdell as shown in Figure II-19.

The different values for heat of pyrolysis obtained for oak and white pine can be qualitatively deduced by comparing their DTG thermograms as in Figure V-3. The DTG curve for oak exhibits a period of constant weight loss beginning

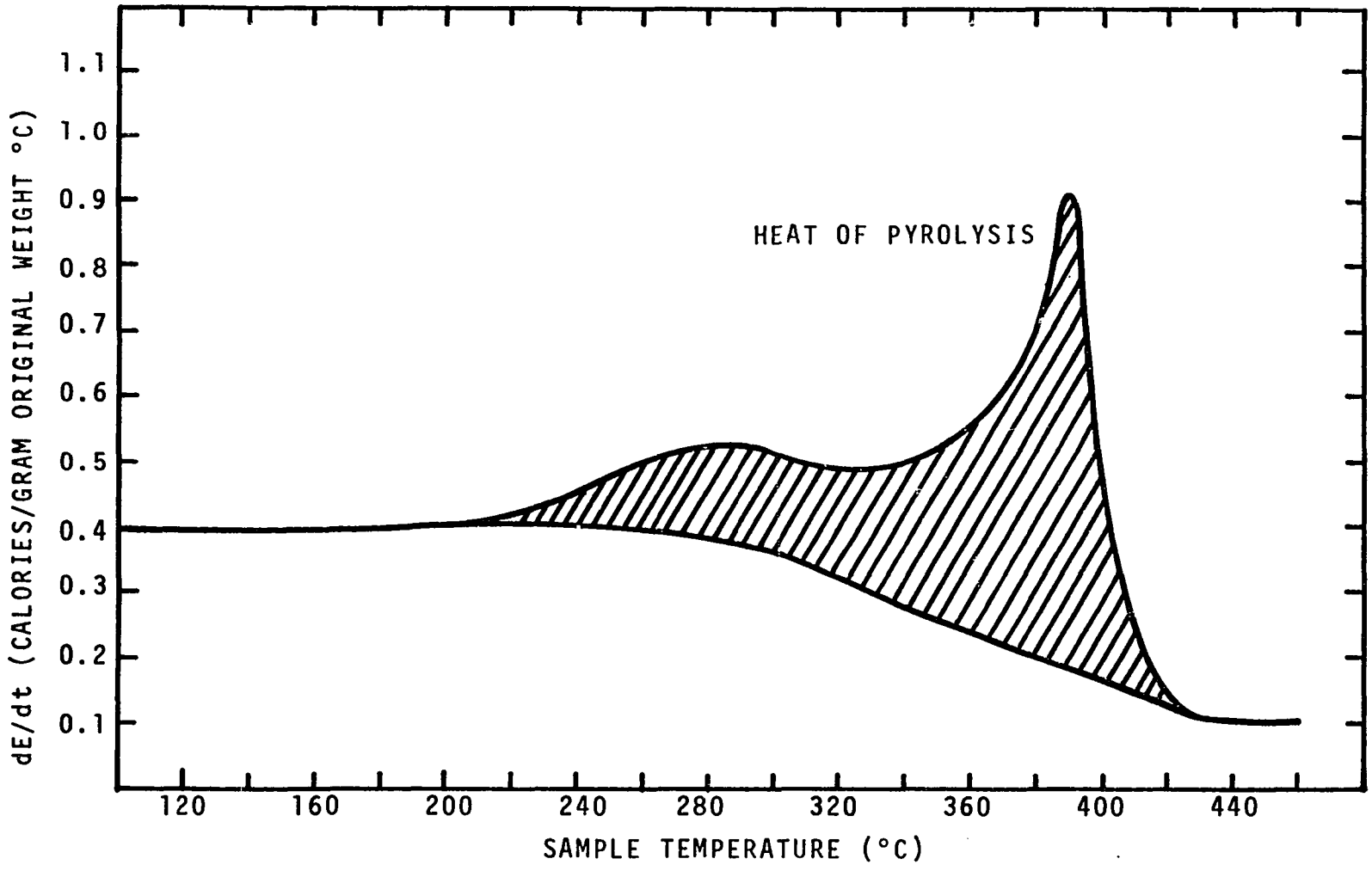

Figure V-1. Estimate of Heat of Pyrolysis for White Pine from DSC Data.

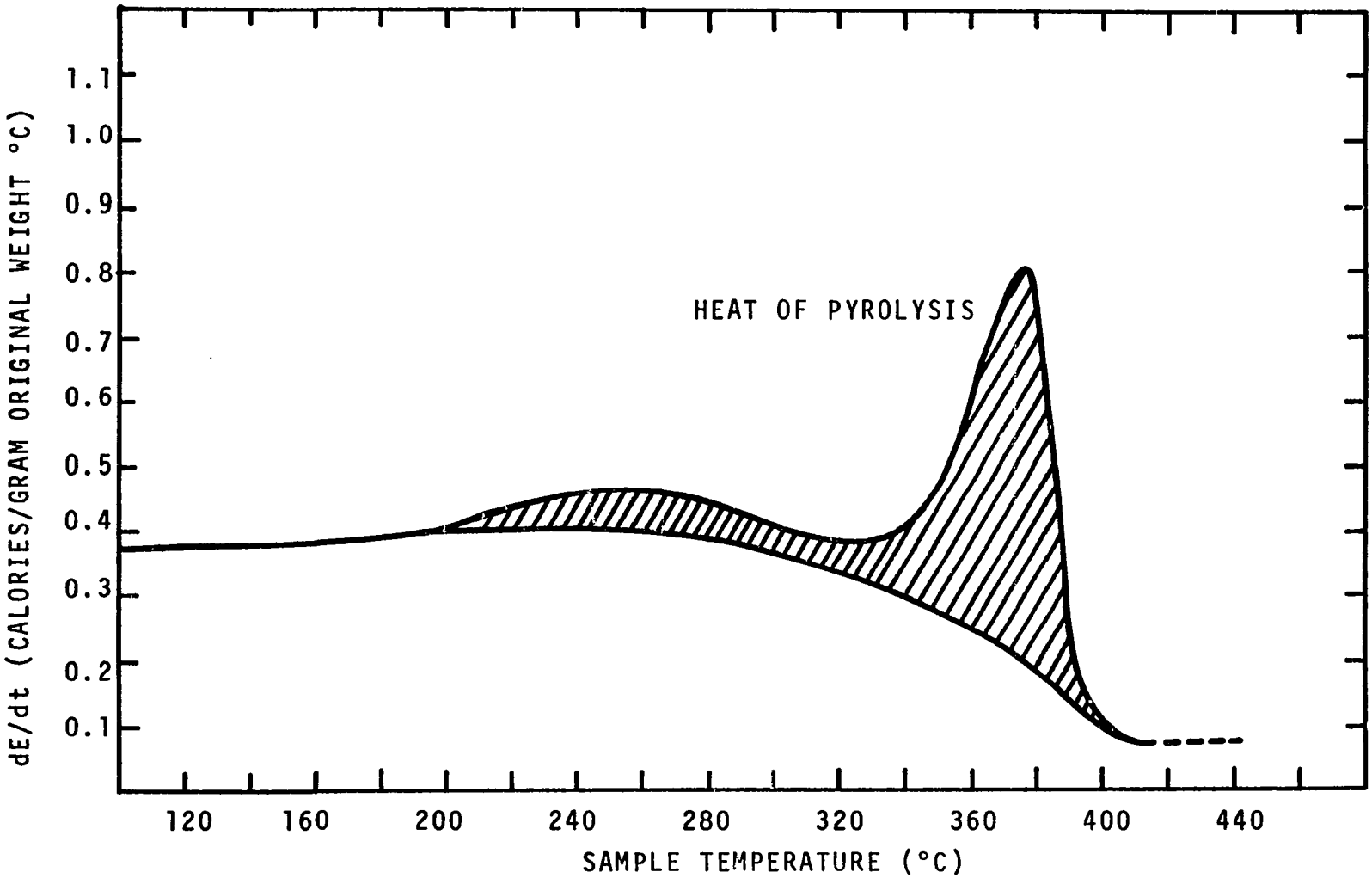

Figure V-2. Estimate of Heat of Pyrolysis for White Pine from DSC Data.

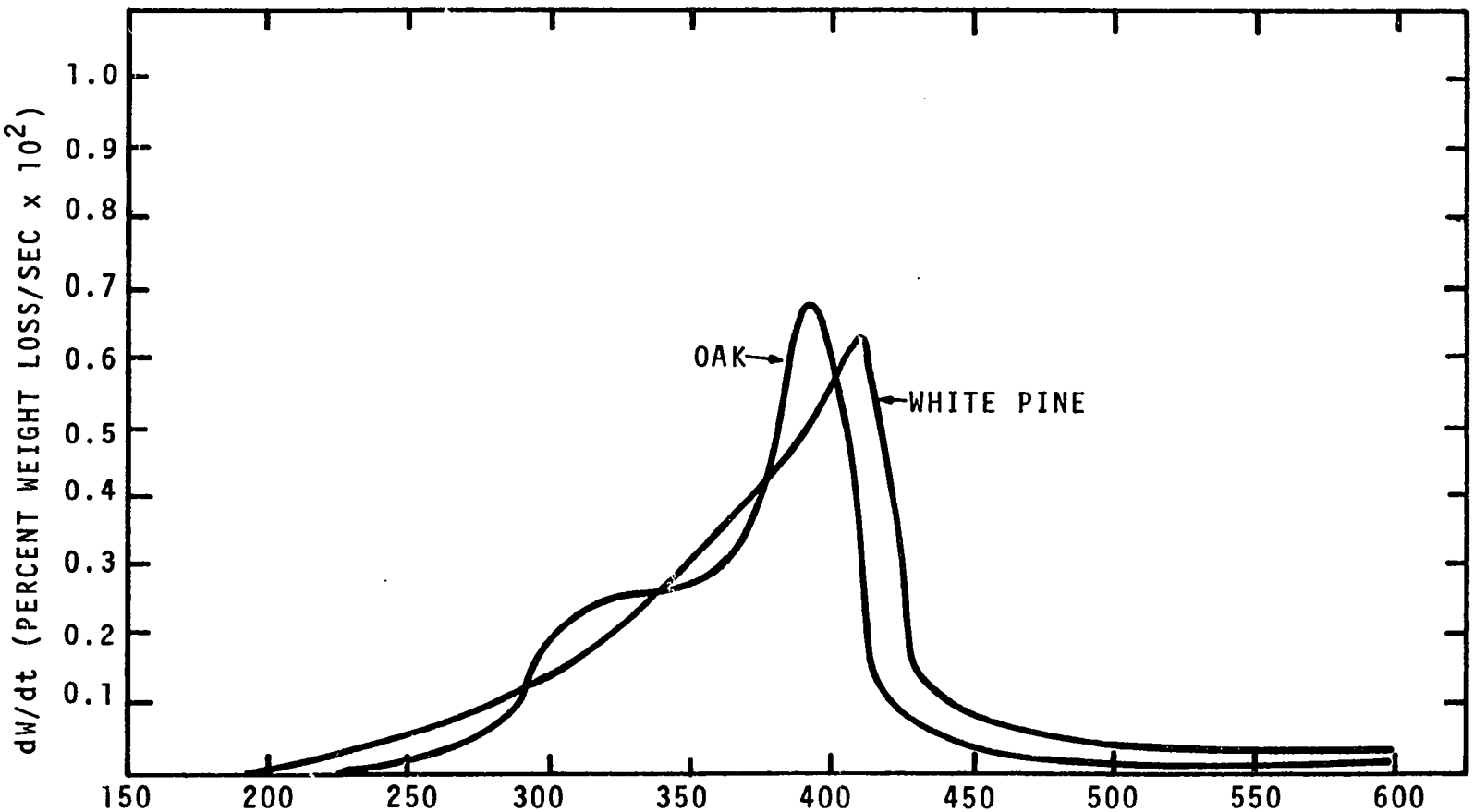

Figure V-3. DTG Curves for White Pine and Oak at a Heating Rate of 20°C/min.

at approximately 320°C and continuing for about 30°C. Over the same range the DTG curves for white pine continue to rise except for a slight discontinuity at about 375°C. Tang (38) has pointed out that the weight loss curves for woods can always be produced by superposition of the weight loss thermograms for the components in each wood. Thus, one would expect that the difference in the DTG and DSC thermograms for white pine and oak can be attributed to composition difference.

The applicability of the energy capacity data to heating rates other than 20°C/min is dependent on demonstrating the effect of heating rate on the chemistry of wood pyrolysis. It has been shown in this work that the overall chemistry of wood pyrolysis is independent of temperature heating rate over the range of heating rates studied. Based on this finding the energy capacity data were extended to higher heating rates. Although this approach does not conclusively prove that the energy of pyrolysis is independent of heating rate over the range of heating rates studied, the results of the TG experiments combined with the excellent agreement between experimental and computed temperature profile and weight loss data strongly supports this position. Additionally, McCarter (28) has recently presented data indicating that the products of wood pyrolysis are independent of heating rate.

It has been suggested that the shift of TG curves to higher temperature with increased heating rate might be

attributed to differences in heat transfer properties between the magnetic standards and wood samples. Two simple experiments were devised to determine the validity of this theory. In the first experiment it was hypothesized that if wood properties are sufficiently different than those of the calibration material, then thermograms for a large wood sample, about 6 mg, should deviate from that for a 2 mg sample. Several such thermograms were obtained for each wood and no difference could be observed. The second experiment was to calibrate the furnace temperature first with the standard aluminum oxide bed and then with an oak bed in the sample pan. The results of this experiment at a heating rate of 80°C/min are summarized in Table V-1. As can be seen the differences between the two calibration procedures are within experimental error.

TABLE V-1

FURNACE CALIBRATION USING ALUMINUM OXIDE AND OAK BEDS

Metal	Magnetic Transition Temp.	Aluminum Oxide Bed	Oak Beds
Alumel	163	163	165
Nickel	354	365	362
Nickoseal	438	440	435
Perkalloy	596	610	615

The shift in the TG curve with heating rate can be computed from the Arrhenius rate expression by replacing temperature with heating rate,

$$- \frac{1}{W_o - W_f} \frac{dW}{dt} = k_o \, e^{-E/R(a+\phi t)} \, W^n \qquad \text{V-1}$$

where ϕ = heating rate (°K/sec)

a = initial temperature (°K)

The kinetic constants, E, n, and k_o, for white pine and oak are summarized in Table III-2.

The white pine and oak activation energies computed in Chapter III are in agreement with those obtained by Akita and Kase (2) and Tang (38) for α-cellulose. It is surprising that a single value of activation energy was obtained for both woods studied since two orders of reaction are indicated for each wood. Most likely there is a slight difference in activation energy, but the difference cannot be resolved using the present procedures.

The value for thermal conductivity of wood char obtained in this study is the first such value reported in the literature. The only similar data is that reported by Nagler (31) for the thermal conductivity of pyrolyzing nylon resins. Before pyrolysis the resin thermal conductivity was found to be 1.0×10^{-4} Btu/ft-sec-°F, and the char thermal conductivity was found to have a value of 2.5×10^{-4} Btu/ft-sec-°F. Qualitatively the increase in thermal conductivity

during pyrolysis can be deduced by comparing electrical and heat conduction properties of the original and pyrolyzed woods. Wood is not an electrical conductor, while wood char which consists of carbon is an electrical conductor. Thus, one would expect wood char to have a higher thermal conductivity than the original wood.

The computed results presented in Chapter IV were obtained without making adjustments in the physical property data. Additionally, microanalytical data, DSC and TG, have been utilized to predict the temperature profile and mass loss during pyrolysis of large wood cylinders. The relative effect of heat conduction, heating rate, and bulk flow on the pyrolysis of wood is demonstrated in Figure V-4. Figure V-4 shows that heating rate and bulk flow are of secondary importance in comparison to heat conduction.

Inclusion in the model of the effect of heating rate is a major extension of the mathematical model. The model was designed (15) to use single valued functions for energy and weight loss as a function of temperature. The temperature correction factor algorithm described in Chapter IV permitted adjustment of the energy and weight loss data such that heating rate could be accounted for in the model. Without this algorithm or a similar algorithm the effect of heating rate could not be incorporated into the model.

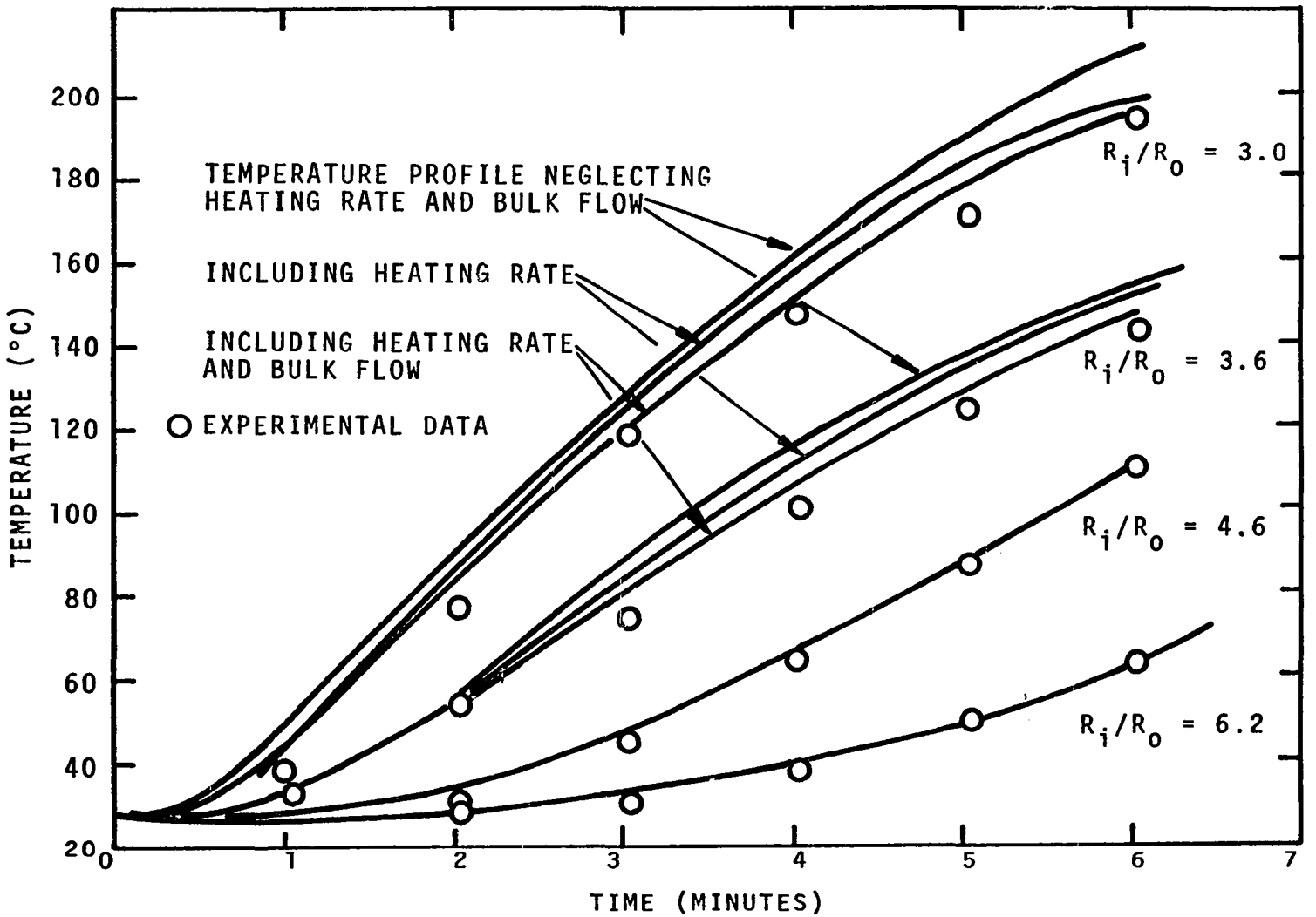

Figure V-4. Effect of Model Modifications on Computed Temperature Profiles.

CHAPTER VI

SUMMARY OF WORK AND SPECULATION ON FUTURE STUDIES

The transient temperature profile and rate of mass loss for pyrolyzing wood can be predicted using the proposed model. Solution of the model for these quantities requires that the sample boundary conditions be defined and the physical and thermal properties of the wood be known. The effect of heating rate on the overall kinetics of wood pyrolysis has been studied. The weight loss data fit an Arrhenius type kinetic expression. The heat of pyrolysis and the sensible heat required to raise the temperature of oak and white pine from 25°C to 450°C have been measured. The thermal conductivity of wood char has been experimentally determined in the transverse grain direction.

Several areas of potential study have come to mind during this work. Included among these are:

1. Criterion for ignition should be studied utilizing the proposed model and experimental ignition data.
2. The effect of air on the pyrolysis of wood should be studied in detail to determine if an additional energy effect does occur in the presence of air.

3. A study of other woods and their components are needed to determine the relationship between heat of pyrolysis and composition.
4. Other polymeric materials such as the synthetic polymers should be studied.

BIBLIOGRAPHY

1. Akita, K. "Studies on the Mechanism of Ignition of Wood." Report of Fire Research Institute of Japan, No. 9 (1959),

2. Akita, A., and Kase, M. "Determination of Kinetic Parameters for Pyrolysis of Cellulose and Cellulose Treated with Ammonium Phosphate by Differential Thermal Analysis and Thermal Gravimetric Analysis." J. of Polymer Science, Part A-1, 5 (1967), 833-848.

3. Arseneau, D. F. "The Differential Thermal Analysis of Wood." Canadian Journal of Chemistry, 39 (1961), 1915-1919.

4. Bamford, C. H.; Crank, J.; and Malan, D. H. "The Combustion of Wood, Part I." Proc. of Cambridge Phil. Soc., 42 (1946), 166.

5. Blackshear, P. L., Jr., and Kanury, A. Murty. "An X-Ray Photographic Study of the Reaction Kinetics of α-Cellulose Decomposition," Pyrodynamics, 4 (1966), 285-298.

6. Broido, A. "Thermogravimetric and Differential Thermal Analysis of Potassium Bicarbonate Contaminated Cellulose." WSCI Paper No. 66-20, 1966 Spring Meeting, Western States Section, The Combustion Institute, Denver Research Institute (April 1966).

7. Brown, D. J. "Errors in Density Measurement During the Pyrolysis of Wood and Related Substances." Combustion and Flame, 15 (1970), 309-311.

8. Burningham, N. W., and Seader, J. D. "Determination of Kinetic Parameters for the Thermal Degradation of Polymers by the Quasilinearization Technique." Paper presented at 161st meeting American Chemical Society (1971).

9. Chung, P. K., and Jackson, M. L. "Thermal Diffusivity of Low Conductivity Materials." Industrial and Engineering Chemistry, 46, No. 12 (1954), 2563-2566.

10. Domansky, Radislov, and Rendos, Frantisek. "Zum Studium der Pyrolysis des Holzes und Seiner Komponenten." Holz als Roh-und Werkstoff, 20 (1962), 473-476.

11. Dunlap, F. "The Specific Heat of Wood." U.S. Dept. of Agriculture, Forest Service Bulletin No. 110 (1912).

12. Freeman, E. S., and Carroll, B. J. Phys. Chem., 62 (1958), 394.

13. Goldfarb, I. J.; McGuchan, R.; and Meeks, A. C. "Kinetic Analysis of Thermogravimetry. Part II. Programmed Temperature." Air Force Materials Laboratory, Wright-Patterson Air Force Base, Ohio, AFML-TR-68-181, Part #2 (1968).

14. Griffiths, Ezer, and Kaye, G. W. "The Measurement of Thermal Conductivity." Proceedings of the Royal Society of London, Series A, 104 (1923), 71-98.

15. Hashemi, H. T. "Heat Conduction with Change of Phase." Unpublished Ph.D. dissertation. University of Oklahoma, Norman, Oklahoma, 1965.

16. Havens, J. A. "Thermal Decomposition of Wood." Unpublished Ph.D. dissertation. University of Oklahoma, Norman, Oklahoma, 1969.

17. Heinrich, H. J., and Kaesche-Krischer, B. "Contributions to the Explanation of Self-Ignition of Wood." Brennstoft-Chemie, 43, No. 5, 142-148.

18. Kanury, A. Murty. "An Evaluation of the Physico-Chemical Factors Influencing the Burning Rate of Cellulosic Fuels and a Comprehensive Model for Solid Fuel Pyrolysis and Combustion." Unpublished Ph.D. dissertation. University of Minnesota, Minneapolis, Minnesota, 1969.

19. Kanury, A. Murty. "A Radiographic Technique to Study Thermal Decomposition Kinetics of Charring Polymeric Solids." Paper presented at 161st meeting American Chemical Society (1971).

20. Keylworth, R., and Chistoph, N. "Contributions to the Study of Thermal Decomposition of Wood by Means of Differential Thermal Analysis." Deutscher Verband Fur Materials Prufung DVM, 2, No. 8 (20 August 1960), 281-288.

21. Klason, Peter. "Theory of the Dry Distillation of Wood." I. Jour. Pract. Chem., 90 (1914), 413-447.

22. Kollman, F. Technologie des Holzes und der Holzwerkstoffs, Vol. 1. 2nd ed. Berlin: Julius Springer, 1936.

23. Koohyar, A. "The Ignition of Wood by Flame Radiation." Unpublished Ph.D. dissertation. University of Oklahoma, Norman, Oklahoma, 1967.

24. Kung, H. C. "A Mathematical Model of Wood Pyrolysis." FM Research Corporation, FMRC Serial No. 19721-6.

25. MacClean, J. D. "Thermal Conductivity of Wood." Heating, Piping and Air Conditioning (July 1940), 459-464.

26. MacClean, J. D. "Rate of Disintegration of Wood Under Different Heating Conditions." American Wood Preserver's Association Proceedings, 47 (1951), 155-169.

27. McAdams, W. H. Heat Transmission. New York: McGraw-Hill Book Company, 1954.

28. McCarter, R. J. "The Pyrolysis of Cellulose at Rates Approaching Those of Combustion." Paper presented at 162nd National American Chemical Society Meeting (1971).

29. Martin, S. "Thermal Radiation Damage to Cellulosic Materials. I. Wood." U.S. Naval Radiological Defense Laboratory. R & D Technical Report USNRDL-TR-102-NS081-001 (10 February 1956).

30. Mitchell, R. L.; Seborg, R. M.; and Millett, M. A. "Effect of Heat on the Properties and Chemical Composition of Douglas Fir Wood and its Major Components." Journal of Forest Products Research Society, 3 (1953), 72-73.

31. Nagler, R. G. "The Thermal Conduction Process in Carbonaceous Char." National Aeronautics and Space Administration Technical Report 32-1010, N67-16556.

32. Panton, R. L., and Rittman, J. G. "Analytical Study of Combustion." Final Report to Air Force Armament Laboratory Ballistics Division (ATB), Elgin Air Force Base, Florida.

33. Roberts, A. F. "A Review of Kinetic Data for the Pyrolysis of Wood and Related Substances." Combustion and Flame, 14 (1970), 261-272.

34. Roberts, A. F., and Clough, G. "Thermal Decomposition of Wood in an Inert Atmosphere." 9th International Symposium on Combustion. New York: Academic Press, 1963.

35. Rowley, F. B. "The Heat Conduction of Wood at Climatic Temperature Differences." Transactions, American Soc. of Heating and Ventilating Engineers, 39 (1933), 313-323.

36. Sandermann, W., and Augustin, Hans. "Chemische Untersuchungen uber die Thermische Fersetzung of Holz Erste Metteilung: Stand der Forschung, Zwerte Metteilung: Unterschungen mit Hilte der DTA." Holz als Roh-und-Werkstoff, 21 (1963), 305-315.

37. Stamm, A. J. "Thermal Degradation of Wood and Cellulose." Industrial and Engineering Chemistry, 48 (1956), 413-417.

38. Tang, W. K. "Study of the Effect of Chemical Treatment of the Thermal Decomposition of Wood." Forest Product Laboratory Report, 1960.

39. Tang, W. K., and Neill, W. K. "Effect of Flame Retardants on Pyrolysis and Combustion of α-Cellulose." J. of Polymer Science, Part C, 6 (1964), 65-81.

40. Tyulpanov, R. S. "Study and Estimation of Thermal Decomposition of Wood." Gidrolizi Lesokhim, Prom 10(6) (1957), 13-14.

41. Wangaard, F. F. "The Transverse Conductivity of Wood." Unpublished Ph.D. dissertation. New York State College of Forestry, 1948.

42. Wangaard, F. F. "Transverse Heat Conductivity of Wood." Heating, Piping, and Air Conditioning, July 1940, 459-464.

43. Weatherford, W. D., Jr., and Sheppard, D. M. "Basic Structure of the Mechanism of Ignition of Cellulosic Materials." Tenth Symposium (International) on Combustion, 1965, 897-910.

44. Welker, J. R. Private communication.

45. Wesson, H. R. "The Piloted Ignition of Wood by Radiant Heat." Unpublished Ph.D. dissertation. University of Oklahoma, Norman, Oklahoma, 1970.

46. Widell, Torsten. "Thermal Investigation into Carbonization of Wood." Acta Polytechnica, Chemical and Metallurgical Series, 1, No. 6 (1949), 35.